DAMAGE DETECTION IN BEAMS BY WAVELET ANALYSIS

A THESIS SUBMITTED TO
THE GRADUATE SCHOOL OF NATURAL AND APPLIED SCIENCES
OF
MIDDLE EAST TECHNICAL UNIVERSITY

BY

HÜSEYİN YANILMAZ

IN PARTIAL FULFILLMENT OF THE REQUIREMENTS
FOR
THE DEGREE OF MASTER OF SCIENCE
IN
MECHANICAL ENGINEERING

DECEMBER 2007

Approval of the Thesis

"DAMAGE DETECTION IN BEAMS BY WAVELET ANALYSIS"

Submitted by **HÜSEYİN YANILMAZ** in partial fulfillment of the requirements for the degree of **Master of Science in Mechanical Engineering Department, Middle East Technical University** by,

Prof. Dr. Canan Özgen
Dean, Graduate School of **Natural and Applied Sciences** _____

Prof. Dr. Kemal İder
Head of Department, **Mechanical Engineering** _____

Prof. Dr. Mehmet Çalışkan
Supervisor, **Mechanical Engineering, METU** _____

Examining Committee Members

Prof. Dr. Y. Samim Ünlüsoy (*)
Mechanical Engineering, METU _____

Prof. Dr. Mehmet Çalışkan (**)
Mechanical Engineering, METU _____

Prof. Dr. H. Nevzat Özgüven
Mechanical Engineering, METU _____

Prof. Dr. Bülent E. Platin
Mechanical Engineering, METU _____

Asst. Prof. Dr. Ahmet Türer
Civil Engineering, METU _____

Date: 17.12.2007

(*) Head of Examining Committee
(**) Supervisor

I hereby declare that all information in this document has been obtained and presented in accordance with academic rules and ethical conduct. I also declare that, as required by these rules and conduct, I have fully cited and referenced all material and results that are not original to this work.

Name, Last Name :Hüseyin YANILMAZ

Signature :

ABSTRACT

DAMAGE DETECTION IN BEAMS BY WAVELET ANALYSIS

YANILMAZ, Hüseyin

M.S., Department of Mechanical Engineering
Supervisor: Prof. Dr. Mehmet ÇALIŞKAN
December 2007, 131 Pages

In this thesis, a method proposed by Han et al. [40] for detecting and locating damage in a structural member was adapted. The method was based on the energies that were calculated from the CWT coefficients of vibrational response of a cantilever beam. A transverse cut at varying depths was introduced. The presence and location of crack was investigated by processing experimentally acquired acceleration signals.

Results of modal analysis and wavelet analysis of the beam with different cut depths were compared. In addition, effect of using different mother wavelets in CWT analysis for damage detection capability was investigated. Acceleration data were analyzed through CWT at different scales and CWT coefficients were calculated. Those CWT coefficients obtained from different scales were evaluated from the standpoint of damage detection. Effectiveness of energy indices associated with CWT coefficients in damage detection was demonstrated as independent of the type of mother wavelet.

Keywords: Damage Detection, Wavelet Transform, CWT Energy Index.

ÖZ

KİRİŞLERDE DALGACIK DÖNÜŞÜMÜ İLE HASAR BELİRLENMESİ

YANILMAZ, Hüseyin

Yüksek Lisans, Makina Mühendisliği Bölümü
Tez Danışmanı: Prof. Dr. Mehmet ÇALIŞKAN
Aralık 2007, 131 Sayfa

Bu tezde, daha önce Han ve diğerleri [40] tarafından önerilmiş yapısal elemandaki bir hasarın varlığını ve yerini belirleyebilecek bir yöntem uyarlanmıştır. Yöntem, ankastre bir kirişin titreşim verilerinden elde edilen Sürekli Dalgacık Dönüşümü (CWT) katsayılarından hesaplanan enerji değerleri üzerine dayanmaktadır. Farklı derinliklerde oluşturulan dikey bir kesiğin varlığı ve yeri deneysel olarak elde edilen ivme sinyalleri işlenerek araştırılmıştır.

Farklı kesik derinliklerindeki kirişin titreşim biçimsel ve dalgacık analiz sonuçları karşılaştırılmıştır. Ek olarak, CWT analizinde farklı ana dalgacıklar kullanımının hasar belirleme yetkinliği üzerindeki etkisi araştırılmıştır. İvme verisi farklı ölçeklerde CWT ile çözümlenmiş ve CWT katsayıları hesaplanmıştır. Farklı ölçekler ile elde edilen CWT katsayıları hasar belirleme açısından değerlendirilmiştir. CWT katsayılarından elde edilen enerji indislerinin ana dalgacık tipinden bağımsız olarak hasar belirlenmesindeki etkinliği gösterilmiştir.

Anahtar Kelimeler: Hasar Belirleme, Dalgacık Dönüşümü, CWT Enerji İndisi

To My Parents and Dear and Devoted Friends

ACKNOWLEDGEMENTS

The author wishes to express his grateful gratitude to his supervisor, Prof. Dr. Mehmet Çalışkan for his guidance, advice, criticism, encouragements and insight throughout the research.

The technical assistance of Mr. Yasin Sarı and Mr. Ahmet Levent Avşar are gratefully acknowledged.

The author would also like to send his very special thanks to Mr. Ekrem Türk for his encouragementsand insight throughout the preparation of this thesis.

The author is greatly indebted to his family for their love and sacrifice.

TABLE OF CONTENTS

LIST OF FIGURES

LIST OF TABLES

NOMENCLATURE

$\psi(t)$	: mother wavelet
$\hat{\psi}(\omega)$	: Fourier transform of $\psi(t)$
ω	: Frequency
a	: Scale number
b	: Translation parameter
F	: Impulse force
A1-A5	: Accelerometer positions
$f(t)$	: Time signal
$\psi_{a,b}(t)$	: Basis function
$\psi^*_{a,b}(t)$	: Complex conjugate of basis function
C(a,b)	: Wavelet coefficients
a	: Depth of crack
b	: Width of crack
FRF	: Frequency Response Function
$f_j^m(t)$	: m^{th} component of j^{th} level decomposed signal $f(t)$
$E_{f_j^i}$	: Energy stored in the component signal $f_j^i(t)$
E_{f_j}	: Signal energy at j^{th} level decomposition
$\overline{E}$	: Uniform energy expression obtained via wavelet coefficients

$E(j)$: Energy of the signal stored in the j^{th} scale of the CWT

E : Total energy of the time signal $f(t)$

WT : Wavelet Transform

WPT : Wavelet Packet Transform

CWT : Continuous Wavelet Transform

FT : Fourier Transform

FWT : Fast Wavelet Transform

STFT : Short Time Fourier Transform

MDLAC : Multiple Damage Location Assurance Criterion

WPD : Waveket Packet Decomposition

WPS : Wavelet Packet Signature

WTF : Wavelet Transmittance Function

WPERI : Wavelet Packet Energy Rate Index

bior6.8 : Biorthogonal wavelet of order 6.8

db7 : Daubechies wavelet of order 7

CHAPTER 1

INTRODUCTION

1.1 General

Monitoring structure condition and detecting structural damage at the earliest possible stage have been a focus of concentrated research recently. There are mainly two reasons that grab the attention of people. The first is the aging phenomena, i.e. more and more structures are getting older while the load they have to carry is either not changing or getting heavier. The second main driving force of this interest is the economics and life loss issues which result from the sudden collapse of the structures.

Different techniques and methods for damage detection are available in the literature which can be classified into either local or global methods. In local methods, it is required that the neighborhood of the damage is known a priori and part of the structure under inspection is readily accessible [1]. Visual, acoustic, magnetic field and eddy current techniques are some examples for local methods. The global damage detection methodologies, on the other hand, most of the time do not require the information for the damage place beforehand. In this technique the condition of a structure is determined and quantified by inspecting changes in its global structural characteristics.

Definition of damage is given as any deviation introduced to a structure, either deliberately or unintentionally, which adversely affect the performance of the system [2]. It is clear from this definition that a comparison is needed between two states of a structure.

1.2 Damage Assessment

One damage identification system commonly classifies four levels of damage assessment [1]:

- Level 1: Determining the presence of damage,
- Level 2: Locating the damage,
- Level 3: Quantifying the damage severity,
- Level 4: Prediction of the remaining serviceability of the structure.

Most currently used techniques, such as visual, acoustic, magnetic field and eddy current, etc., are effective yet local in nature. It is required to know the neighborhood of the damage a priori and the portion of the structure to be inspected should be readily assessable. The global damage identification methods, on the other hand, quantify the condition of a structure by examining deviations of its global structural characteristics. Vibration-based damage assessment which is the mostly used global damage identification method is usually carried out in three steps:

1. Data collection,
2. Extraction of condition index,
3. Assessment of structure condition through the analysis of indices.

A fundamental issue with the use of vibration-based damage assessment methods is to seek some damage indices that are sensitive to structural damage [4]. The damage indices that have been demonstrated with various degrees of success include natural frequencies, mode shapes, mode shape curvatures, modal flexibility, modal strain energy, etc.

Doebling et al. [1] and Farrar et al. [5] summarized the comprehensive historic development of damage assessment methodologies based on these indices as well as pointed out their applicability and limitations. Techniques such as the Fourier transform (FT) are usually used for processing the measured signals in system identification so that modal properties are obtained to be used in damage assessment. The structural damage is typically a local phenomenon which tends to be captured by higher frequency signals [3]. The Fourier analysis transforms the signal from a time-based or space-based domain to a frequency-based one. However, the time or space information may be lost during performing such a transform and it becomes sometimes very difficult determining time of occurrence or place of a particular event. To overcome this difficulty, the short-time Fourier transform (STFT) was proposed by Gabor [6]. This windowing technique analyzes only a small portion of the signal at a time. The STFT is mapping a signal into a 2-D function of time or space and frequency. However, the transformation has the drawback that the information about time or space and frequency can be obtained with a limited precision that is determined by the size of the window. A higher resolution in time or space and frequency domain cannot be attained simultaneously since once the window size is chosen, it is the same for all frequencies. The wavelet transform (WT) is precisely a new way to analyze the signals, which overcomes the problems that other signal processing techniques exhibit. Wavelet functions are composed of a family of basis functions that are capable of describing a signal in a localized time (or space) and frequency (or scale) domain [7].

The wavelet packet transform (WPT) is an extension of the WT, which provides a complete level-by-level decomposition of signal [8]. Coifman and Wickerhauser [9] defined wavelet packets as alternative bases formed by the linear combinations of the usual wavelet functions. One further step of WT is continuous wavelet transform (CWT) which is defined as the sum over all time of the signal multiplied by scaled, shifted versions of the wavelet function. In this study CWT is applied both to the mode shapes and acceleration signals of a cracked beam with various damage levels. The results of CWT are then used for calculation of energy indices and plotting the coefficients for different damage cases.

1.3 Objective and Scope of the Thesis

In this study, it is aimed to compare effectiveness of vibration based damage detection techniques. Natural frequencies, mode shapes and frequency response functions are to be used for modal analysis where continuous wavelet transform (CWT) results are to be utilized for wavelet analysis. In addition, one of the methods [4] using wavelet transform for damage detection is to be adapted both for the acceleration and mode shape data. Furthermore, effect of using different mother wavelet types on damage assessment of the same measurement data is aimed to be compared. Also, the same mother wavelet with different scale numbers is to be used to see the effect of scaling number on the damage detection. Thesis was organized in 6 chapters.The second chapter summerizes the literature in the field. Wavelet analysis and motivation for this study were given in chapter 3. Test setup and collection and processing of data were given in chapter 4. Results were discussed in chapter 5. Finally, the study was summerized and concluded in chapter 6.

CHAPTER 2

LITERATURE REVIEW

A literature survey has been carried out to establish present state of art on available techniques in structure health monitoring and diagnostics. Subjects of this survey have been classified under the topics related to detection of effects on natural frequencies and on mode shapes as well as wavelet transform applications.

2.1 Natural Frequencies

Dimarogonas [10] and Chondros [11] modeled the crack as a local flexibility and they obtained the local flexibility by experiments. They also developed a spectral method to identify cracks in various structures relating the crack depth to the change in the first three natural frequencies of the structure for known crack position.

Cawley and Adams [12] developed an experimental method to estimate the location and the depth of the crack from the changes in the natural frequencies. In all of the method, the model of the damage was important.

Petroski [13] proposed a technique in which the section modulus was appropriately reduced to model a crack. Another approach has been to model the crack by a local flexibility matrix Dimarogonas [14].

In the case of transverse vibrations of beams Chondros and Dimarogonas [15]; Rizos et al. [16]; Liang et al. [17]; Ostachowicz and Krawkczuk [18], reduced the flexibility matrix to one rotational spring inserted at the site of the crack to represent the crack, where the stiffness of the spring was related to the size of the crack.

Specifically, Chondros and Dimarogonas [15] gave a method to detect cracks in welded joints. Rizos et al. [16] applied this technique and detected the crack location through the measurement of amplitudes at two points on the component.

Liang et al. [17] studied a case and indicated that the characteristic equation could be solved to obtain the value of stiffness for a given natural frequency and the crack location.

Ruotolo and Surace [19] claimed that most detection techniques for crack damage in a beam are applicable only in existence of a single crack in the beam. The authors propose a damage assessment method for identifying multiple cracks in beam structures. The proposed method is based on two optimization techniques: genetic algorithms and simulated annealing. By combining these two optimization techniques, local minima/maxima are avoided and global extrema are sought. Here, the objective function is formed as a function of the difference between the measured and calculated frequencies and mode shapes.

Williams and Messina [20] formulated a correlation coefficient that compared changes in a structure's resonant frequencies with predictions based on a frequency-sensitivity model derived from a finite element model. This approach was termed Multiple Damage Location Assurance Criterion (MDLAC).

Chaudhari and Maiti [21] proposed a method for modeling transverse vibration of a geometrically segmented cantilever slender beam using the Frobenius method of solving an Euler-Bernoulli type differential equation. Then, using the first three frequencies, the authors solved an inverse problem to locate and quantify a crack in the beam.

Hanselka et al. [22] proposed an online monitoring technique, which used an onboard microcontroller to extract modal properties when the structure was in use. For damage diagnosis, the authors solved an inverse eigen value problem trying to estimate the stiffness changes from the measured modal properties.

Morassi [23] presented a diagnostic technique based on the determination of some Fourier coefficients of the stiffness variation caused by damage. This study focused on identifying notches in axially vibrating beams. First, the eigen functions of the analytical model were expanded as a series of the eigen functions of the undamaged beam, and it was imposed that this analytical model have the same frequencies as the experimentally estimated frequencies of the damaged structure.

Aydoğan [24] introduced a new method to detect and locate a crack in a structural component in his study. The method proposed was an extension of a previously developed technique for identification of non-linearity in vibrating multi degree-of-freedom systems. The method exploited nonlinear frequency response functions for the detection and identification of cracks in structures.

2.2 Mode Shapes

Doebling and Farrar [25] examined changes in the frequencies and mode shapes of a bridge as a function of damage. This study focused on estimating the statistics of the modal parameters using Monte Carlo procedures to determine if damage has produced a statistically significant change in the mode shapes.

Ahmadian, Mottershead, and Friswell [26] proposed a damage detection procedure that used measured displacements of a structure and an existing analytical model to locate faults.

Sun [27] stated that damage assessment using mode shape vectors generally involves analyzing differences between the measured modal vectors before and after damage. Mode shape vectors are spatially distributed quantities; therefore, they provided information that could be used to locate damage. However, large numbers of measurement locations were required to accurately characterize mode shape vectors and provide sufficient resolution for determining the damage location.

Ettouney et al. [28] discussed a comparison of three different structural health monitoring techniques applied to a complex structure. All three of the techniques were based on knowing the mode shapes and natural frequencies of the damaged and undamaged structure.

2.3 Wavelet Analysis

Wang and McFadden [29] used the wavelet transform to analyze actual gearbox vibration signals in the time domain and the local features of the signals were presented. Their works indicated that the gear damage could be correlated to features in time versus wavelet scale plots.

Sung et al. [30] presented the application of the wavelet transform to detect the impact damages in composite laminates.

The acoustic emission waves generated by impact loads are analyzed by wavelet transformation and the differences in these waves were found.

Zhang et al. [31] used numerically simulated dynamic response data to locate damage. The use of multiple impact positions was proposed to improve the result. The effects of sensor position, damage depth and severity of damage were discussed.

Liew and Wang [32] proposed an application of spatial wavelet theory to crack identification in structures. They calculated the wavelets along the length of the beam based on the numerical solution for the deflection of the beam. In order to find the position of crack from the wavelet data, an excitation that oscillated rapidly along the length of the beam was used to excite the beam. The crack location was then indicated by a peak in the variations of some of the wavelets along the length of the beam.

Chang and Chen [33] presented a method for structure damage detection. The wavelet transform was used to analyze spatially distributed signals (e.g. mode shapes) of the structure. The flexural vibration equations of the Timoshenko beam containing a transverse crack were obtained and then these results were analyzed by wavelet transformation. The crack position could be effectively detected by the present approach even though the crack was very small.

Chang and Chen [33] also investigated vibration damage detection of a Timoshenko beam by spatial wavelet based approach. First, the mode shapes of the Timoshenko beam containing a transverse crack were obtained. The crack was represented as a rotational spring. Then these spatially distributed signals were analyzed by wavelet transformation.

Naldi and Venini [34] briefly explored the use of wavelets to detect damage in structural components. The authors numerically simulated damage in a beam constrained in all but the axial direction. The damage was simply a 20% reduction in axial stiffness at one-third the distance from the end. The coefficients of the Daubechies wavelet were used to locate the damage, and a harmonic excitation was applied to the beam. Then, the stiffness reduction, which varies from 50% to almost 0%, was detected using the first seven Daubechies wavelet coefficients in the vicinity of the damage.

Lu and Hsu [35] carried out investigations considering a discrete wavelet transform; they analyzed dynamical structural aspects on 1-D truss structures and flexible strings, respectively.

Biemans et al. [36] used Daubechie's wavelet coefficients to detect crack growth in the middle of a 400 × 150 × 2 mm rectangular aluminum plate with 6 piezoceramic sensors mounted symmetrically around the crack. Static loading, sinusoidal loading, and Gaussian white noise were provided by one of the sensors, and the crack growth was monitored by the remaining sensors. The authors demonstrated that classical Fourier analysis could yield misleading results. In fact, some cracks had virtually no effect on frequency components of measured signals. They, however, showed that certain Daubechies wavelet coefficients provided a reasonable indicator of crack presence.

Wang and Deng [37] discussed a structural damage detection technique based on wavelet analysis of spatially distributed structural response measurements. This approach was based on a premise that damage in a structure causes the structural response perturbations at the damage sites and that the local perturbations were often discernable in wavelet components. Comparisons between the Haar and Gabor wavelets were made by conducting static and dynamic simulations on simply supported beams and plates with crack damage. Cracks ranged in thickness, size, and displacement fields, to which the wavelet analyses were applied and were calculated. In all cases, the methods demonstrated the ability of the wavelets to capture the crack location.

Peng and Chu [38] presented a summary about the application of the wavelet in machine fault diagnostics, including the following main aspects: the time–frequency analysis of signals, the fault feature extraction, the singularity detection for signals, the denoising and extraction of the weak signals, the compression of vibration signals and the system identification. Some other applications were introduced briefly as well, such as the wavelet networks, the wavelet-based frequency response function, etc.

Sun [27] proposed a method based on wavelet packet decomposition (WPD) to process vibration signals of a structure that undergoes characteristic changes due to damage. Based on WPD, a novel damage condition index, wavelet packet signature (WPS), was formulated and proposed as indices for structure condition assessment. The method for evaluating the sensitivity of WPS under different damage scenarios was proposed. After comparing with the sensitivity of other dynamic properties such as natural frequencies and mode shapes the results showed that proposed index was more likely to indicate damage than modal properties.

Hughes et. al. [39] developed a combined time series and wavelet analysis technique to improve damage detection in either thick, complex geometry, or non-homogeneous materials. A wavelet transmittance function (WTF) was defined as the ratio of continuous wavelet transforms from the time responses at different locations on a structure. A new damage indicator was developed based upon wavelet transmittance function. A simulated model was illustrated to highlight the potential of the new damage indicator on a thick aluminum specimen. Then, experimental signal data from two sets of different experiments conducted on thick structures with a crack and a delamination were analyzed using the wavelet transmittance function to detect the presence and extent of the damages as reflected on the WTF maps.

Han et al. [40] proposed a damage detection index called wavelet packet energy rate index (WPERI), for the damage detection of beam structures. They decomposed the measured dynamic signals into the wavelet packet components and the wavelet energy rate index was computed to indicate the structural damage. The proposed damage identification method was firstly illustrated with a simulated simply supported beam and the identified damage was satisfactory with assumed damage. Afterward, the method was applied to the tested steel beams with three damage scenarios in the laboratory. Despite the presence of noise during measurement, the identified damage pattern was comparable with the tests.

Both simulated and experimental studies demonstrated that the WPT-based energy rate index was a good candidate index that was sensitive to structural local damage.

Kim and Kim [41] used Gabor wavelets to detect a crack in a simply supported beam. They not only estimated the presence of the damage by a wavelet-based approach but also its extent.

Kim and Mehlem [42] provided a review of the research that had been conducted on damage detection by wavelet analysis.

They classified the wavelet-based methods for damage detection into three categories: (1) variation of wavelet coefficients, (2) local perturbation of wavelet coefficients in a space domain, and (3) reflected wave caused by local damage. The first category was normally used to find the existence and severity of damage. This variation was usually caused by the change of modal properties of a structure. The second category was to localize the damage in structures. It involved detecting the irregularity of wavelet coefficients observed near the location of the crack. The third category was used to measure the severity as well as the location of damage. It was based on the analysis of the wave reflected by local damage in the structure.

Liew and Wang [32] used the wavelet theory to identify the crack in a simply supported beam with a transverse on-edge nonpropagating open crack. The eigen theory was also used to compare to wavelet theory. A mathematical model of the cracked beam was derived and the wavelet expressions in the space domain were proposed. It was concluded that wavelet analysis could be easily applied to the eigen functions compared to the application of the eigen theory.

For the eigen value analysis, the abrupt change of eigen functions always occurred in the higher-order modes, which results were generally inaccurate. It was stated that the wavelet analysis would not encounter this problem.

Spanos et. al. [43] used spatial wavelet transform (WT) for damage detection in Euler–Bernoulli beams subject to static loads. It was shown that by applying the WT on the difference between the displacement responses of the damaged and the undamaged beams for various loading conditions, boundary effects were eliminated and damage-related local maxima were clearly identified in the WT modulus map.

Estimates of damage locations and amplitudes were then obtained by two separate optimization procedures, in which each damaged section was modeled by an equivalent 'reduced-stiffness' spring. The effectiveness of the method was assessed using digitally-simulated data obtained via cubic interpolation on a finite number of nodal displacements.

Ovanesova and Suarez [44] subjected a fixed-end beam to dynamic and static concentrated loads and the responses were numerically calculated. Although the detection procedure did not require knowledge of the response of the undamaged structures, they also applied the wavelet analysis to their response signals.

The responses (i.e. deflected shapes) were processed with the wavelet transform to detect any feature in the signals other than those associated with the normal discontinuities. They found that a sudden peak, which occurred due to unknown sources, pinpointed the presence of a crack. They also concluded that, among those available for the present study, the biorthogonal wavelet of order 6.8(bior 6.8) was the most appropriate wavelet for crack detection in beams.

Castro et. al. [45] used free longitudinal vibrations for damage detection in rods via the CWT with the position as an independent variable. Local decreases in density and stiffness were considered, of very small size and intensity, to model the damage. The presence of a peak in the CWT allowed localization of the defect, while the linear relationship between the amplitude of this peak and the intensity of the defect permitted its quantification. The most relevant result of this study stemmed from the comparison of the different modes of vibration with regards to their capacity of detection of the defect. The first eight modes of vibration were considered; and the capacity of detection was shown to depend on the combination of two factors: the order of the used mode and the location of the defect.

Law et. al. [46] derived the sensitivity of wavelet packet transform component energy with respect to local change in the system parameters analytically from the dynamic response sensitivity. They used measurements from two states of the structure in a sensitivity-based method for damage detection. Authors showed that the wavelet packet transform containing a structural vibration mode was most suitable for the identification with a larger energy content and higher sensitivity to the parameter change. The proposed method was also shown both analytically and numerically not to be sensitive to measurement noise. The method could differentiate damages at close proximity to each other with good resolution with very short duration of measured data from only two sensors. An experimental result from a steel beam also confirmed the effectiveness of the proposed method.

Li et. al. [47] proposed a damage detection method based on a continuous wavelet transform and applied this method to analyze flexural wave in a cracked beam. For flexural waves obtained from FEM or experiments, some useful characters of the incident, reflected and transmitted waves at a certain frequency was extracted by the Gabor wavelet to exactly identify the damage location and its extent.

2.4 Overview of Literature Survey

Damage detection through vibration measurements has attracted much interest over the years. A substantial amount of work has been conducted on natural frequency and mode shape based damage detection methods in the past. Recently, a new vibration based damage detection technique that utilizes a mathematical tool called wavelet transform has been the focus in the field. A lot of studies using wavelet transform as a damage detection tool are being carried out in the vibration based damage detection field. Many different approaches in this new way of data analysis are being studied. Results obtained from these studies seem more promising in terms of damage identification when compared to modal analysis results.

CHAPTER 3

WAVELET ANALYSIS AND MOTIVATION FOR THE STUDY

3.1 Wavelet Analysis

3.1.1 Background

The most well known tool of signal analysis has been Fourier analysis, which breaks down a signal into constituent sinusoids of different frequencies. To put it another way, Fourier analysis is, as a mathematical technique, for transforming our view of the signal from time-based to frequency-based domain. For many signals, Fourier analysis is accepted as very useful because the signal's frequency content is of great importance. Then, the question why advanced techniques like wavelet analysis are needed must be addressed.

Fourier analysis has a serious drawback, which is the loss of time information in transforming to the frequency domain. In other words, when looking at a Fourier transform (FT) of a signal, it is impossible to tell when a particular event took place.

If statistical properties of signals do not change with time, that is, if it is what is called a stationary signal, this drawback is not very important.

However, much of the signals contain numerous nonstationary or transitory characteristics: drift, trends, abrupt changes, and beginnings and ends of events [53]. This part of the signal is usually important and FT lacks the capability to detect the characteristics in that part.

In an effort to correct this deficiency, Fourier transform was adapted to analyze only a small section of the signal at a time — a technique called windowing the signal. Gabor's adaptation, called the Short-Time Fourier Transform (STFT), mapped a signal into a two-dimensional function of time and frequency The STFT represented a sort of compromise between the time- and frequency-based views of a signal. It became possible to answer questions about both when and at what frequencies a signal event occurred. However, precision was limited and determined by the size of the window. While the STFT compromise between time and frequency information can be useful, the drawback is that once you choose a particular size for the time window, that window is the same for all frequencies. Many signals require various window sizes to determine more accurately either time or frequency.

Wavelet analysis represents the next logical step: a windowing technique with variable-sized regions. Wavelet analysis allows the use of long time intervals where we want more precise low-frequency information, and shorter regions where we want high-frequency information.

Time-based, frequency-based, STFT, and wavelet-based views of a signal are illustrated in Figure 3.1.

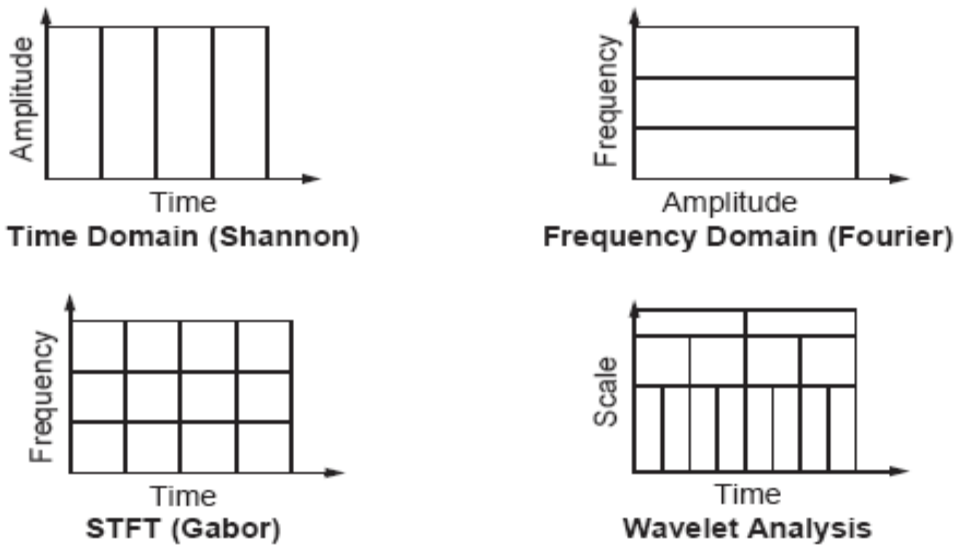

Figure 3.1 Different views of a signal [53]

3.1.2 Theory

A wavelet is a waveform of effectively limited duration that has an average value of zero:

$$\int_{-\infty}^{+\infty} \psi(t)dt = 0 \,, \qquad (1)$$

The function $\psi(t)$ is called the mother wavelet and it must satisfy the wavelet admissibility condition:

$$\int_0^{+\infty} \frac{|\hat{\psi}(\omega)|^2}{\omega} d\omega < \infty, \quad \text{.....(2)}$$

where $\hat{\psi}(\omega)$ is the Fourier transform of $\psi(t)$.

While Fourier analysis consists of breaking up a signal into sine waves of various frequencies, wavelet analysis breaks up a signal into shifted and scaled versions of the original (or mother) wavelet, which are called either basis functions or wavelet kernel and can be expressed by:

$$\psi_{a,b}(t) = \frac{1}{\sqrt{|a|}} \psi\left(\frac{t-b}{a}\right) \quad \text{.....(3)}$$

Usually, a is called the dilation (stretching or compression) parameter whereas b is the translation parameter, both being the real numbers. The wavelet transform of continuous or discrete version correlates the function $f(t)$ with $\psi_{a,b}(t)$.

The degree of correlation is calculated as a numeric value which represents how close the wavelet is correlated with the specified section of the signal. The higher the number is, the more the similarity would be. To put it another way, if the signal energy and the wavelet energy are equal to one, coefficient number may be interpreted as a correlation coefficient.

The continuous wavelet transform (CWT) is the sum over all time of the signal multiplied by a scaled and shifted version of a mother wavelet [44].

$$C(a,b) = \frac{1}{\sqrt{a}} \int_{-\infty}^{+\infty} f(t)\psi^*(\frac{t-b}{a})dt \quad \text{.....(4)}$$

$$= \int_{-\infty}^{+\infty} f(t)\psi^*{}_{a,b}(t)dt \,,$$

where * denotes complex conjugation and *C(a,b)* are the wavelet coefficients. *C(a,b)* is two-dimensional in the time-scale plane (*a,b*), where the term scale instead of frequency is used. Large-scale is for low frequency, and vice versa.

3.1.3. Properties of Wavelets

Cohen et. al. [48] and Daubechies [7] briefly introduced many types of wavelets, characteristics and performance of which vary based on their associated properties. Ovanesova and Suarez [44] stated a few of the most relevant properties as: (1) regularity; (2) support; (3) number of vanishing moments; and (4) symmetry which were briefly defined in the same study.

Since there are many mother wavelets available in this area, one has to decide which wavelet to use. Although most of the time this is determined by trial-and-error method, one can eliminate some of them by examining the properties, some of which were given above.

The wavelet selection criterion given by Ovanesova and Suarez [44] was adapted in this study for the proper wavelet selection. Consequently, bior 6.8 was selected as the most suitable (see Figure 3.2) for the purpose sought in this study. The selection criteria are summarized as follows:

- Ability to allow carrying out a fast wavelet transform (FWT),

- Satisfying symmetry and exact reconstruction of the analyzed signal,
- Regularity of the wavelet.

Figure 3.2 Biorthogonal wavelet: bior 6.8

Note that two graphs for the same wavelet were given above. The reason is that the one on the left is used for decomposition whereas the one on the right is for reconstruction.

To see the effects of different mother wavelets in the damage detection process, two additional ones were also selected for CWT. The first one was from db families which were developed by Daubechies [7] based on the solution of a dilation equation. The one adopted in this study, db7, is given in Figure 3.3.

The second was the Morlet wavelet which was also used by Hughes et.al.[39] because of its direct conversion capability between scale and frequency. This wavelet is illustrated in Figure 3.4.

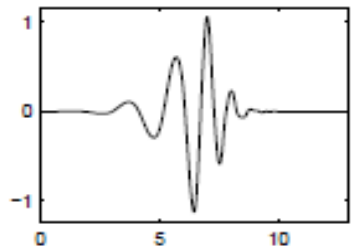

Figure 3.3 Daubechies family wavelet: db7

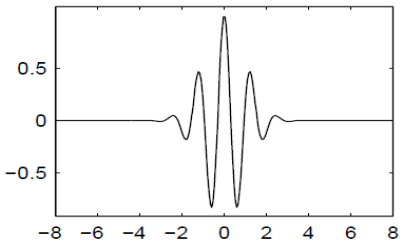

Figure 3.4 Morlet wavelet

3.2 Motivation for the Study

Substantial amount of vibration-based damage detection techniques and vast number of research studies have been conducted in the field. Almost every method for damage assessment has an inherent drawback. For example, processing temporal signals with traditional Fourier transform (FT) has some inherent incapability in identifying damages accurately. Gurley and Karem [49] reported that FT fails in presenting the time or space information and lacks the important characteristics that commonly observed in the signals measured from naturally-excited structures. Moreover, Doebling et. al. [1] addressed that FT is actually a data reduction process as a result of which information concerning the damage condition might be lost.

Farrar et. al. [50] summarized structural health monitoring studies that have appeared in the technical literature between 1996 and 2001. In this study, quite a lot different applications of FT on vibratory response data were investigated.

It was previously stated that wavelet transform (WT) can be thought of as an extension of FT with variable window location and size. This property of windows allowed signals to be represented by series expansion where each term is one of the basis wavelets multiplied by its magnitude [27]. When compared to FT which uses sine and cosine functions as bases, basis wavelets are local functions having scale (frequency) and position (time) as parameters of definition. This property makes WT capable of revealing aspects of data that other signal analysis techniques miss, like trends, breakdown points, discontinuities in higher derivatives, and self-similarity. Furthermore, because it affords a different view of data than those presented by traditional techniques, wavelet analysis can often compress or de-noise a signal without appreciable degradation [53].

With regards to the above mentioned issues, the goals of this study can be listed as follows:

- To compare the effectiveness of modal and wavelet analysis techniques on the damage detection of a cantilever beam with a cut introduced at various degrees of depth,
- To adapt the damage assessment index of wavelet packet energy rate index (WPERI) to CWT analysis results,
- To see the effect of different types of mother wavelets used in CWT for damage assessment of the same measurement data.

CHAPTER 4

EXPERIMENTAL SETUP

4.1 Test Setup

A rectangular cross-section cantilever beam, made from aluminum is shown in Figure 4.1. Its dimensions as well as the positions of the applied force and accelerometers are depicted in Figure 4.1. The cross-hatched part of the beam was clamped while the other end was free. The beam was hit vertically by an impact hammer which is depicted as F in Figure 4.1.

A data acquisition unit of Brüel & Kjær type 3560C was used for the measurement of both impulse forcing and acceleration response of the beam. It allows up to 17 input channels and a control unit to be connected. Software programme Pulse LabShop v.10.1.0.15 was used for the modal analysis of the measured response data. The software supports both classical and operational modal analysis. It also supports graphically driven test, linking the measurement directly to the on-screen test object geometry. The picture of the measurement setup is illustrated in Figure 4.2.

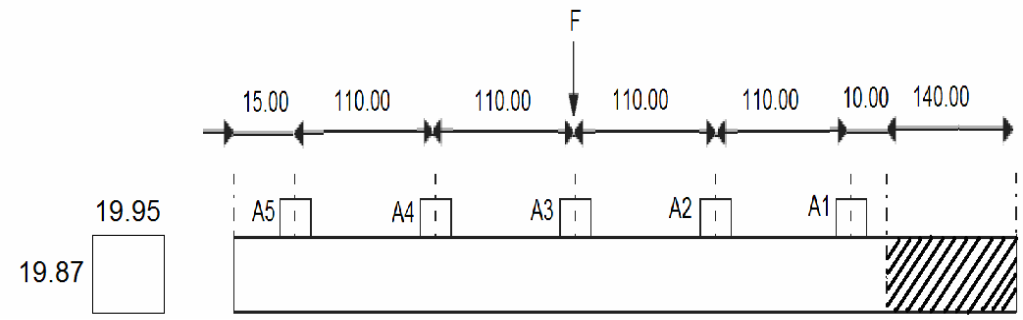

Figure 4.1. Schematic drawing of the test beam (All dimensions are in mm)

Upper frequency for the measurement was set to 1.6kHz. In order to smooth and reduce the measurement noise, data collection at each measurement point was repeated 5 times and then, the data was averaged. The forcing was always applied at the place shown as F in Figure 4.1 while the accelerometer was moved along the beam from position A1 to A5. Exponential windowing was applied to the measurement data.

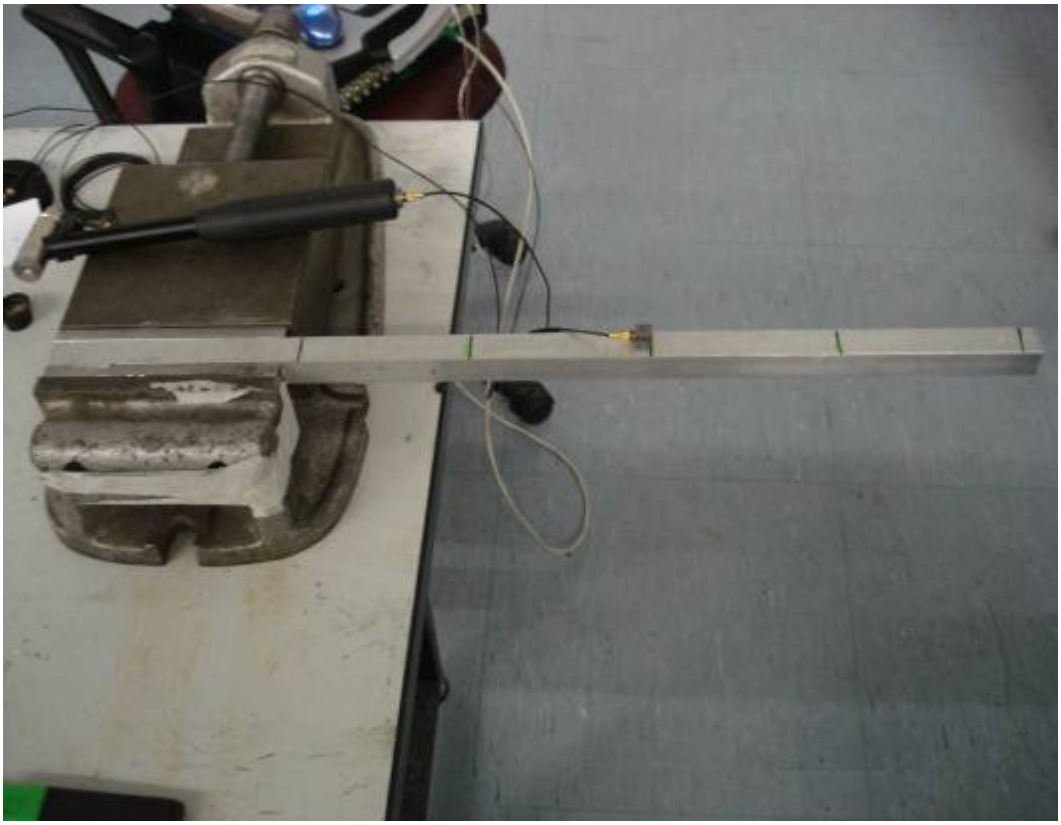

Figure 4.2. Experimental setup

For each measurement 4096 data points were collected and sampling ratio was 2.56. Impulsive loading was supplied by an impulse hammer and accelerometer used was Brüel & Kjær 8206 and 4507, respectively. Impact hammer was used together with type 2646 Deltatron conditioning amplifier which supported automatic DC offset compensation, detection including out-of-band frequencies and overload detection showing incorrect conditioning.

Some of the important features of the impact hammer that was used are;

- 22.7 mV/N sensitivity,
- Full scale range of 220 N,
- Upper frequency limit of 20 kHz.

Three different damage scenarios were tested on the beam. The position and geometry of the damage was given in Figure 4.3. Dimensions of the cut for different damage levels, which were measured using a micrometer, were also summarized in Table 4.1.

Table 4.1 Dimensions of the cut for different damage cases

Damage Case	a (mm)	b (mm)
Undamaged	0	0
Case 1	1.64	1.64
Case 2	7.80	1.64
Case 3	12.06	1.64

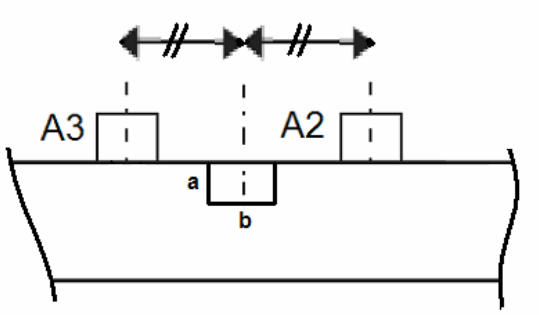

Figure 4.3 Section of the test beam

In order to assure that measurement setup was established correctly and data collected was accurate, cantilever beam from the test setup was modeled and modal analyses were performed by finite element model analysis software ANSYS ®. Afterwards, the beam was excited by an impulse hammer and each time transverse vibrational data from measurement points A1 to A5 was collected with an accelerometer. Measurement data was then processed by Pulse LabShop v.10.1.0.15 software programme for modal information extraction of the test beam. A picture of the Pulse analysis software while performing measurements is given in Figure 4.4.

The geometry, boundary conditions and material properties were supplied to ANSYS ® software for the modal analysis. The first three mode shapes obtained from the ANSYS ® software analysis are given in Figures 4.5, 4.6, and 4.7, respectively.

The first three natural frequencies which were obtained both from the measurements and through the ANSYS ® software were given in Table 4.2.

The differences of the experimental and analytical results were acceptable which indicated that measurement setup was accurate enough. However, there can be some small differences which can be due to the followings;

- Different algorithms of ANSYS ® and Pulse LabShop v.10.1.0.15 software analysis programmes which were used for the modal analysis,
- Inherent noise from the analyzer,
- Effect of the test setup to the measurement.

The frequency response function (FRF) of the undamaged beam was also obtained from the measurement data, the graph of which was given in Figure 4.8.

Both graphs of the measurement data and the curve fit to the same measurement data were given in the same figure.

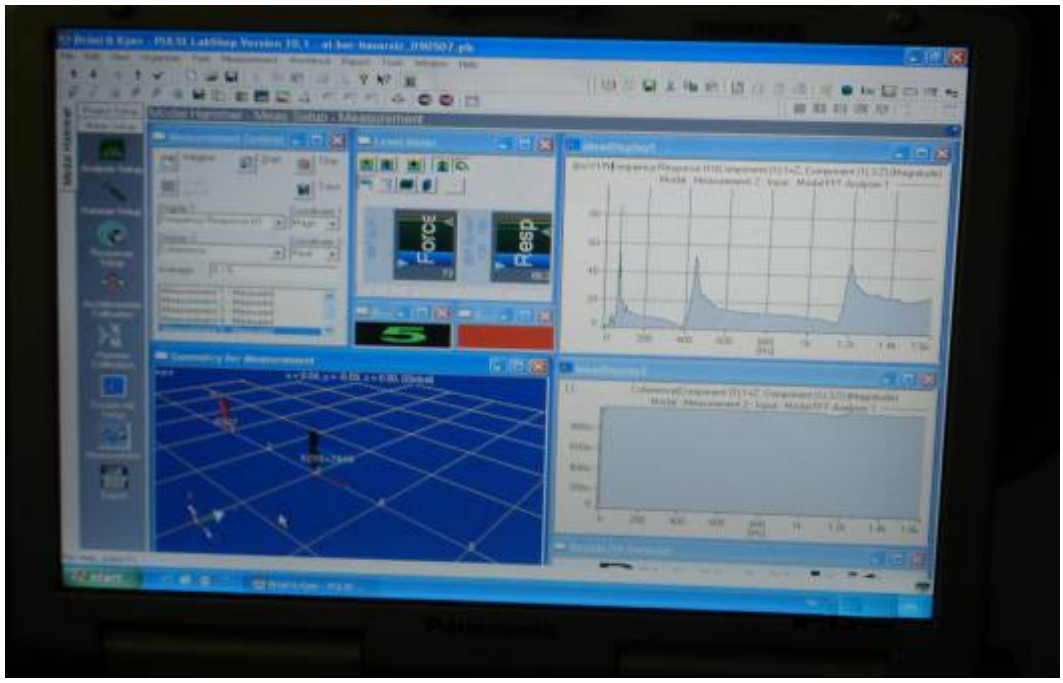

Figure 4.4 A view from Pulse LabShop v.10.1.0.15

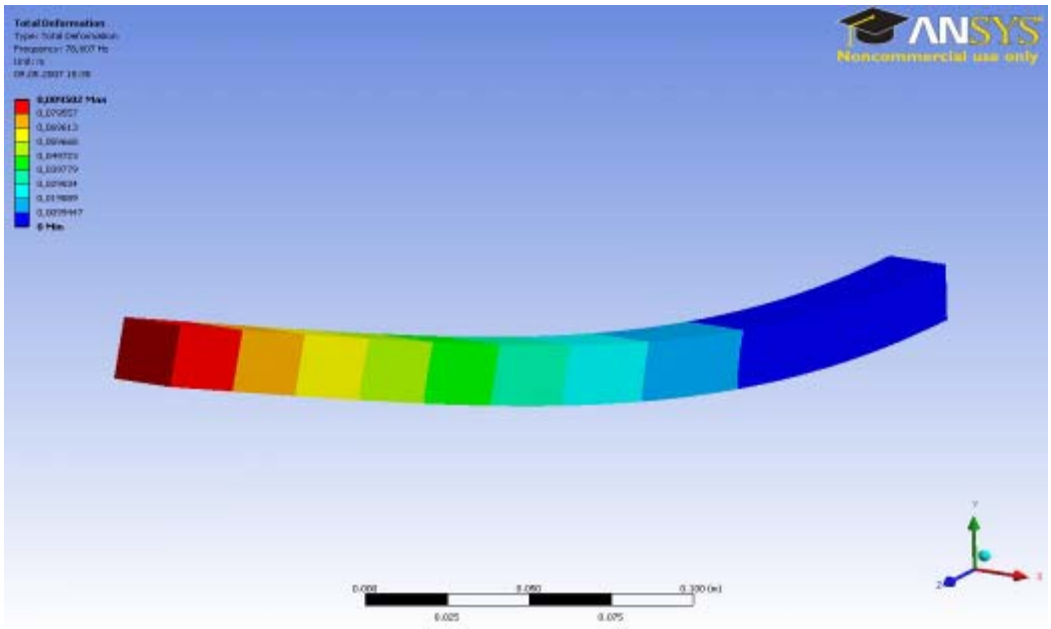

Figure 4.5 Mode shape 1 of undamaged beam obtained via ANSYS ® software

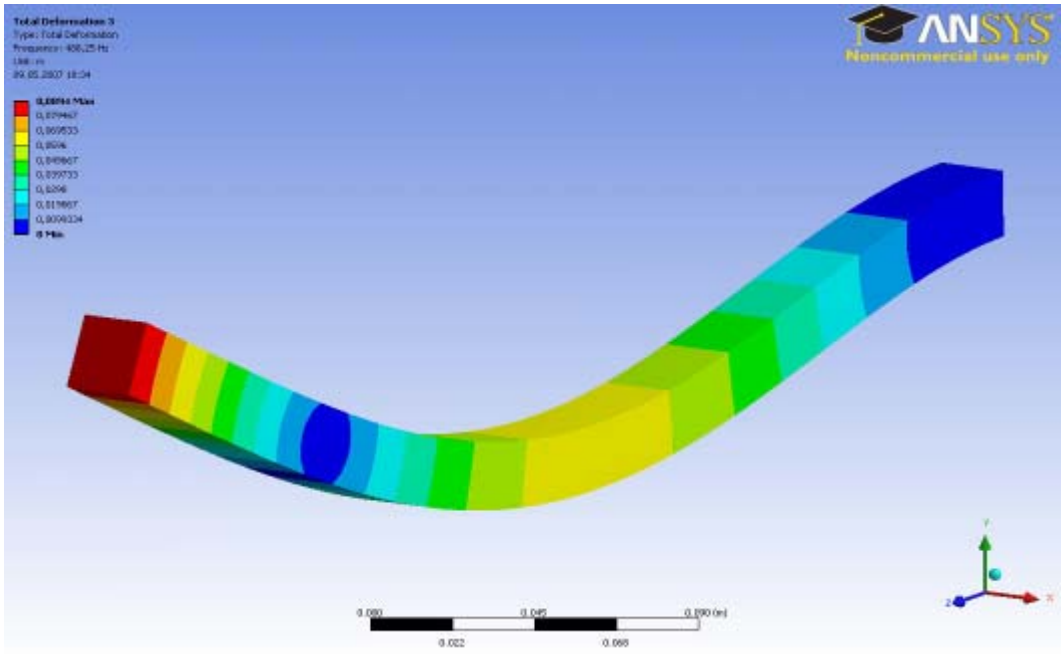

Figure 4.6 Mode shape 2 of undamaged beam obtained via ANSYS ® software

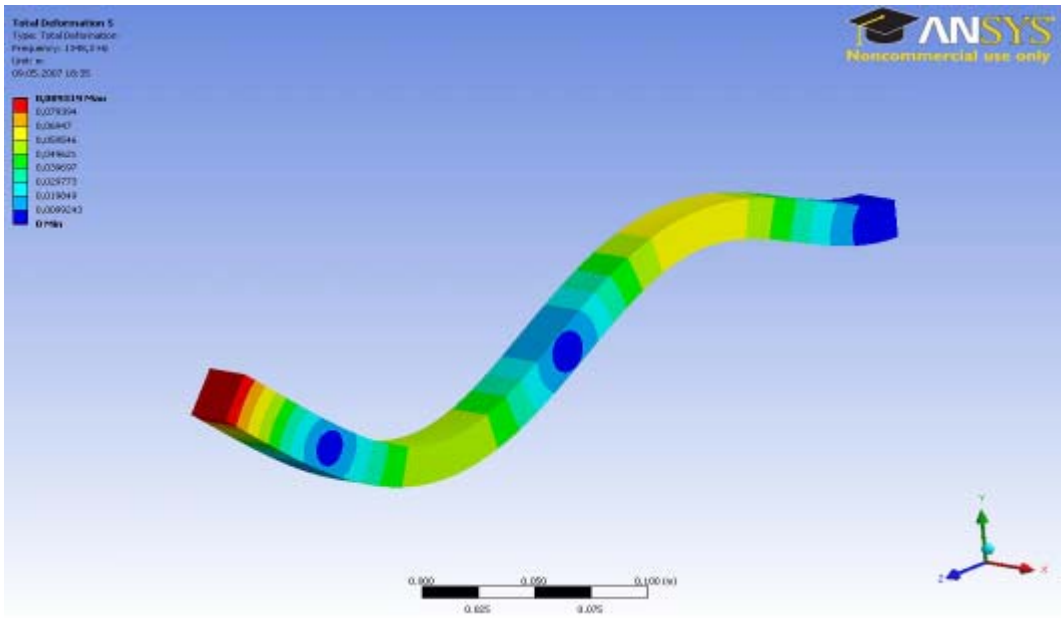

Figure 4.7 Mode shape 3 of undamaged beam obtained via ANSYS ® software

Figure 4.8 Frequency Response Function (FRF) of the Undamaged Beam

Table 4.2 First three natural frequencies of the undamaged test beam

Natural Frequency (Hz)	ANSYS ® software	Measurement Data
First	67.5	65.3
Second	427.8	441
Third	1198.5	1190

4.2 Damaging the Beam and Data Collection

A saw tooth was used to introduce damage to the beam. The damage was given at the position as shown in Figure 4.3 and the damage level was increased step by step according to the values given in Table 4.1. Data collection for all the damage cases as well as for each measurement point was done according to the procedure given below;

1. Cut the beam at the specified location,
2. Measure the dimensions of the cut,
3. Hit the beam at position as shown in Figure 4.1,
4. Record both the forcing and transverse response of the beam at position A1,
5. Repeat steps 3 and 4 for 5 times and calculate the average,
6. Repeat steps 3, 4 and 5 for measurement points A2, A3, A4, and A5.

Time history of forcing and time response at measurement point A2 of undamaged beam are given in Figures 4.9 and 4.10, respectively, as an example.

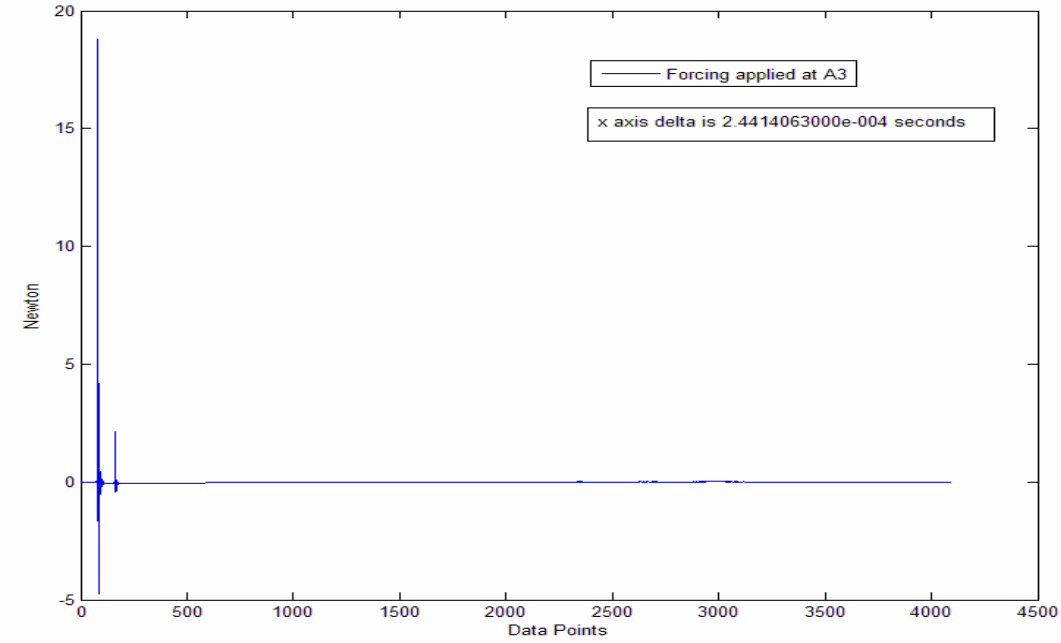

Figure 4.9 Time history of forcing applied at A3 for undamaged case

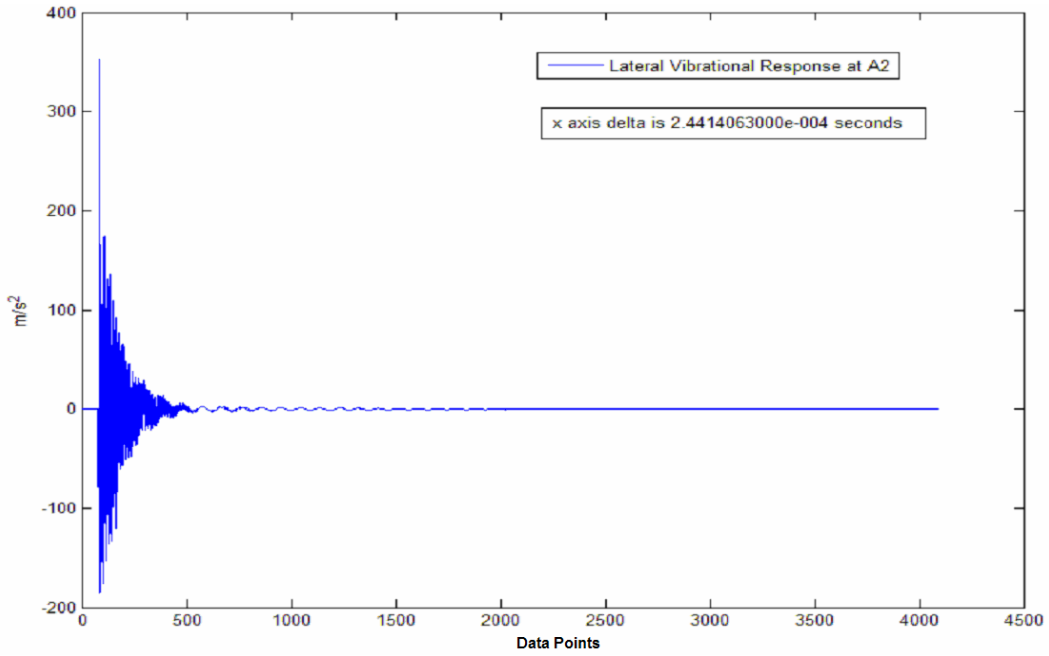

Figure 4.10 Time response of point A2 for undamaged case

4.3 Processing the Measurement Data

4.3.1 Modal Analysis

After collection of data from each measurement point for different damage cases it was supplied to the Pulse LabShop v.10.1.0.15 software programme for modal analysis. Some natural frequencies of the beam for four different damage cases were obtained. These cases were tabulated in Table 4.3.

It was noticed that for all damage cases some of the natural frequencies were quite close in value. This was something expected since some lateral modes were also excited. When the mode shapes which were saved in the movie format were inspected, the modes which were not vibrating in the vertical plane were eliminated. In addition, some modes vibrating in vertical plane were not fitting to any of first three mode shapes of the undamaged beam Thus, Table 4.4 was obtained after the aforementioned filtering.

The mode shapes that were calculated from the measurement results were not quite smooth since only five measurement points were utilized for data collection. The first three mode shapes obtained from the measurements were supplied to Microsoft Excel ® software. Fifth order curves were fit to the measured mode shapes since curve fitting tool of the software allowed at most a fifth order curve fit. The same procedure was repeated for all damage cases. The first three mode shapes obtained from the measurements of all damage cases were given in Figure 4.31, Figure 4.33, and Figure 4.35, respectively. Moreover, first three mode shapes obtained by curve fitting to the measurement data were also shown in Figure 4.32, Figure 4.34, and Figure 4.36, respectively. The zero value of the axis along the beam length of Figures 4.31 to 4.36 does not correspond to the fixed end of the beam but it is the point 10 mm away from the fixed end.

Furthermore, equations resembling the first three mode shapes obtained via curve fitting were given in Table 4.5-7, respectively for different damage cases.

In addition, FRFs for all the damage cases were estimated using the same modal analysis software. For each measurement point and also for all the damage cases FRFs were estimated. These were displayed in Figure 4.11 to Figure 4.30.

Table 4.3 First Several Natural Frequencies of the beam for different damage levels

NATURAL FREQUENCY	UNDAMAGED [Hz]	CASE 1 [Hz]	CASE 2 [Hz]	CASE 3 [Hz]
1	65.3	40.1 80.6 87	40.9 81.8 86	35.7 76.6 84
2	441	434 444 511	419 426 424	387 401
3	1190	1200	1180	1140

Table 4.4 First Three Natural Frequencies of the beam for different damage levels

NATURAL FREQUENCY	UNDAMAGED [Hz]	CASE 1 [Hz]	CASE 2 [Hz]	CASE 3 [Hz]
1	65.3	40.1	40.9	35.7
2	441	434	419	387
3	1190	1200	1180	1140

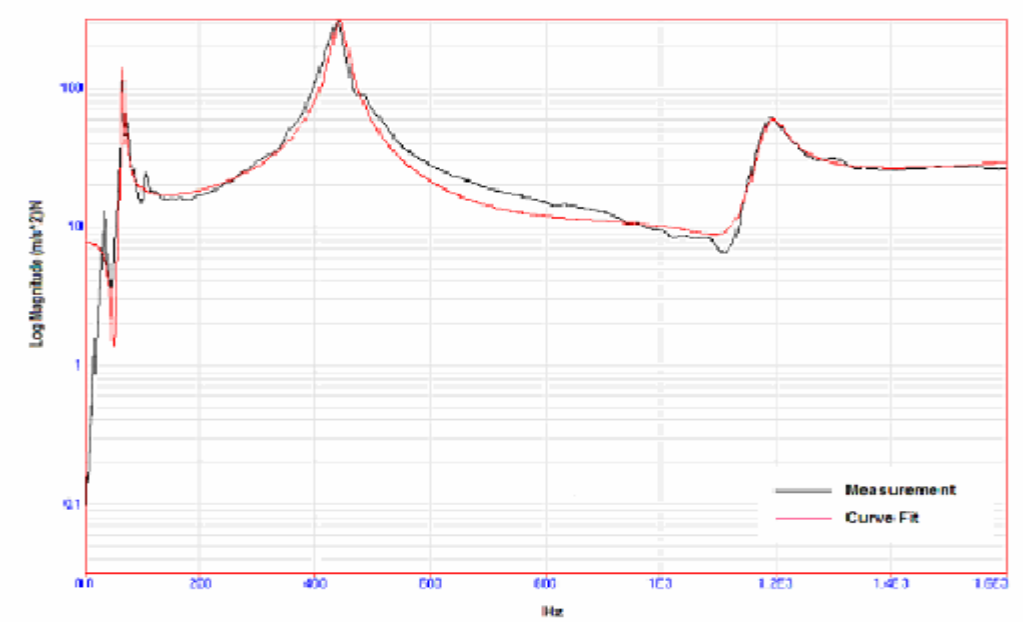

Figure 4.11 FRF calculated from response of point A5, Undamaged case

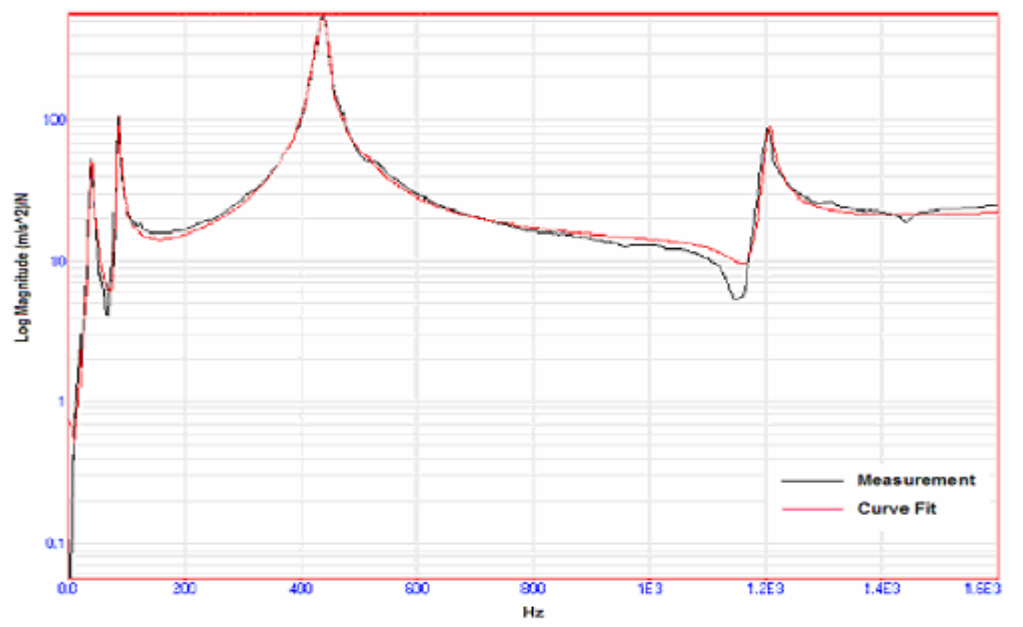

Figure 4.12 FRF calculated from response of point A5, Damage case 1

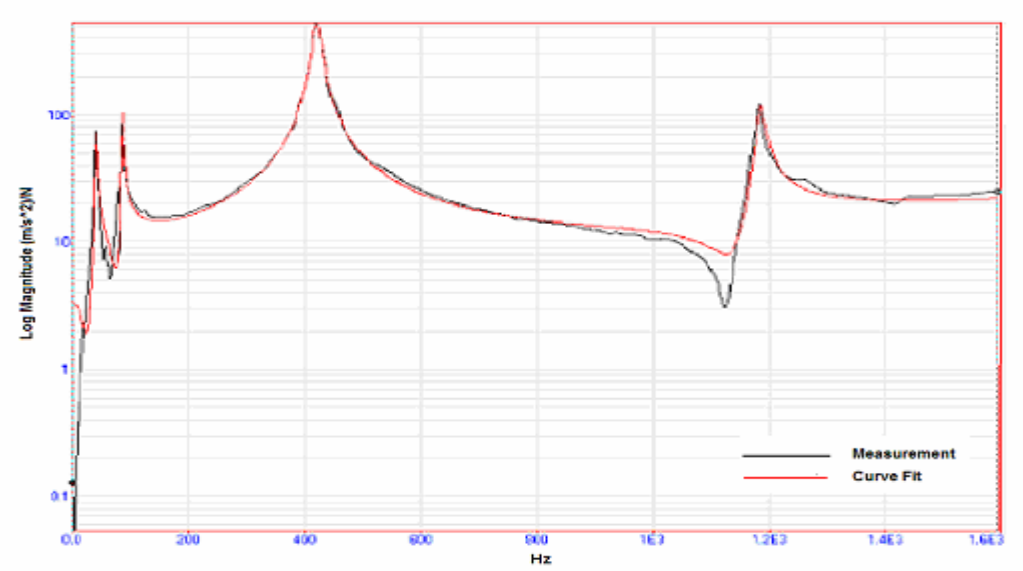

Figure 4.13 FRF calculated from response of point A5, Damage case 2

Figure 4.14 FRF calculated from response of point A5, Damage case 3

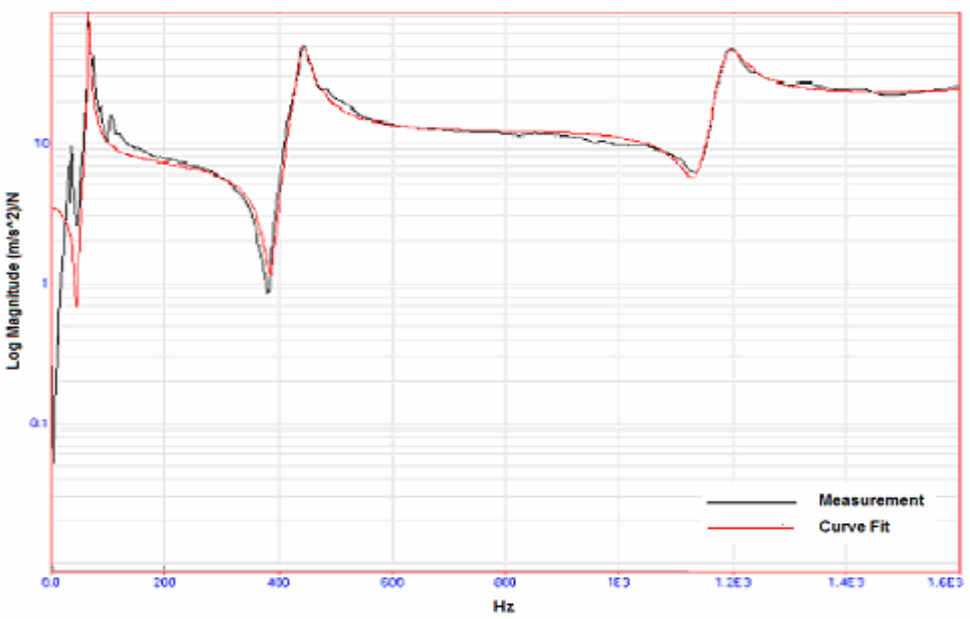

Figure 4.15 FRF calculated from response of point A4, Undamaged case

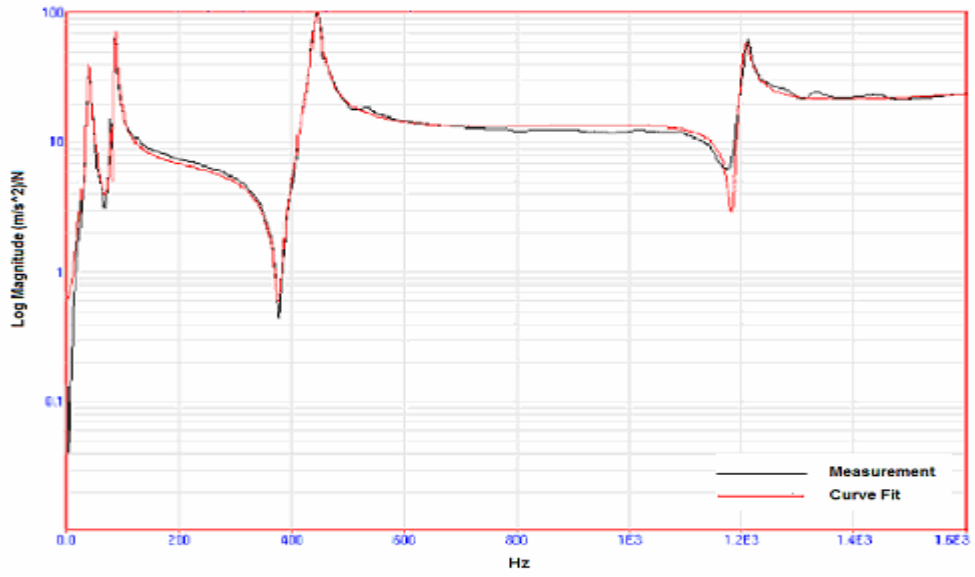

Figure 4.16 FRF calculated from response of point A4, Damage case 1

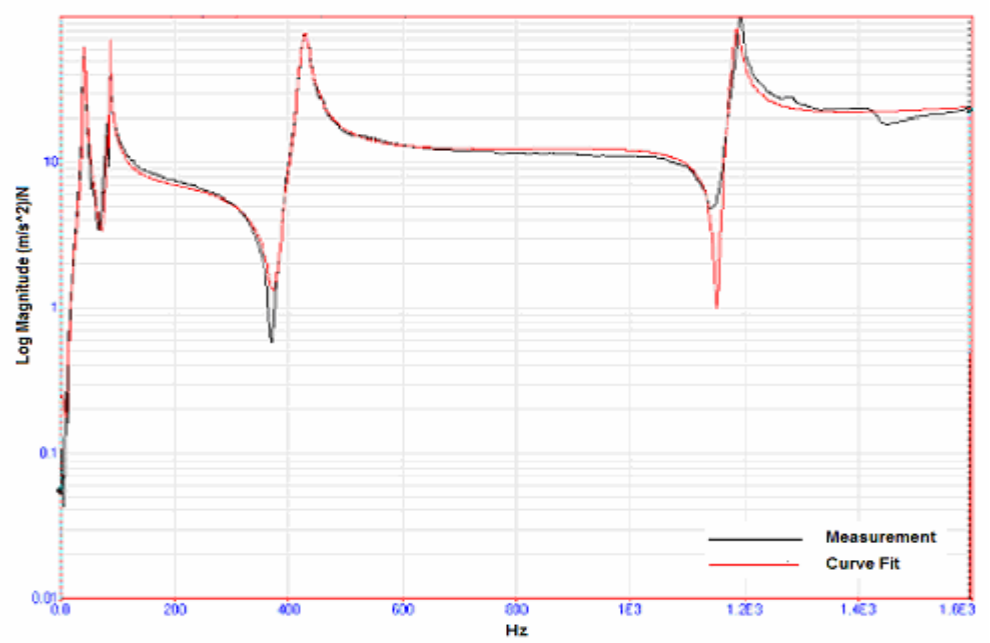

Figure 4.17 FRF calculated from response of point A4, Damage case 2

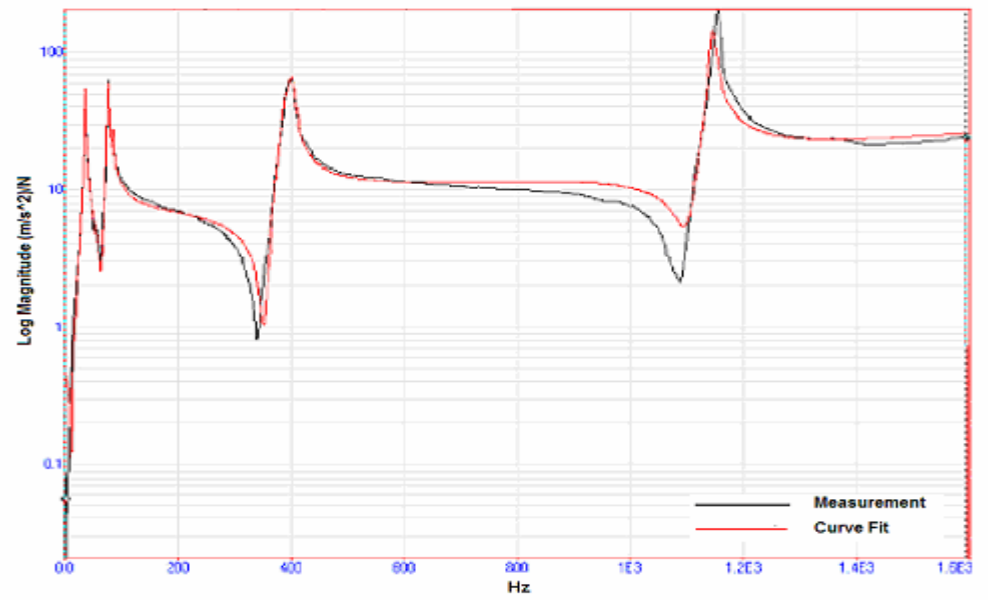

Figure 4.18 FRF calculated from response of point A4, Damage case 3

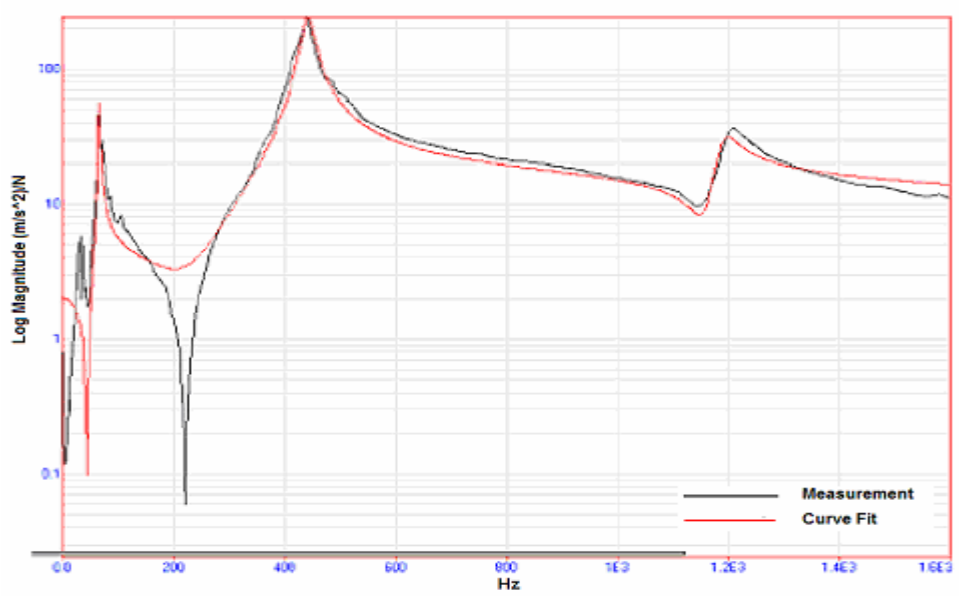

Figure 4.19 FRF calculated from response of point A3, Undamaged case

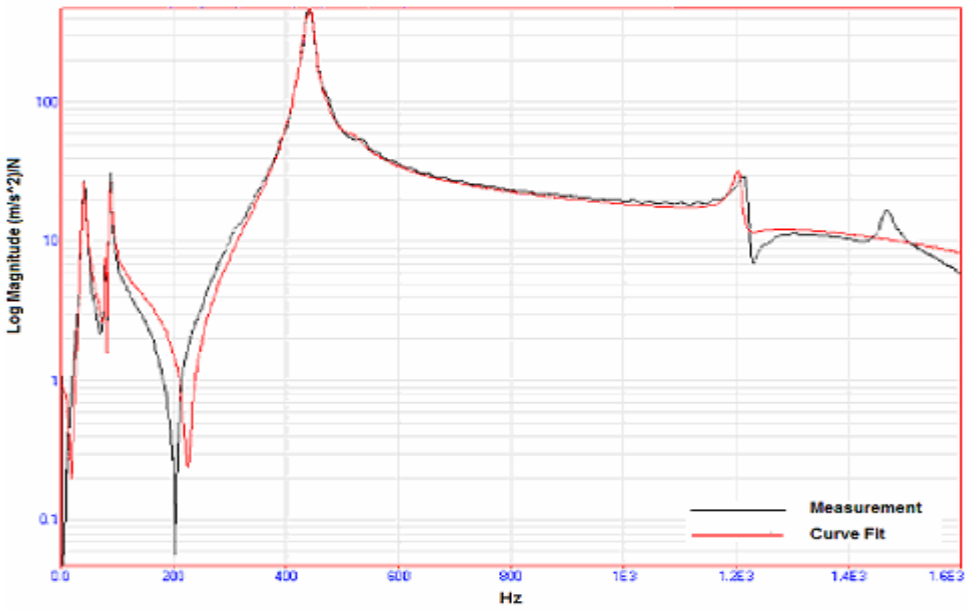

Figure 4.20 FRF calculated from response of point A3, Damage case 1

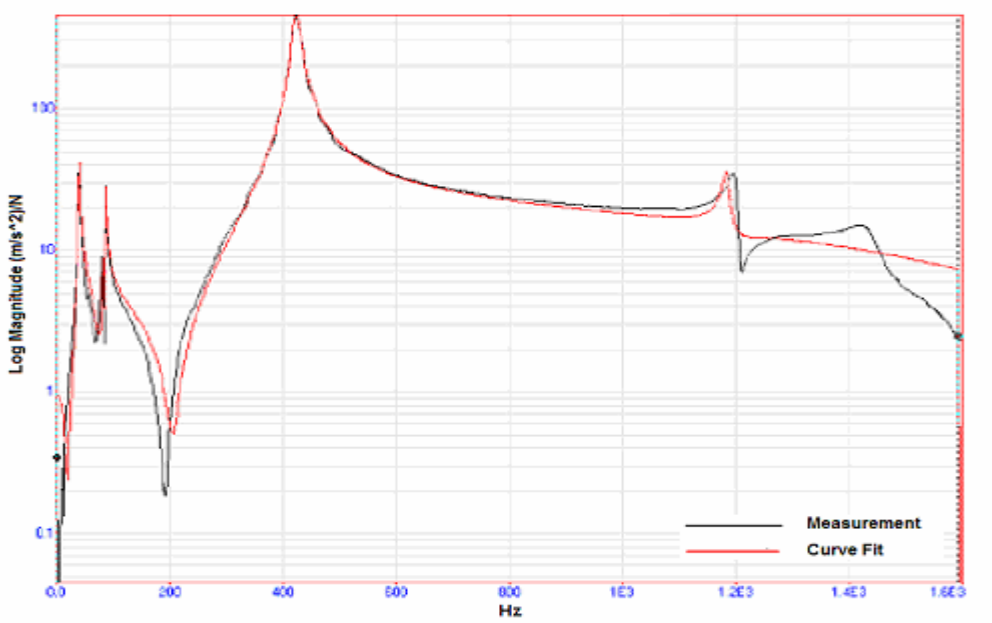

Figure 4.21 FRF calculated from response of point A3, Damage case 2

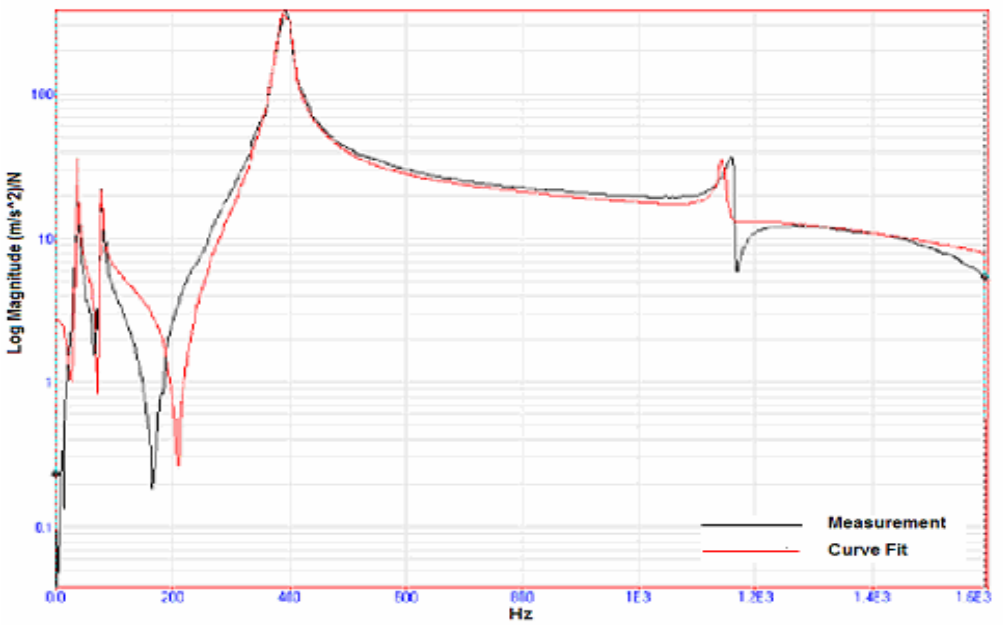

Figure 4.22 FRF calculated from response of point A3, Damage case 3

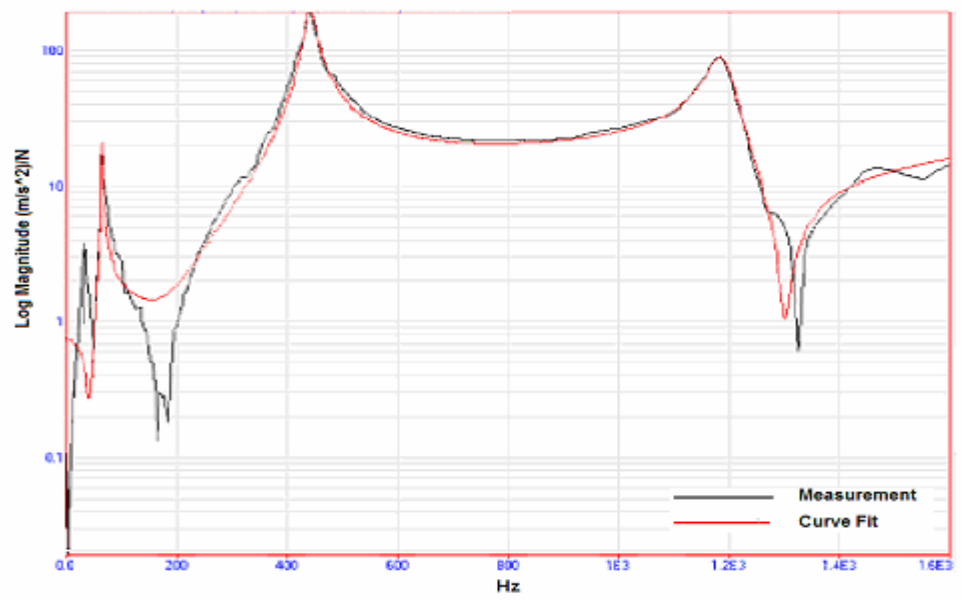

Figure 4.23 FRF calculated from response of point A2, Undamaged case

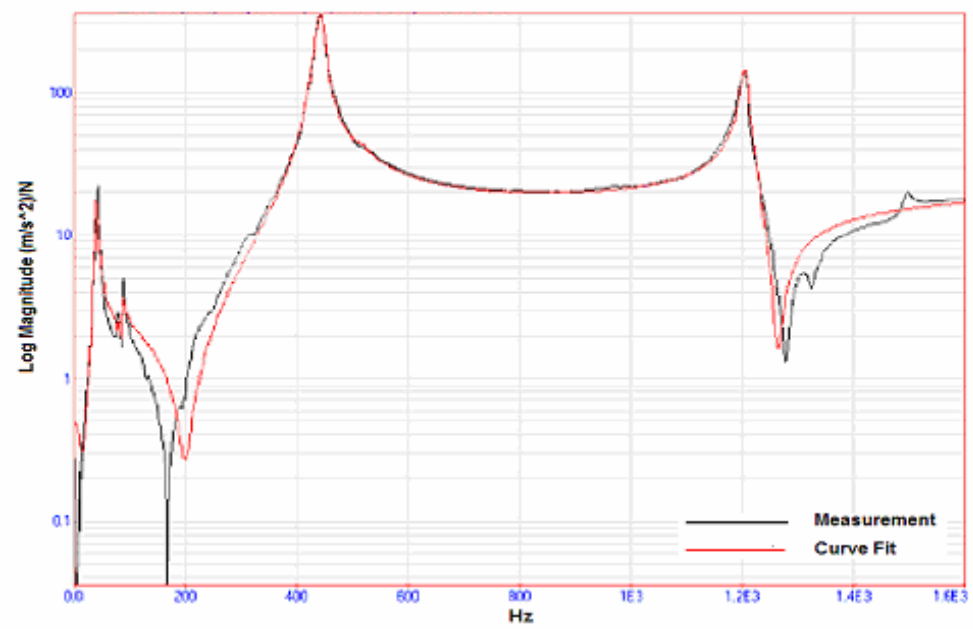

Figure 4.24 FRF calculated from response of Point A2, Damage case 1

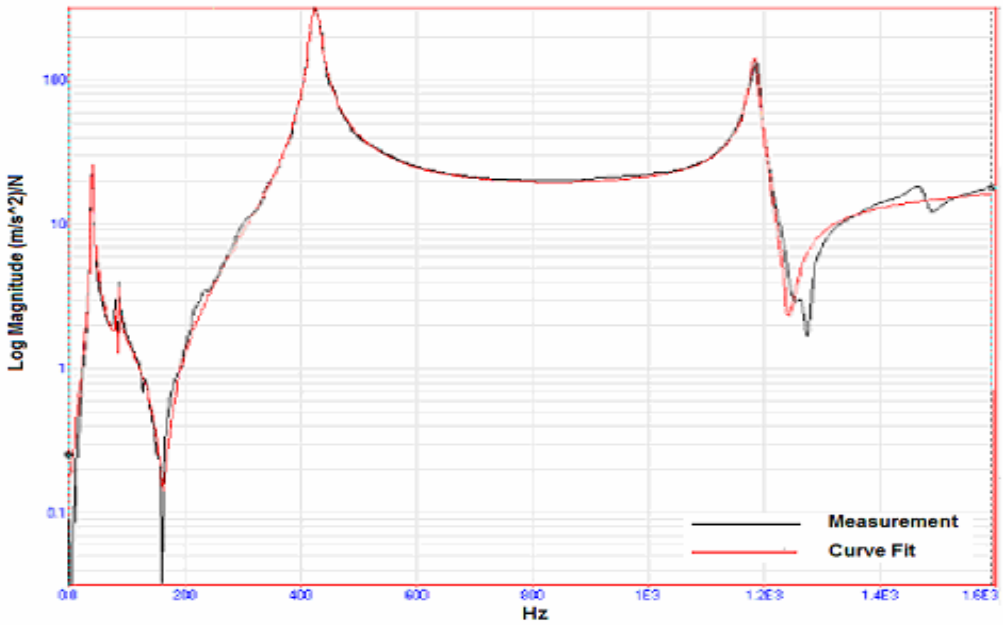

Figure 4.25 FRF calculated from response of point A2, Damage case 2

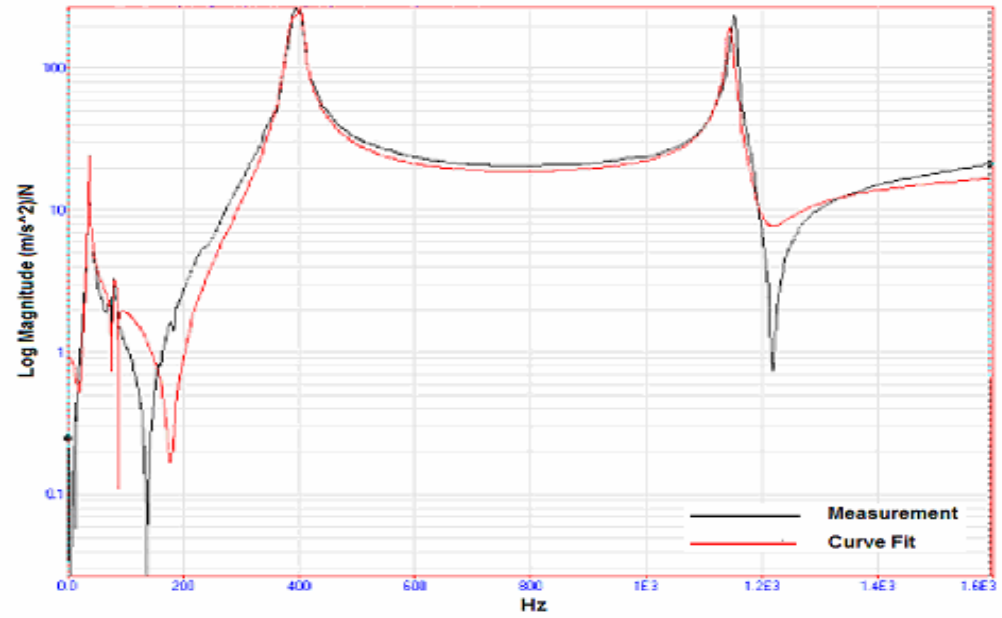

Figure 4.26 FRF calculated from response of point A2, Damage case 3

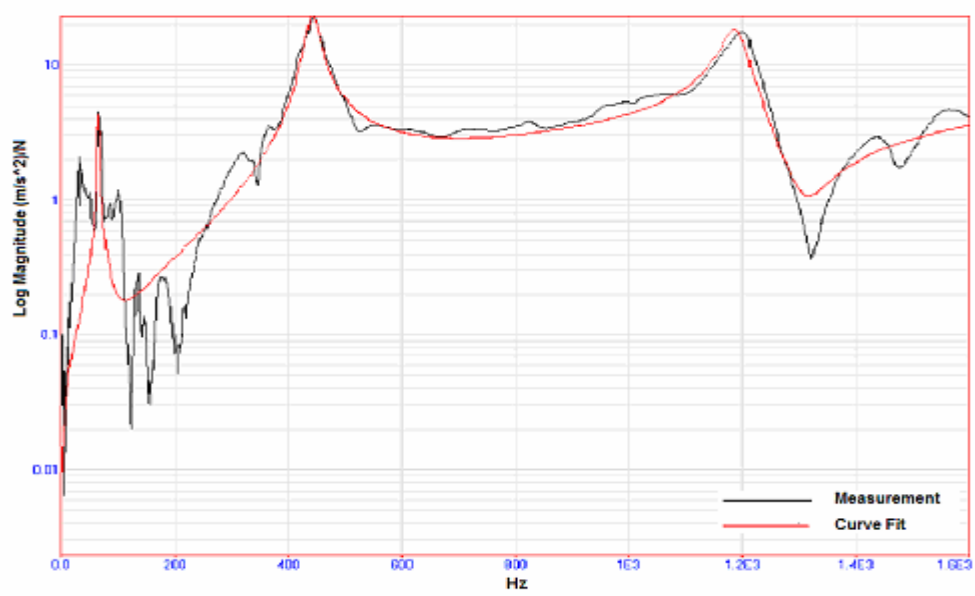

Figure 4.27 FRF calculated from response of point A1, Undamaged case

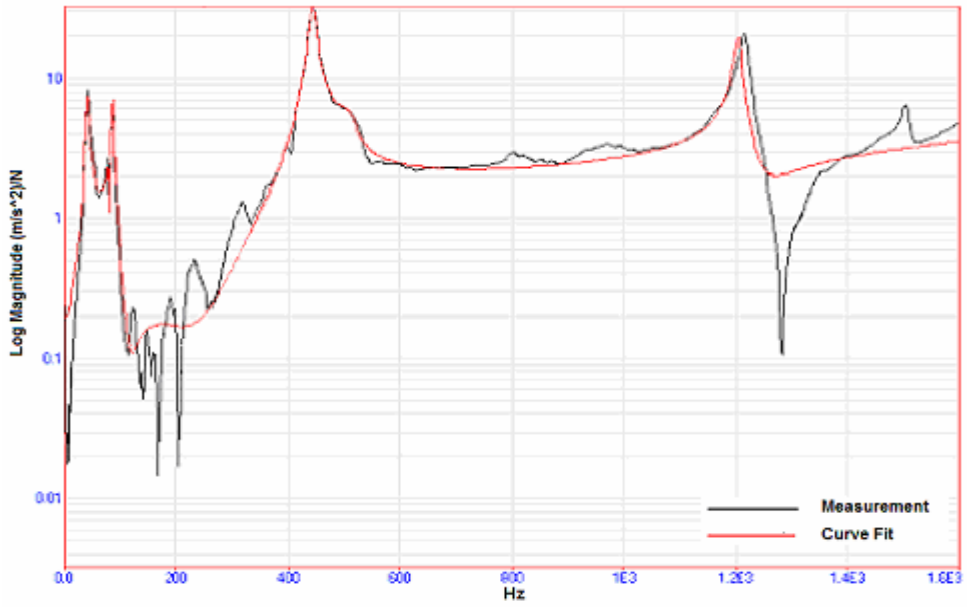

Figure 4.28 FRF calculated from response of point A1, Damage case 1

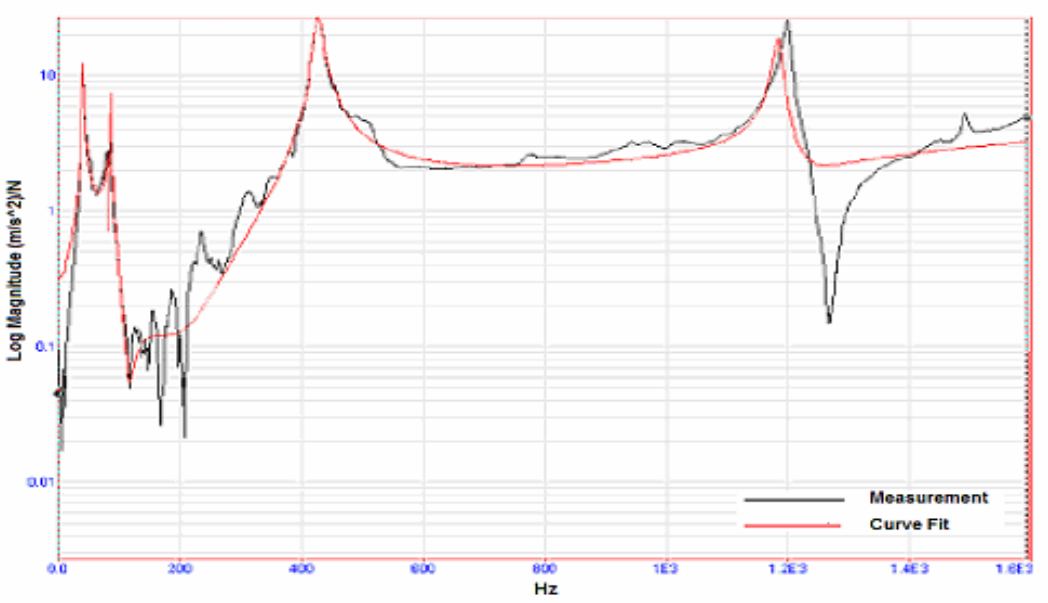

Figure 4.29 FRF calculated from response of point A1, Damage case 2

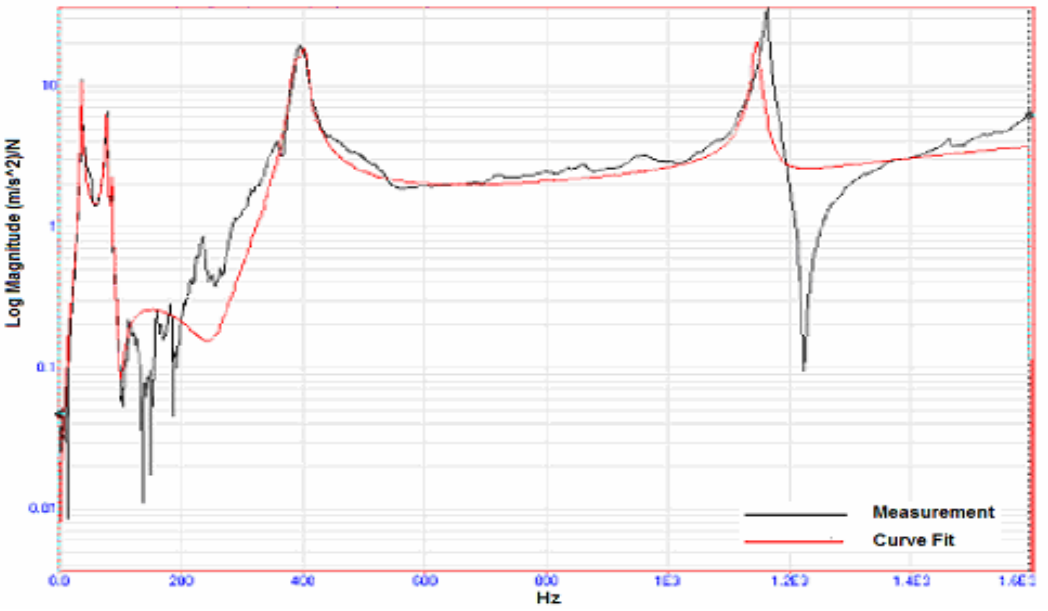

Figure 4.30 FRF calculated from response of point A1, Damage case 3

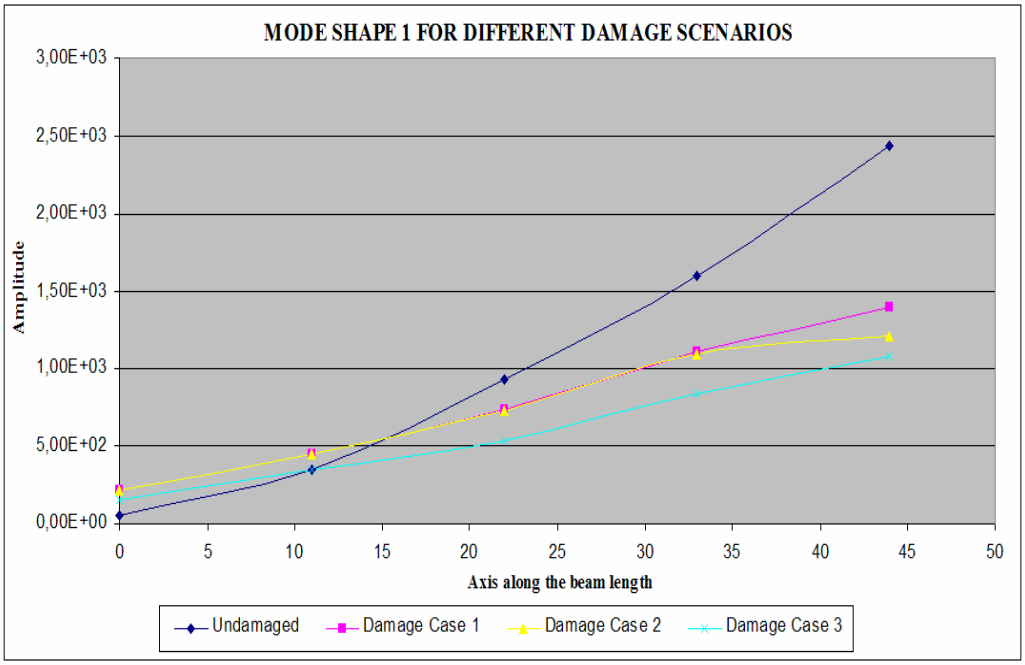

Figure 4.31 Mode shape 1 obtained from measurements of all damage cases

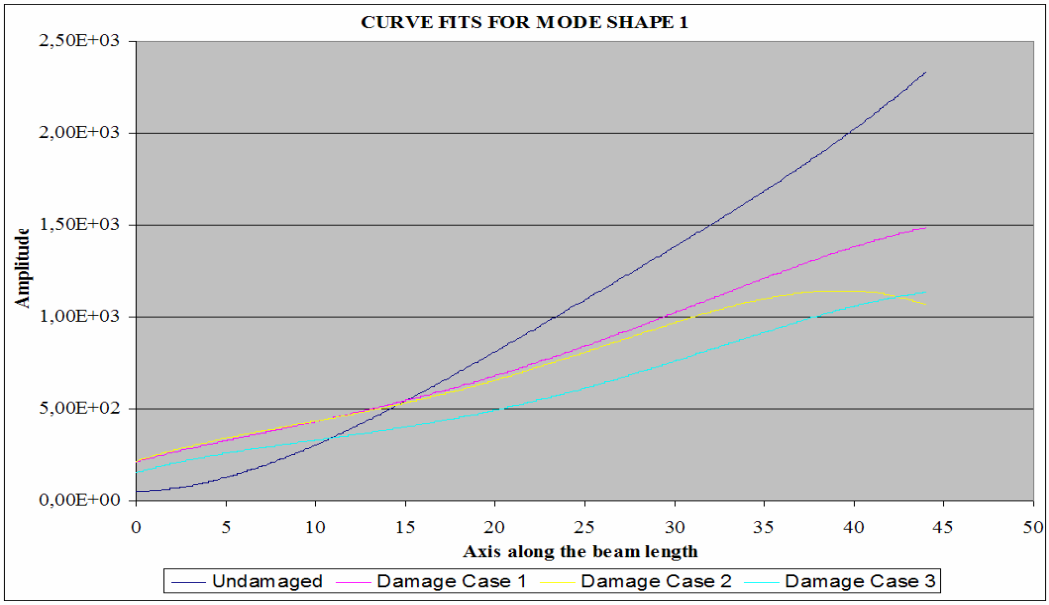

Figure 4.32 Mode shape 1 obtained via curve fitting to all damage cases

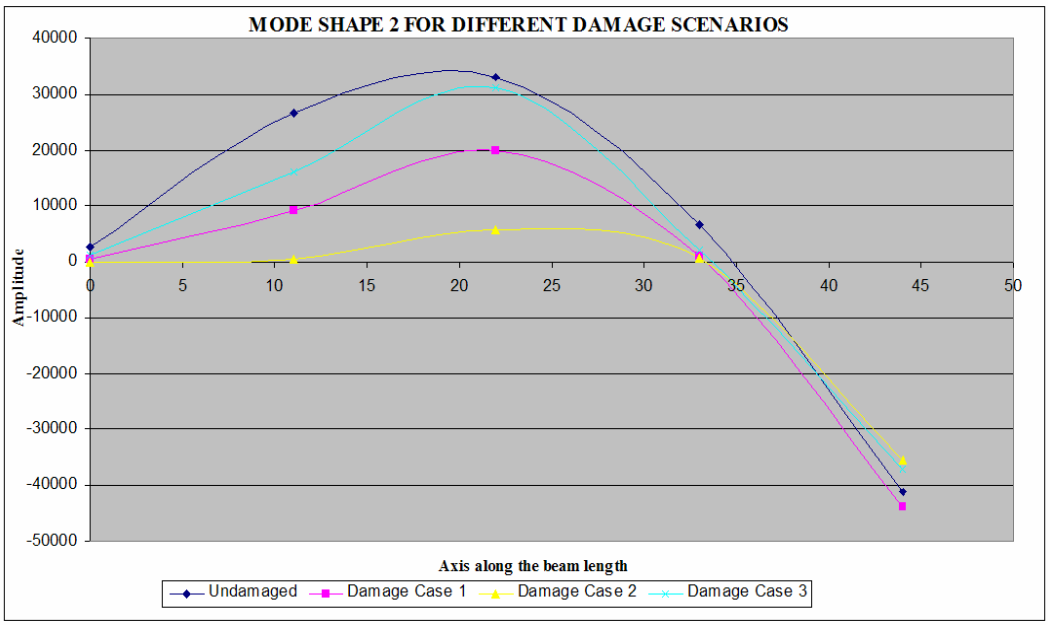

Figure 4.33 Mode shape 2 obtained from measurements of all damage cases

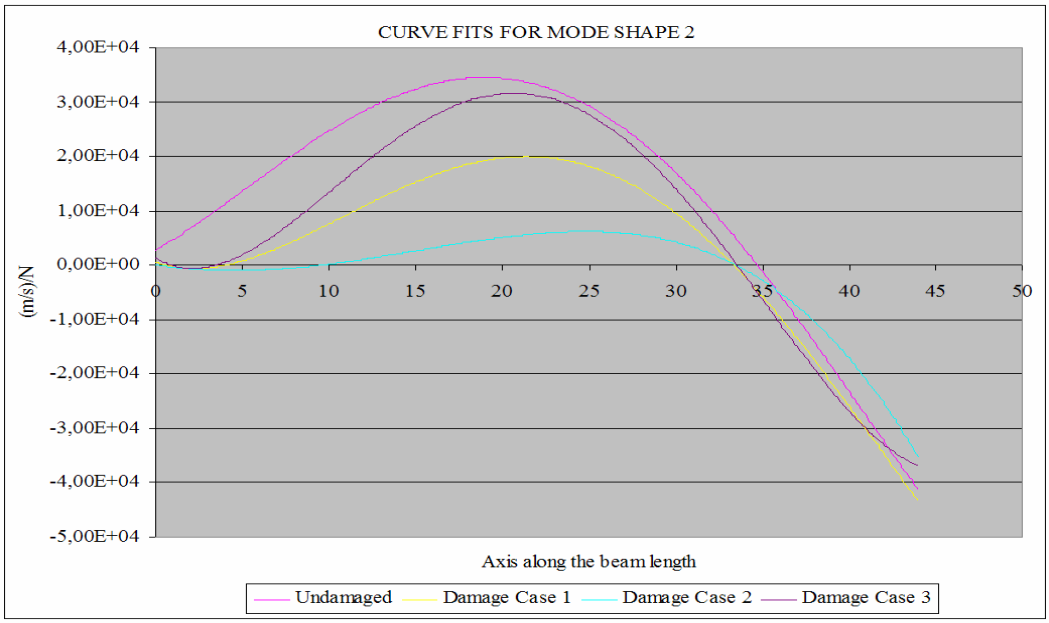

Figure 4.34 Mode shape 2 obtained via curve fitting to all damage cases

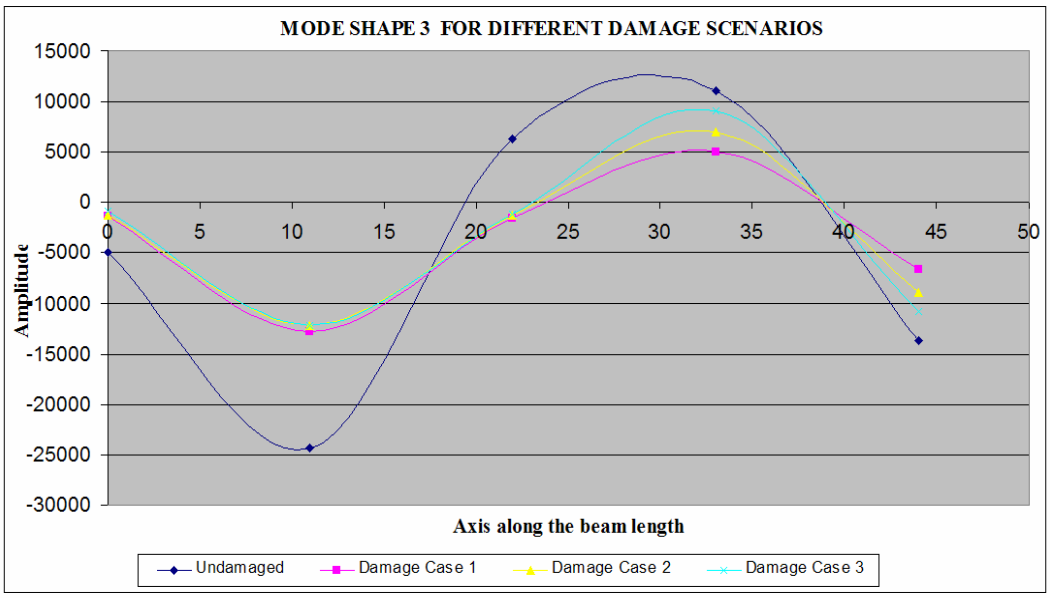

Figure 4.35 Mode shape 3 obtained from measurements of all damage cases

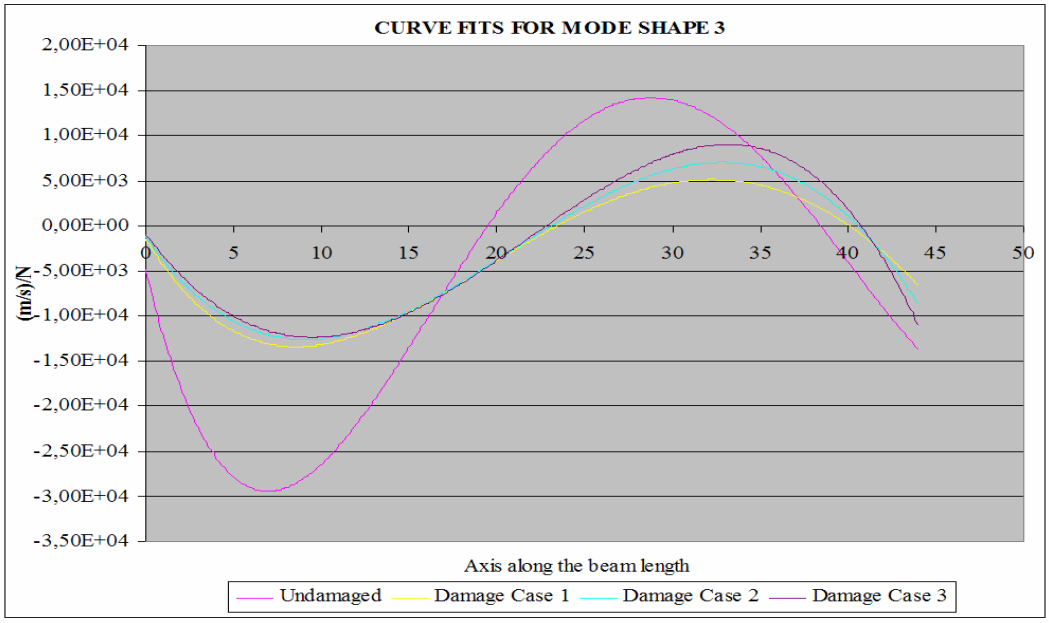

Figure 4.36 Mode shape 3 obtained via curve fitting to all damage cases

Table 4.5 Equations obtained via curve fitting for mode shape 1 for all damage cases

Mode Shape 1	
Undamaged Case	$y(x) = 0.001x^4 - 0.08x^3 + 3.1x^2 - 1.6x + 49.7$
Damage Case 1	$y(x) = -0.001x^4 + 0.05x^3 - 0.8x^2 + 26.2x + 211.6$
Damage Case 2	$y(x) = -0.001x^4 + 0.09x^3 - 1.8x^2 + 32.4x + 213.9$
Damage Case 3	$y(x) = -0.001x^4 + 0.07x^3 - 1.6x^2 + 27.5x + 152.2$

Table 4.6 Equations obtained via curve fitting for mode shape 2 for all damage cases

Mode Shape 2	
Undamaged Case	$y(x) = 0.078x^4 - 7.14x^3 + 98.1x^2 - 1846.3x + 2742.5$
Damage Case 1	$y(x) = 0.100x^4 - 10.54x^3 + 271.1x^2 - 1048.1x + 501.4$
Damage Case 2	$y(x) = -0.017x^4 - 0.76x^3 + 58.3x^2 - 474.7x + 7.4$
Damage Case 3	$y(x) = 0.223x^4 - 20.26x^3 + 480.8x^2 - 1781.8x + 1183.8$

Table 4.7 Equations obtained via curve fitting for mode shape 3 for all damage cases

Mode Shape 3	
Undamaged Case	$y(x) = 0.207x^4 - 23.22x^3 + 798.7x^2 - 8025.8x - 4908.1$
Damage Case 1	$y(x) = 0.038x^4 - 5.91x^3 + 255.6x^2 + 3173.8x - 1463.6$
Damage Case 2	$y(x) = 0.008x^4 - 3.59x^3 + 201.8x^2 - 2794.6x - 1216.1$
Damage Case 3	$y(x) = -0.017x^4 - 1.76x^3 + 164.9x^2 - 2600.2x - 890.9$

4.3.2 Wavelet Analysis

The feasibility of applying the WPT to the vibration signals was investigated by Yen and Lin [51]. The authors defined wavelet packet node energy index and concluded that the node energy representation could be used for signal feature classification. Han et. al. [3] also proposed the wavelet packet energy index to identify the locations and severity of damage. For this purpose, the signal energy E_f at j level was defined as

$$E_{f_j} = \int_{-\infty}^{+\infty} f^2(t)dt = \sum_{m=1}^{2^j}\sum_{n=1}^{2^j}\int_{-\infty}^{+\infty} f_j^m(t) f_j^n(t)dt. \quad \text{.....(4)}$$

$$E_{f_j^i} = \sum_{i=1}^{2^j} E_{f_j^i}, \quad \text{.....(5)}$$

which is the simplification of (4) and $E_{f_j^i}$ was considered as the energy stored in the component signal $f_j^i(t)$.

However, in their study approach by Tsai et. al. [52] was followed with some modifications. Squared wavelet coefficients were normalized uniformly to obtain the energy expression:

$$\bar{E} = \frac{1}{m \times n} \sum_{i=0}^{m-1} \sum_{j=0}^{n-1} \left| C_{ij} \right|^2 \quad \text{.....(6)}$$

where C_{ij} stands for the wavelet coefficients of each section, m representing the interval on the time axis, and n the interval on the scale.

Instead of the expression (6) the following equation was used for the energy calculations of the measurement signals in this study:

$$E(j) = \sum_{i=1}^{m} \left| C_{ji} \right|^2 \quad \text{.....(7)}$$

where $E(j)$ was defined as the energy of the signal stored in the j^{th} scale of the CWT. It should be noted that the total energy of the measured signal is the summation of the energies at all the scales of CWT.

$$E = \sum_{j=1}^{n} E(j) \quad \text{.....(8)}$$

In equations (7) and (8), m was similarly used for the interval on the time axis, and n was used for the interval on the scale.

The continuous wavelet transform of the measured signals was accomplished by MATLAB R2006a ® wavelet4 toolbox [53]. Both acceleration signals from each measurement points and the mode shape data obtained through curve fitting to measurement results were processed via CWT tool of the wavelet toolbox of MATLAB R2006a ®. Table 4.8 summarizes which mother wavelet with the shown scale number was applied to which data set for calculation of coefficients of CWT process.

The force applied for data collection from each measurement point was different for each data set since only one accelerometer was used each time to record the response of the beam. Thus, amplitude of the response was affected by changes in the impulsive excitation. In order to eliminate the effect of forcing from the response data, energy of the forcing signal was also calculated with the same procedure applied to the response data. Then, the energy of the response signal was divided to the energy of the corresponding forcing signal. This normalization process was carried out scale by scale i.e., energies in the same scale numbers were divided.

Wang and Deng [37] state that spatially distributed signals can also be equally analyzed with wavelets, although wavelets are usually used for signal analysis in the time domain,. This can be done by simply replacing time coordinate with a spatial coordinate of interest.

In the light of the above argument, coefficients of CWT of the first three mode shapes were calculated [53].

In this case the normalization of the signal energy was not necessary since mode shapes were not excitation dependent. Also, the total energy made up of all the energies of each separate scale at data points were calculated instead of separately calculating the scale wise energies. It was anticipated that changes in the total energy of data points along the beam length could reveal the damage location more easily.

Table 4.8 Different wavelets and scales applied to different data sets

	db7 8	db7 64	db7 128	Morlet 16	Morlet 128	Bior 6.8 16	Bior 6.8 128
Vibration, A1	X	X		X		X	
Vibration, A2	X	X		X		X	
Vibration, A3	X	X		X		X	
Vibration, A4	X	X		X		X	
Vibration, A5	X	X		X		X	
Mode shape 1			X		X		X
Mode shape 2			X		X		X
Mode shape 3			X		X		X

CHAPTER 5

RESULTS AND DISCUSSION

5.1 Introduction

This chapter is devoted to the study of three damage levels of a beam with a lateral cut to test and demonstrate the applicability of the method suggested. The cuts were formed in a controlled fashion on the cantilever beam.

Modal analysis results, i.e., natural frequencies, mode shapes and accelerance FRFs, were examined to see the effect of the cut on the test beam. In section 5.3, the wavelet analysis results of CWT applied to the first three mode shapes as well as to the transverse vibration data of each measurement point for different damage cases were utilized for the detection and localization of the cut. Both coefficients of CWT and energy plots for different damage levels were used in the assessment of these vibration based techniques.

5.2 Modal Analysis Results

5.2.1 Natural Frequencies

Change in natural frequencies for varying damage levels were calculated and results were tabulated in Table 4.4. When the table is inspected, it is seen that all natural frequencies except the first one the beam do not change significantly for the applied damage levels. The drop in the first natural frequency for the initial damage level is as high as 38 % whereas it is approximately 1 % for the remaining modes. The amount of deviation of the first natural frequency of the cut beam was surprisingly high which could be a good indicator of damage. If deviation in the first natural frequency of the cut beam is considered as an exception, it could be concluded that deviations of the natural frequencies do not relieve information for the presence of damage in the beam. Since those results were obtained from measured data it is necessary to take into consideration the effect of measurement errors. Yet, the deviation observed for the first natural frequency is not believed to be due to the measurement errors. Also, information regarding the location and severity of the cut could not be obtained from the natural frequency changes of the beam.

5.2.2 Mode Shapes

Mode shapes were depicted in Figures 4.31 to 4.36. As explained before Figures 4.31, 4.33 and 4.35 were obtained from actual measurements. All modes of the test beam preserved their shapes while amplitude of each point was reduced as a result of the cut introduced. The magnitude at measurement points of the mode shape 1 dropped consistently with the cut depth. The same behavior at measurement points of the other mode shapes was not observed. Although there was a decrease in amplitudes of measurement points for the first damage level of the latter two modes, the same was not true for the damage cases 2 and 3. The trend of mode shapes 2 and 3 was different from that of the first one.

So it was not possible to generalize the behavior seen at mode shape 1 which was the magnitude reduction of measurement points with the increase at the damage level.

However the biggest drop in magnitudes of mode shapes 2 and 3 occurred at the section of the beam located around 12 cm from the fixed end, which was very close to the damage position.

All in all, deviations observed in mode shapes for different damage cases imply that some changes are present within the structure. Also behavior of the beam portion located between distances 10 and 15 cm from the fixed end for mode shape of 2 and 3 was good candidate for the localization of the cut. Yet, the aforementioned alterations at lower levels were also seen at other parts of the beam, which made it difficult to identify the damage.

5.2.3 Frequency Response Functions

For each damage case 5 separate points were used for data collection, which was used for FRF calculations. Since four different damage scenarios were tested, total number of FRFs is 20. As given before the measurement point A1 is the one closest to the fixed end while A5 is closest to the free end of the beam.

When the Figures 4.11 to 4.30 are studied the following points are observed:

- The magnitude and horizontal position of the peaks around 100 Hz, 450 Hz and 1200 Hz were changing with the advance of the cut depth,
- The slope of the curves around the peak points was getting sharper as the damage level increased,
- Peak around the 1200 Hz for the undamaged case of point A3 turned to valley after the damage.

Also for points A5, A4, and A3 the magnitude of peak around 100 Hz always dropped with increase of the damage level whereas this was not the case for points A2 and A1 at the same frequency. One interesting point is the shift of the resonant and anti-resonant frequencies around the 1200 Hz of the FRF of point A3. It is worth mentioning that while taking measurement from point A3 the accelerometer was placed very close to the cut since forcing was always applied at the position of A3.

To sum up, although there were some changes both at the horizontal position (natural frequency) and amplitude of FRFs, those were small in magnitude when compared to the undamaged values. Neglecting the odd behavior of FRF of point A3 at 1200 Hz, it was clear that no information was available on the position and on the extent of the damage. Thus damage identification with this technique is found to be rather limited.

5.3 Wavelet Analysis Results

5.3.1 CWT Applied to Mode Shape Data

The first thing that should be pointed out was that the data that was analyzed was obtained by curve fitting to the original measurement data. The main reason behind this approach was that since original mode shape signal was made up of five data points, the highest scaling number allowed for CWT was two which, if used, could result in a limited number of coefficients, namely 8. In order to increase the allowable scaling number for CWT process, mode shape equations obtained from the curve fitting step was used in the analysis. Since the original mode shape data was very approximate, original mode shape data in the CWT process was not used.

Although the modified data set was smoother than the original one it was still the approximation which could still make the damage assessment process more difficult.

The x-axis of the mode shape curves span from 0 to 45 cm, 0 representing the nearest measurement point (A1) to the fixed end and 44 cm representing the closest measurement point (A5) to the free end.

The mother wavelets and the scale numbers used for the CWT of the mode shape data were summarized in Table 4.8. The same scaling number was chosen for all the wavelet types so that results of CWT could be more easily evaluated to see the effect of using different mother wavelets.

The coefficients of CWT, which were plotted in color proportional to their magnitude, corresponding to mode shape 1 data were given in Figures 5.60, 5.61, and 5.62. The common behavior observed in these graphs was that the region lying around the left of position 50 mm and at high scale values was subjected to some small changes in magnitude for all the wavelet types used. Another effect which was observed for all wavelet types was around 150 mm free end of the beam and at high scales, which was the section of beam where the damage was introduced. These differences observed by different wavelet types could be a sign for the damage. Moreover the effect of damage on results obtained by using different wavelets was most easily followed in the graph obtained through db7 wavelet. On the contrary, results obtained via using bior 6.8 wavelet were the least sensitive to damage whereas Morlet results were in between. The former two seemed to be more sensitive than the latter.

For the coefficients of CWT of mode shape 2 obtained with bior 6.8 wavelet, changes in the magnitude of coefficients at high scales and at position around 50 mm were observed. This deviation was also observed in the results obtained by using Morlet and db7 wavelets. In addition, high scale coefficients at the position around 150 mm changed comparatively much, where db7 and Morlet wavelets were used as analyzing wavelet.

Again, this part of the beam was exactly where the cut was introduced. There was a general drop in the magnitude of the coefficients when using the db7 wavelet. Furthermore, changes all over the coefficients map for different wavelet types were observed even though the order of which was not high. From Figures 5.63, 5.64, and 5.65 the most sensitive mother wavelet was observed as Morlet whereas the bior 6.8 was the least sensitive for the mode shape 2 results. As observed in the mode shape 1 results the region horizontal position of which was around 150 mm showed the existence and the location of the cut. The reason why a second region which was formed around the 50 mm point in x-axis was not clear but it could be related with the end effect of the beam which was fixed.

For the CWT coefficients obtained by analyzing mode shape 3 curve where different wavelets had been used, there was a general reduction in interested regions of the coefficients map as the damage was introduced. Specifically, the results obtained by using db7 analyzing wavelet showed that around both the 100 mm and 350 mm point along the beam length and also at high scaling numbers, magnitude of coefficients decreased as the damage level was increased. A very similar situation was also observed in the results where bior 6.8 mother wavelet was used as the analyzing wavelet. The only difference from the previous case was the increase of coefficients around the 350 mm point where coefficients were reduced in the former one. Although the case where Morlet was used as the analyzing wavelet showed similar results, there were two differences: (1) In addition to changes seen at 100 mm point there was another point 150 mm where the same shift was observed. (2) The region on the right was not around the 350 mm point but instead it was located in the proximity of 250 mm. Even though the effect of using 3 different wavelets for CWT coefficient calculations showed very similar results, it can be said that more precise damage location estimation could be made from results obtained by Morlet analyzing wavelet. The related graphs were illustrated in Figures 5.66, 5.67, and 5.68.

For the total energy calculations the coefficients obtained from the processes above were used in the following equation:

$$E_i = \sum_{j=1}^{n} E_i(j) \quad \text{.....(9)}$$

where i represents the time scale, i.e., in this case the position increment. Equation 9 was utilized with the CWT coefficients of the mode shape data.

At each point, which were separated 1 mm from each other along the beam length, the total energy composed of all the scale wise energies was computed.

The results obtained for the mode shape 1 data show no significant change in the energy distribution over the beam length for different mother wavelets of bior 6.8, db7 and morlet, where scaling for CWT was selected as 128 for all. Thus, the following notes were summarized from the previous analysis:

- The energy magnitude around the 150 mm position was altered as the damage was introduced to the structure. Yet, the deviation of this energy value, as the depth of cut increased, did not show any consistency for all the different wavelet types used.
- The only information that could be extracted from the related figures without any doubt was the presence of a change in the structure.

The situation where the results of CWT coefficients of mode shape 2 data was used was also not very promising. Again there existed inconsistency within the results obtained by using various mother wavelets at different damage levels.

For example, the energy level calculated at position 154 mm from Figure 5.72, where bior 6.8 was selected as the analyzing wavelet, initially increased as the cut was formed. Then, as the cut depth was increased the energy level dropped. Finally, the highest energy amplitude was obtained for the highest damage level. This observation was also recorded for cases where other wavelet types were utilized in the CWT process. Hence, this analysis could only reveal the presence of a structural change giving no information for the position and extend of the cut. Also, sensitivities of different mother wavelets in differentiating the energy change with respect to damage were very close to each other.

Results obtained by analyzing the mode shape 3 data were the most informative among the first two cases with regard to damage identification. When Figures 5.75, 5.76, and 5.77, which were obtained by employing Morlet, db7, and bior 6.8 analyzing wavelets, respectively, were inspected it was seen that the energy values at the 150 mm and 129 mm positions were reduced consistently as damage level was increased. This behavior observed in different results obtained by using different mother wavelets pinpointed the location of the cut as well as its presence. Again, using different analyzing wavelets for the same data did not reveal any significant differences to damage sensitivity among the different wavelets employed.

In brief, the mode shape 1 and 2 data analysis results did not indicate any significant information for the damage identification except the presence of a structural change in the beam. The results were not consistent. Since, as the damage level was increased, the sign of change at each step was not the same.

That is to say the energy of a point was increasing for the first two levels of the damage whereas it was decreasing for the last level. The only informative case was the one where mode shape 3 data was analyzed. In this case the energy difference with each higher damage level around the cut position was decreasing.

This information was the basis for the prediction of both the existence and location of the damage.

5.3.2 CWT Applied to Acceleration Data

The results of the normalized energy calculations for various mother wavelets as well as for all measurement points were given in Figures 5.1 to 5.20.

The observations from the figures of the results for different measurement points are explained below:

Point A1, A3, A4, and A5:

- Energy level dropped as the damage level increased for the scale numbers higher than 3 where the analyzing mother wavelet was db7 with scale number of 8.
- When the above mentioned wavelet with scaling number of 64 was used a similar decrease in the energy level for scale numbers between 4 and 10 was observed. Also the peak of each curve representing different damage cases moved towards the right.
- Similar changes that were experienced in the previous step were also observed when the analyzing mother wavelets of Morlet and bior 6.8 with scaling of 16 were used.
- Results very similar to that of point A1 were obtained except the scale ranges where energy deviation occurred.

Point A2:

- Being different from A1 results, a small increase at the first level damage was observed with db7 of scales 8 and 16 which dropped as the damage level increased. Also, for the scaling of 16 peaks shifted a little towards the higher scales.
- For Morlet and bior 6.8 being the mother wavelets with scale of 16, a drop was seen in the energy levels between the scales 4 and 8 and an increase in energy levels for the scales 9-13 was observed.

A similar interpretation methodology that was used for the energy curves of the measurement points was used for the CWT coefficients curves of the same points. The related pictures were displayed in Figures 5.21 to 5.59.

Point A1:

- The magnitude of middle scale coefficients, obtained through the analysis with bior 6.8 mother wavelet of scale 16, was reduced so that some disappeared at the higher data points, i.e., at these frequencies of the signal they lived shorter as the damage was introduced to the structure.
- The above situation was also observed for mother wavelets of Morlet with scaling of 16 and db7 with scale number of 8. In addition, the magnitude of the lowest scale coefficients increased at the data points that were not visible for the undamaged case. That is to say higher frequency content of the measurement signals lived longer and the magnitudes of coefficients got higher as the damage level increased.

- For the case with db7 of scale 64, middle scale coefficients appeared at shorter intervals along the data axis, which was actually the time axis. Also higher scaled coefficients were eliminated at longer data points, meaning they were not present at times that they were before as the damage was introduced to the beam.

Points A2 and A3:

- Lowest scale values of coefficients of point A2 increased both in magnitude and in the range along the data points for wavelets of bior 6.8 and morlet of scale 16 and for db7 of scale 8. The x-axis range for middle scale coefficients was shortened for morlet with scale of 16.
- For the db7 of scale 64, higher scale coefficients of point A2 and A3 disappeared at relatively high data points as depth of cut increased.
- The overall magnitude of the coefficients for point A2 was not regularly changing while the damage level was increased whereas it was reduced for point A3.
- The length along the data points that they extend was reduced for middle scale coefficients of measurement point A3 as the structure was damaged.

Point A4:

- Not a regular change of the magnitude of coefficients was observed for all different mother wavelets.
- Middle scale coefficients dropped in value while lowest scale coefficients increased in magnitude at longer data points for bior 6.8 of scale 16, morlet of scale 16, and db7 of scale 8.

- A similar situation to that of point A1 with mother wavelet of db7 with scale 64 was observed as the damage level increased.

Point A5:

- A general drop in the magnitudes of the wavelet coefficients for bior 6.8 with scale 16, morlet with scale 16, and db7 of scale 8 was seen.
- The result with db7 of scale 64 was similar to that of point A4 analyzed with the same mother wavelet with scaling of 64.
- For the morlet wavelet with scale 16, no significant change was observed except the overall magnitude drop.

When the results that were discussed in this section were inspected a general trend in the analyzed data can be summarized as follows:

1. Analyzing the signals at higher scale levels revealed the periodicity change more clearly than those with the lower scale analysis results,
2. A regular change, which was reduction of the magnitude, of the CWT coefficients throughout the whole figure was only obtained for points A3 and A5,
3. Usually, coefficients obtained at lower scales increased both in magnitude and along the data point range towards the right. To put it another way, high frequency content of the measurement signals was higher in amplitude and lasted longer in time,
4. Magnitude of the coefficients belonging to middle scale ranges were reduced as well as the time they lived was shortened.

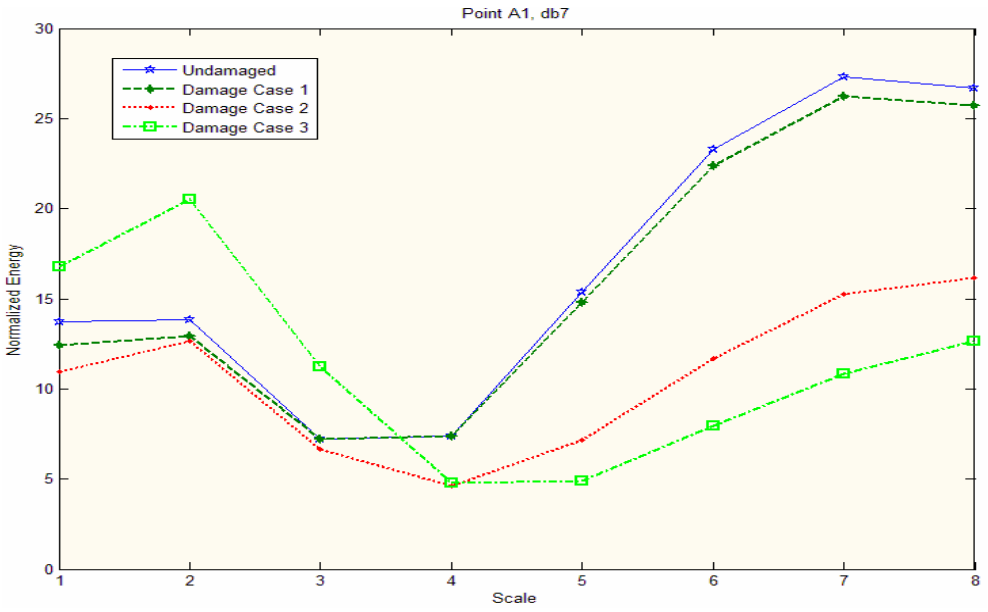

Figure 5.1 Scale wise normalized energy of point A1, db7 with scale 8

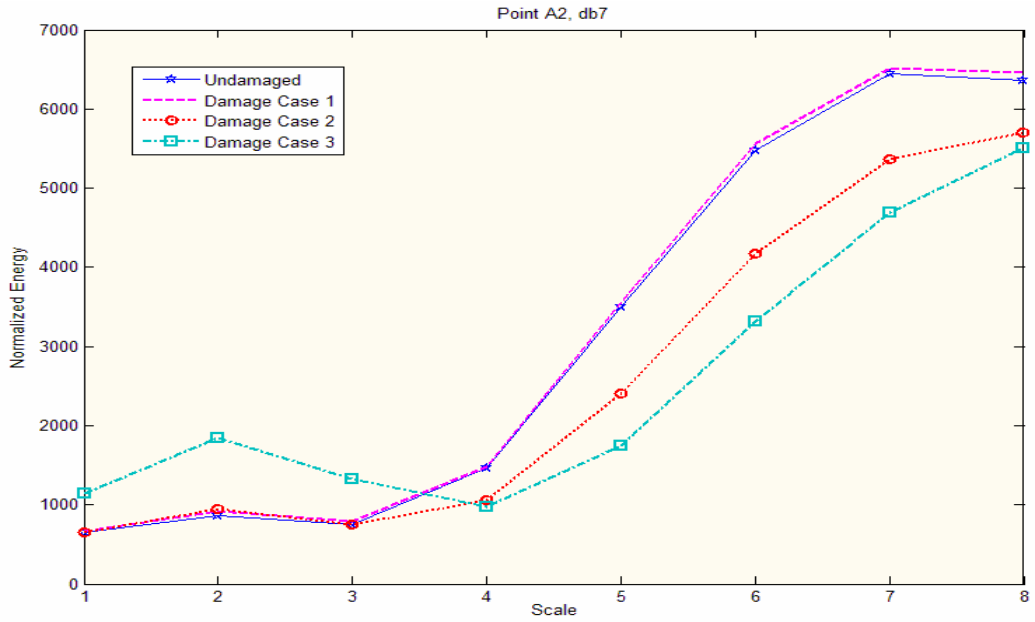

Figure 5.2 Scale wise normalized energy of point A2, db7 with scale 8

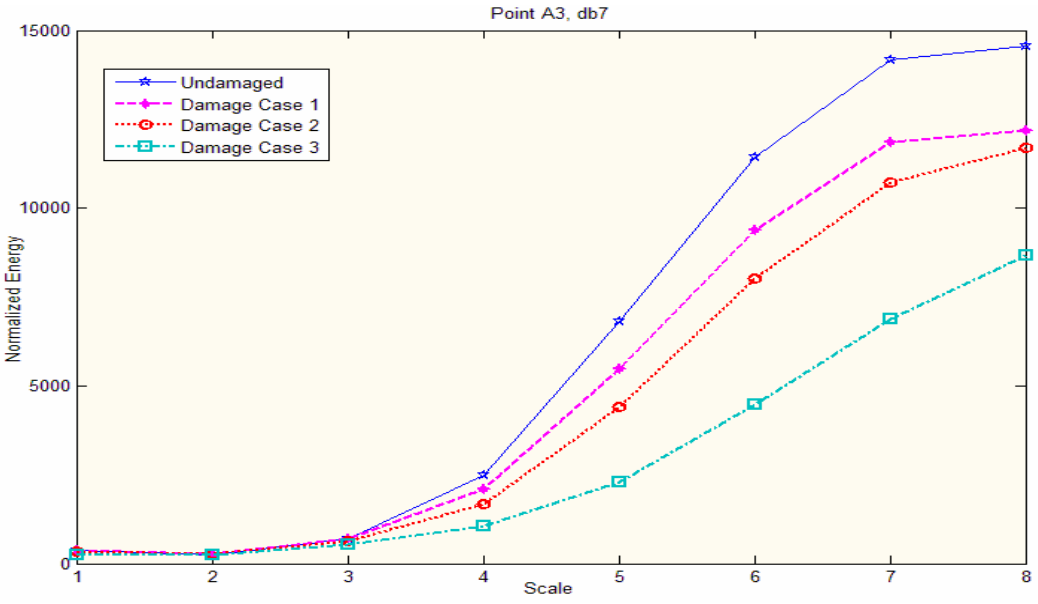

Figure 5.3 Scale wise normalized energy of point A3, db7 with scale 8

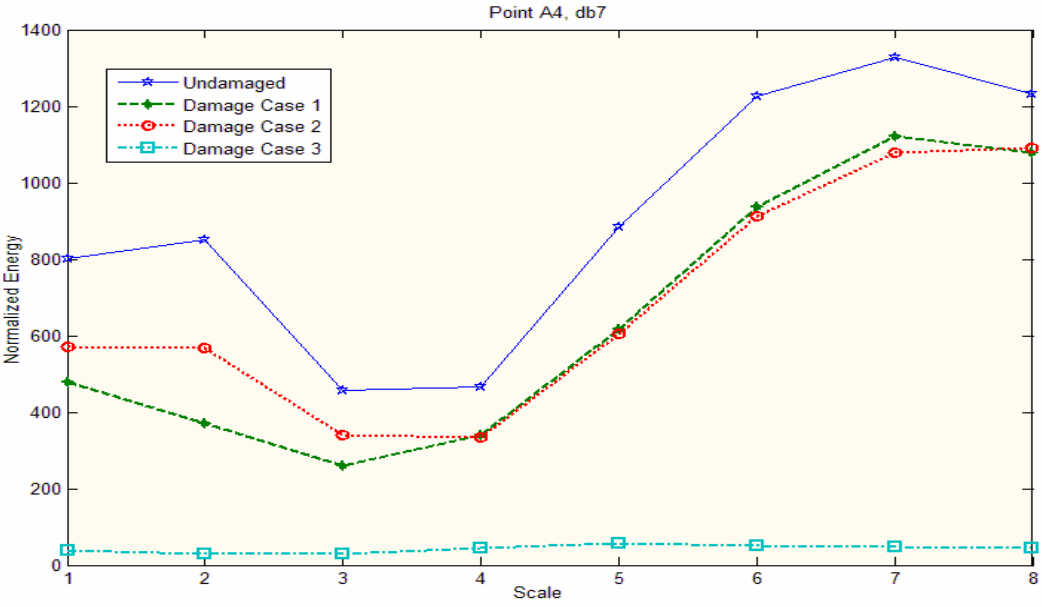

Figure 5.4 Scale wise normalized energy of point A4, db7 with scale 8

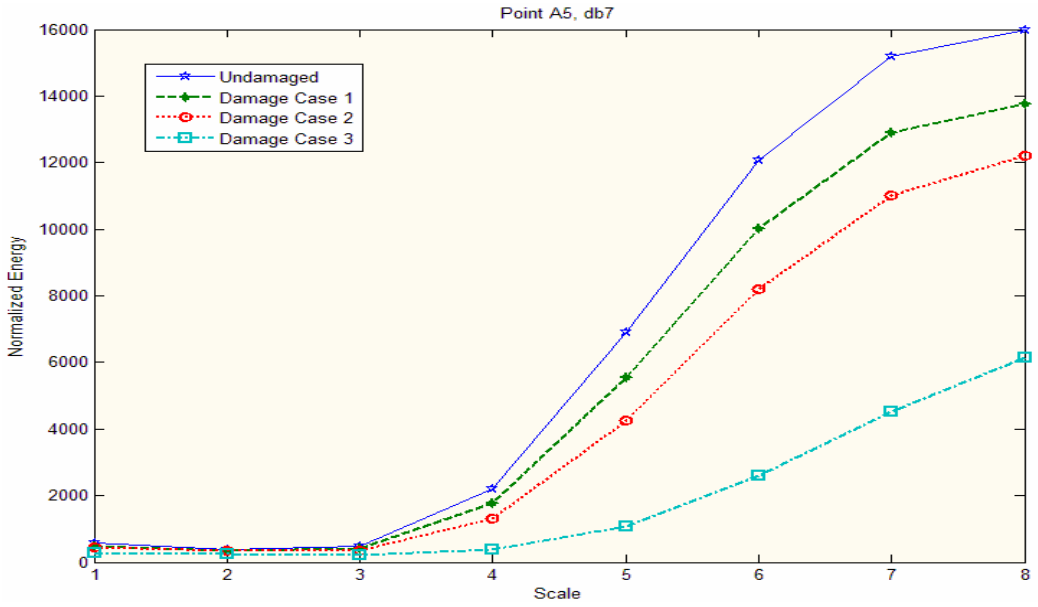

Figure 5.5 Scale wise normalized energy of point A5, db7 with scale 8

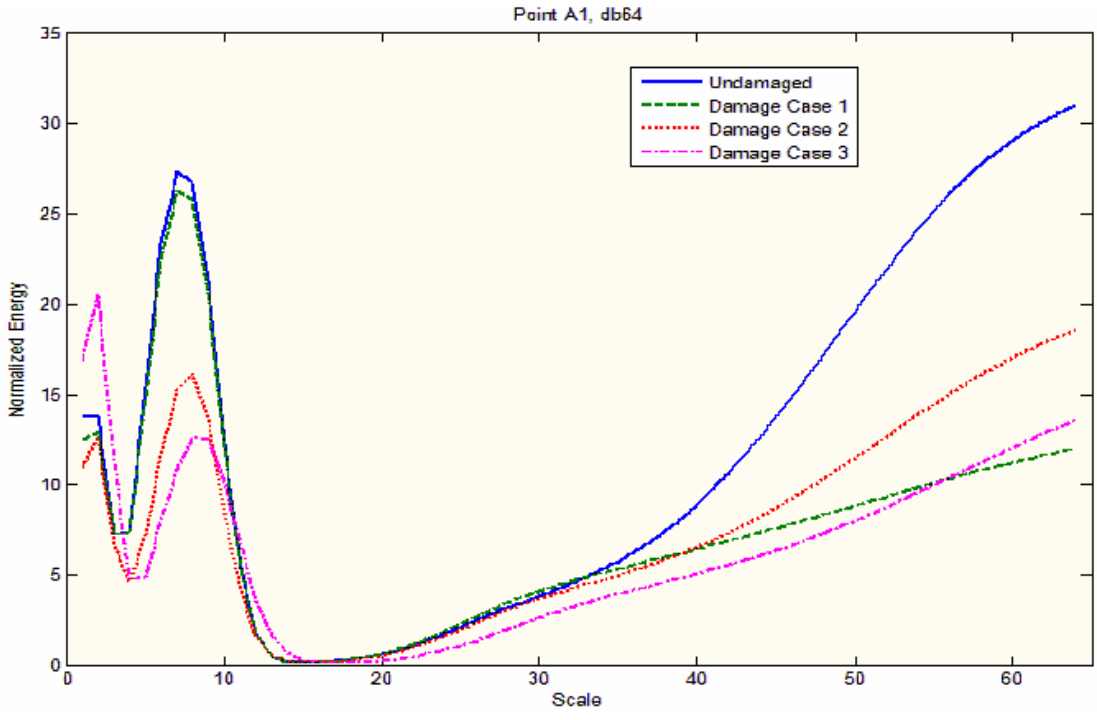

Figure 5.6 Scale wise normalized energy of point A1, db7 with scale 64

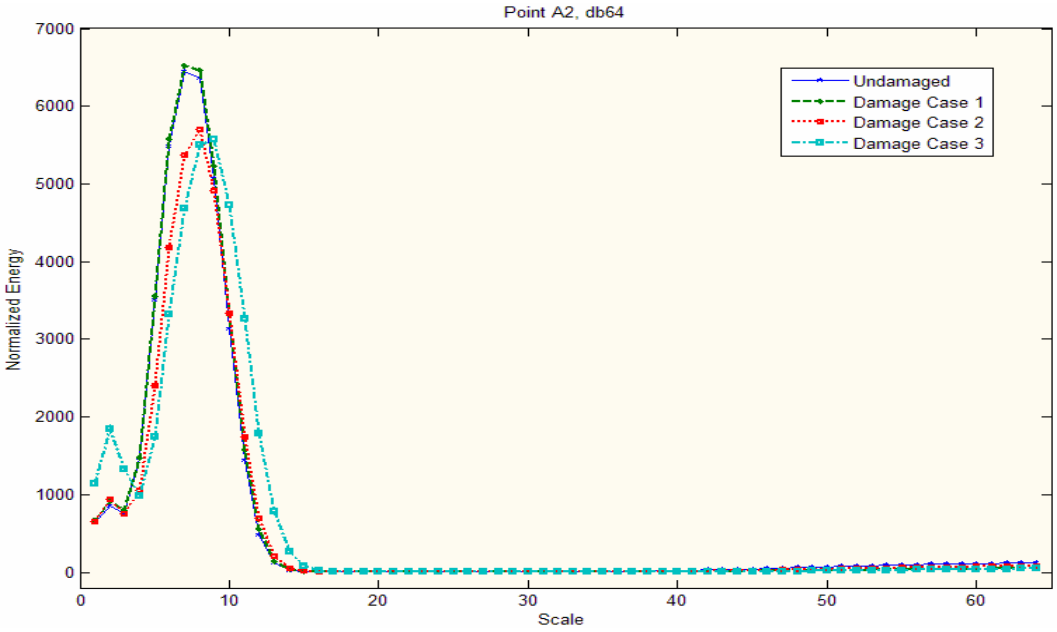

Figure 5.7 Scale wise normalized energy of point A2, db7 with scale 64

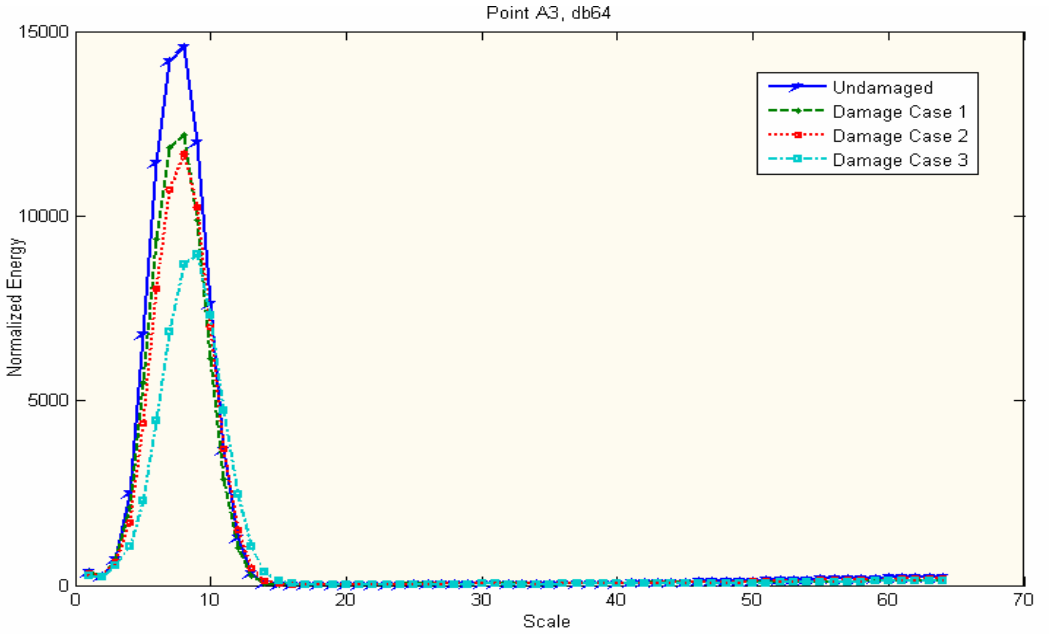

Figure 5.8 Scale wise normalized energy of point A3, db7 with scale 64

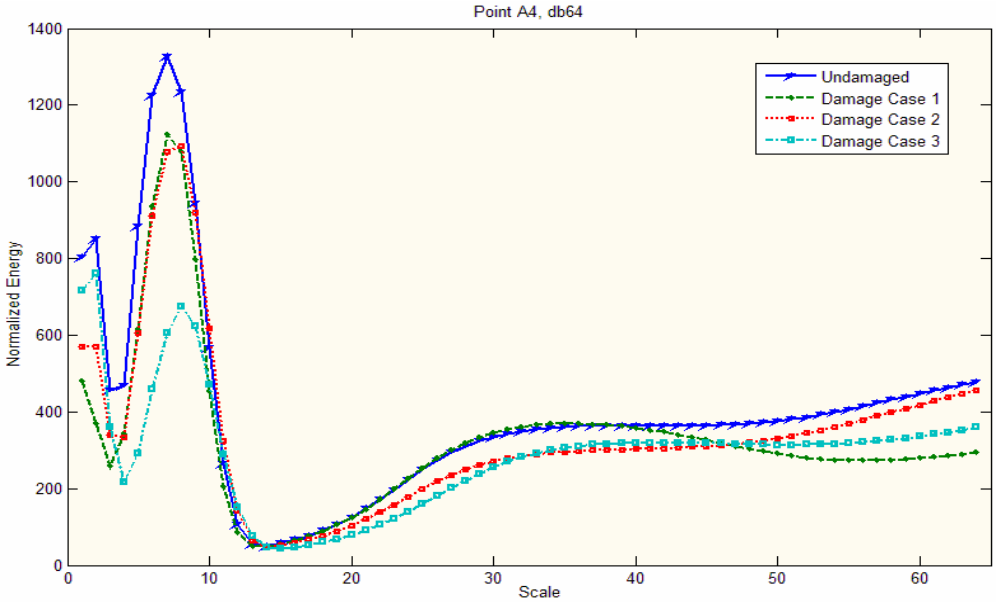

Figure 5.9 Scale wise normalized energy of point A4, db7 with scale 64

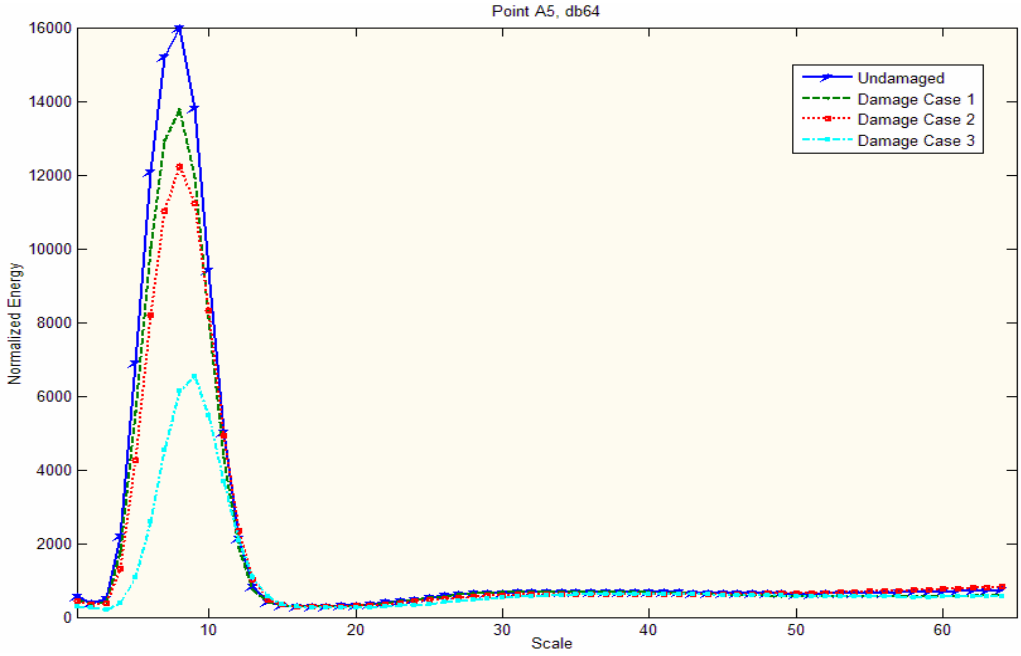

Figure 5.10 Scale wise normalized energy of point A5, db7 with scale 64

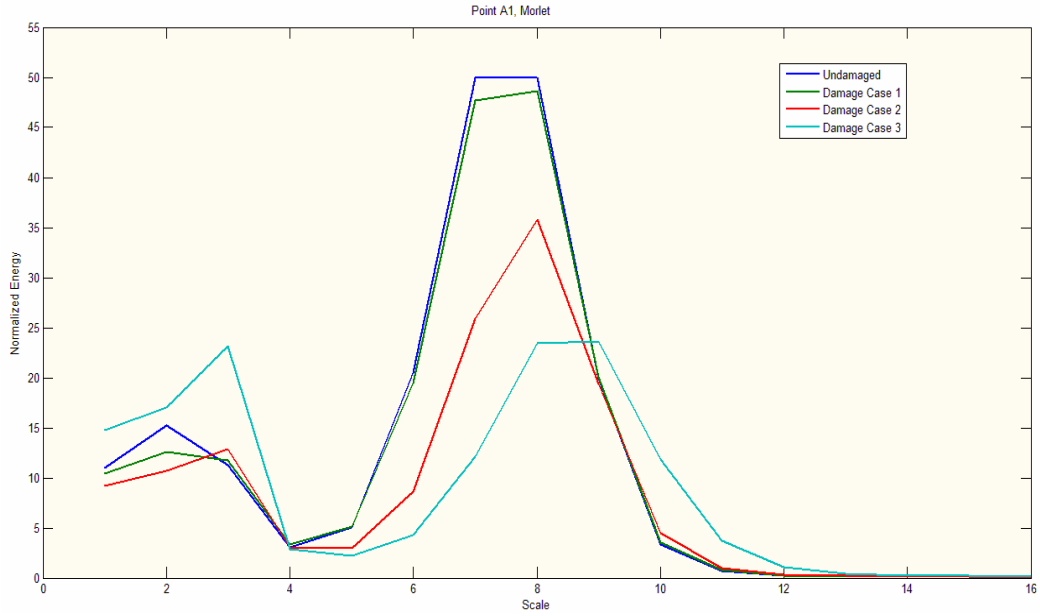

Figure 5.11 Scale wise normalized energy of point A1, morlet with scale 16

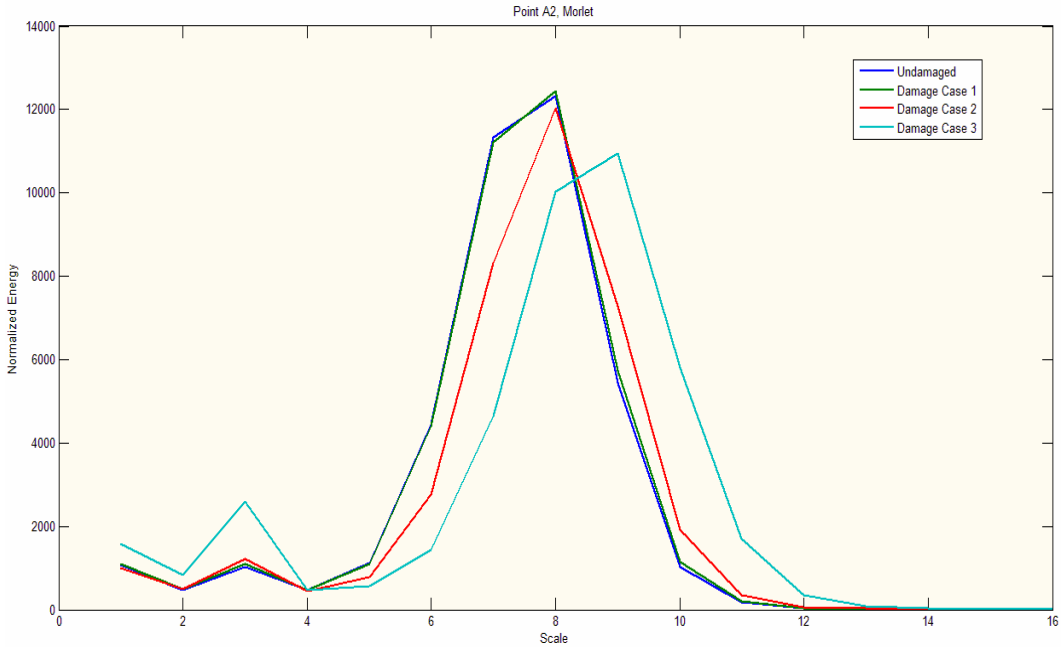

Figure 5.12 Scale wise normalized energy of point A2, morlet with scale 16

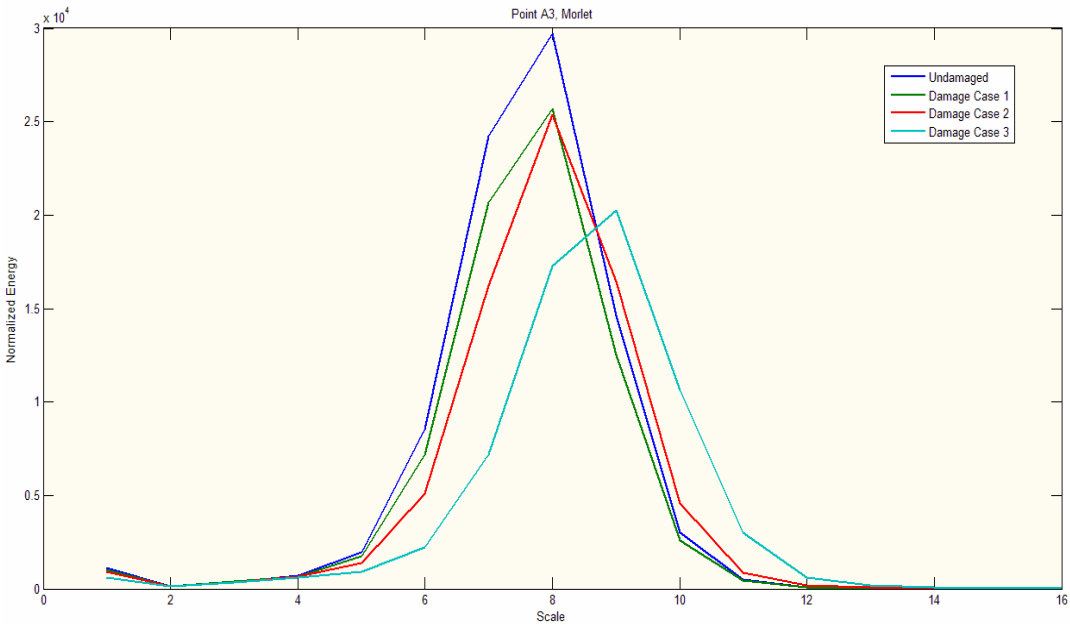

Figure 5.13 Scale wise normalized energy of point A3, morlet with scale 16

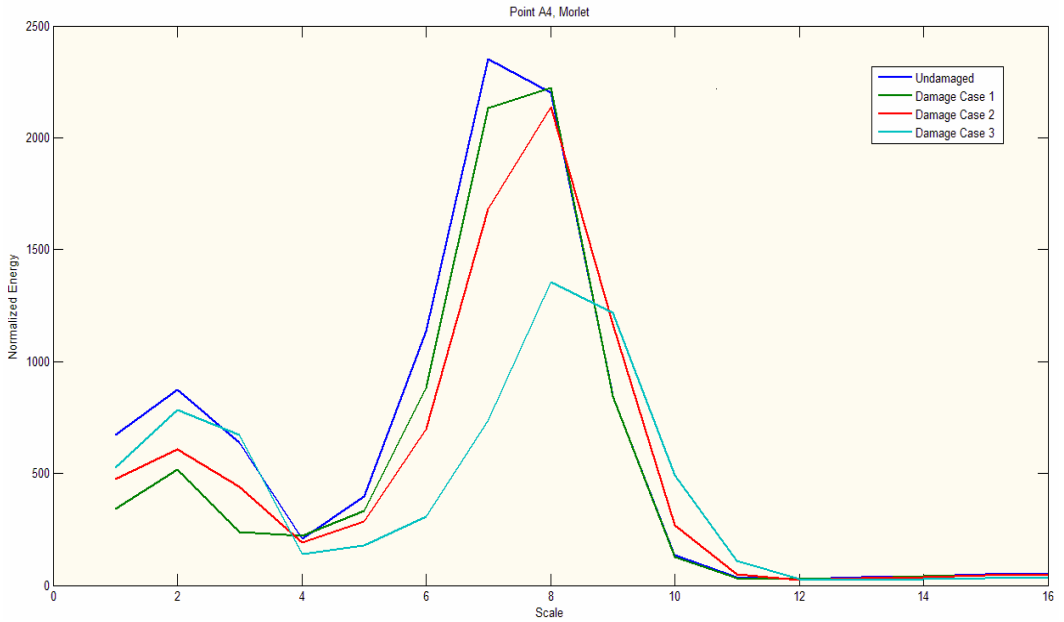

Figure 5.14 Scale wise normalized energy of point A4, morlet with scale 16

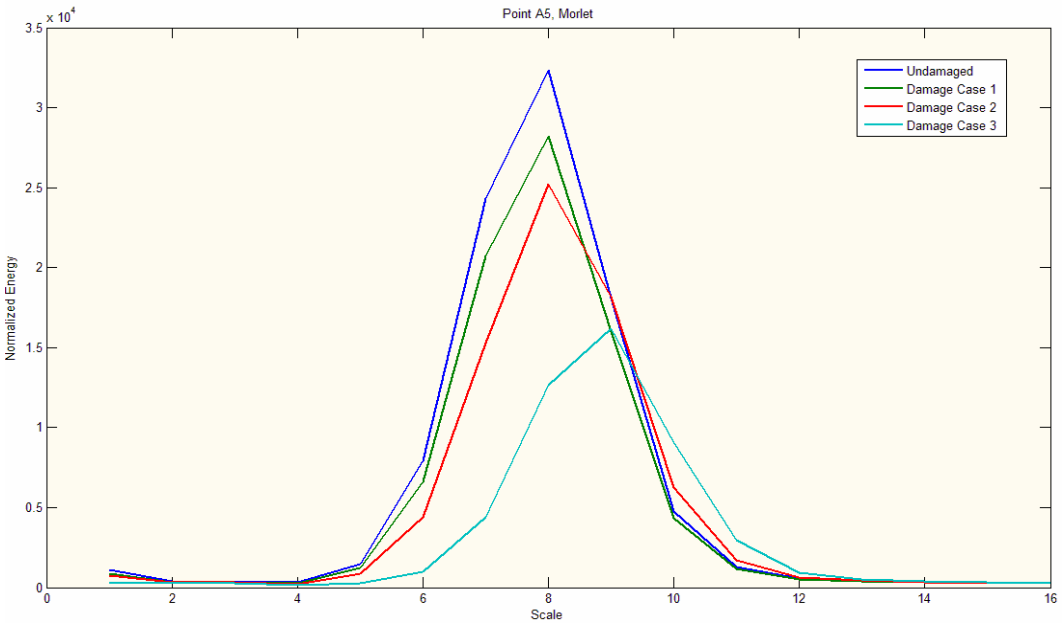

Figure 5.15 Scale wise normalized energy of point A5, morlet with scale 16

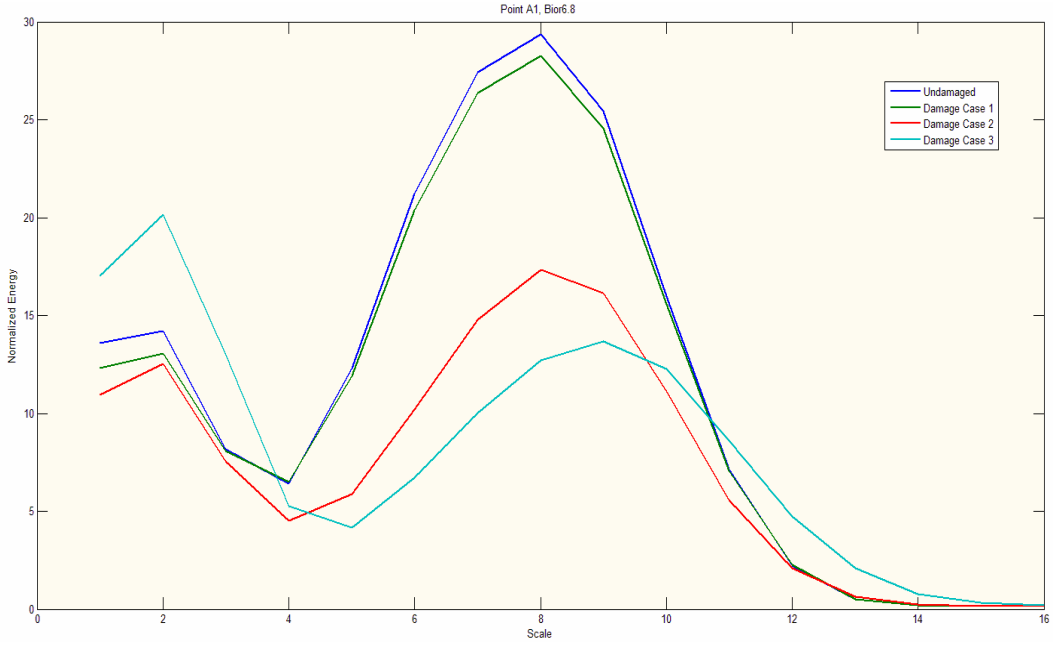

Figure 5.16 Scale wise normalized energy of point A1, bior 6.8 with scale 16

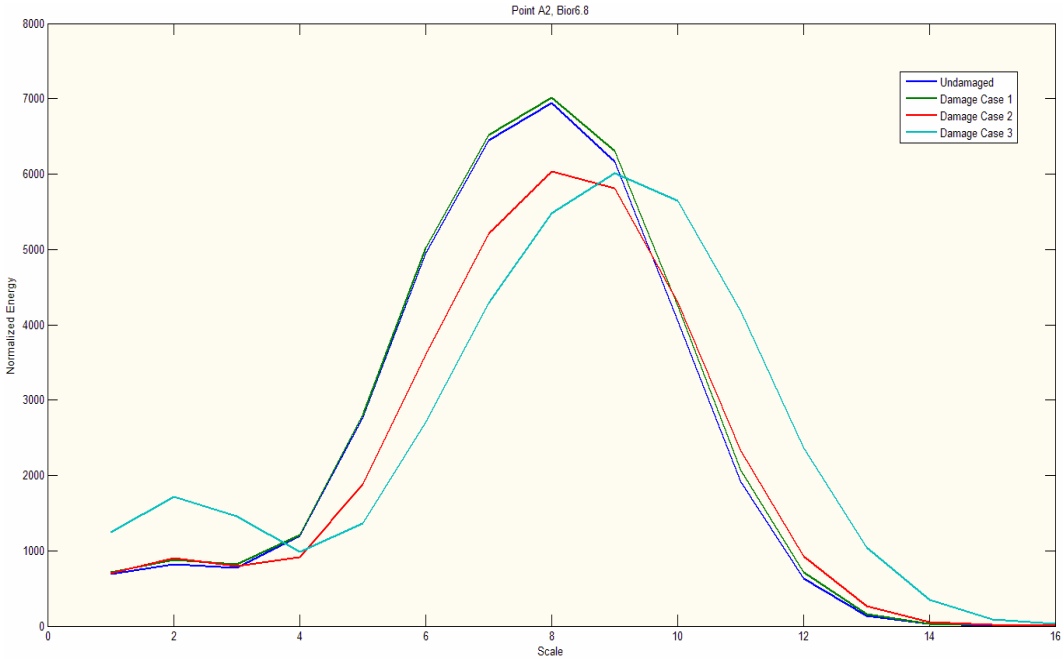

Figure 5.17 Scale wise normalized energy of point A2, bior 6.8 with scale 16

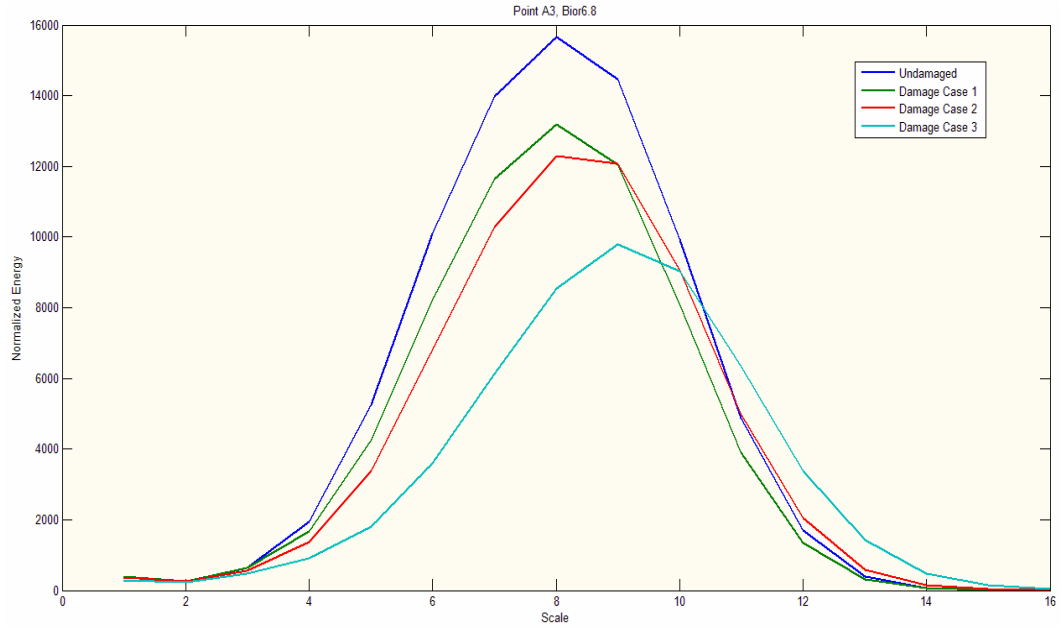

Figure 5.18 Scale wise normalized energy of point A3, bior 6.8 with scale 16

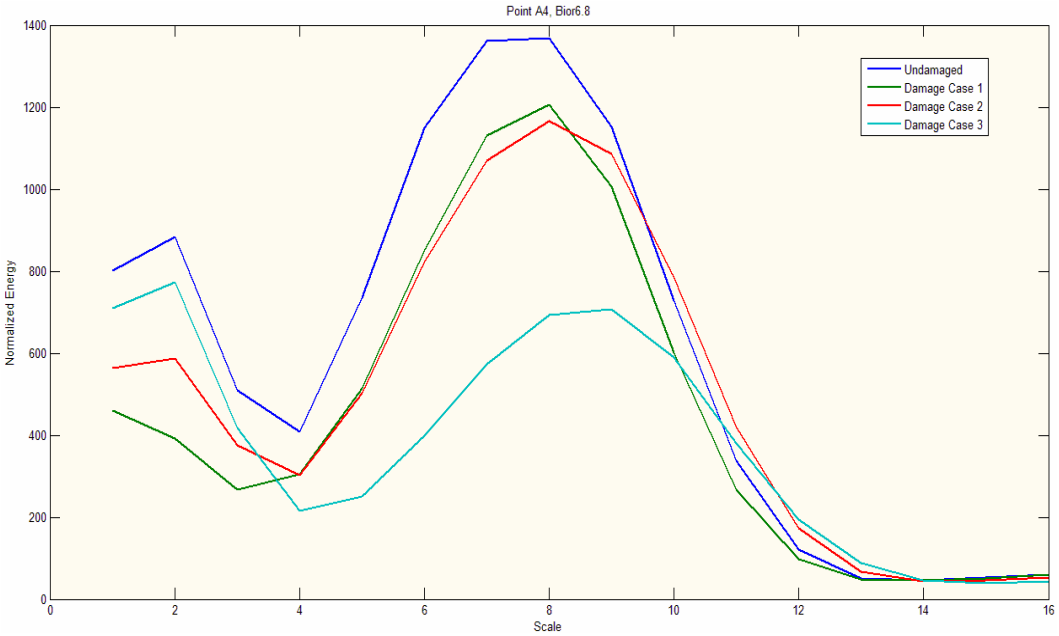

Figure 5.19 Scale wise normalized energy of point A4, bior 6.8 with scale 16

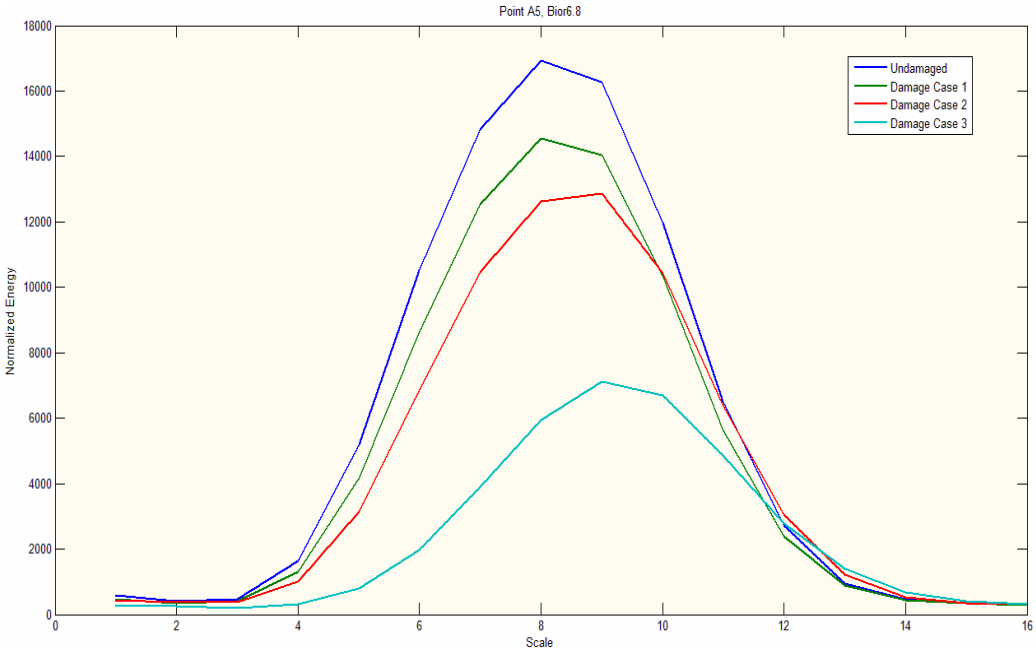

Figure 5.20 Scale wise normalized energy of point A5, bior 6.8 with scale 16

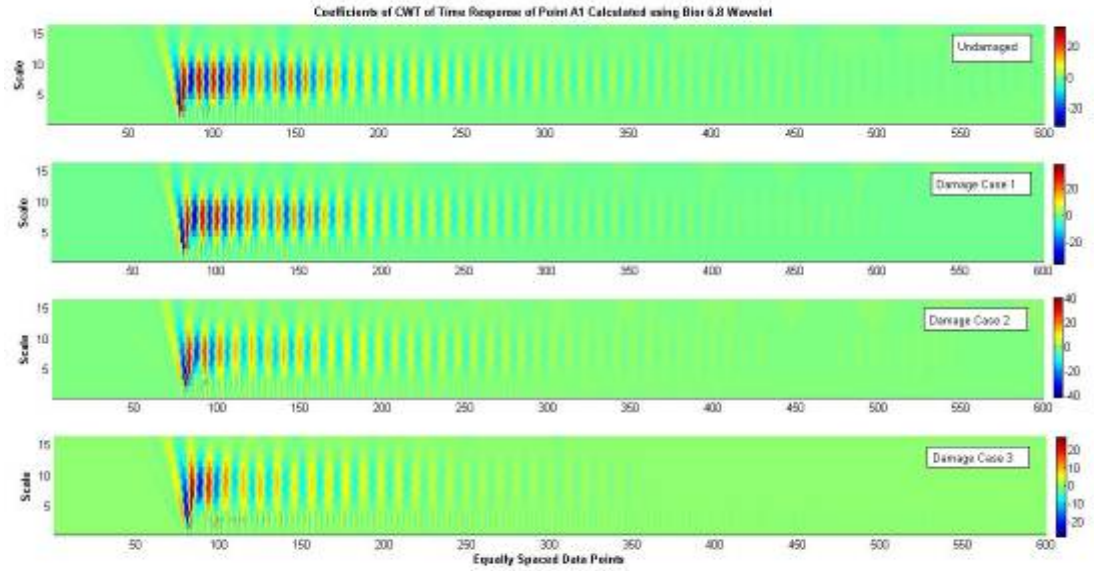

Figure 5.21 Coefficients of CWT of response data of point A1, bior 6.8 with scale 16

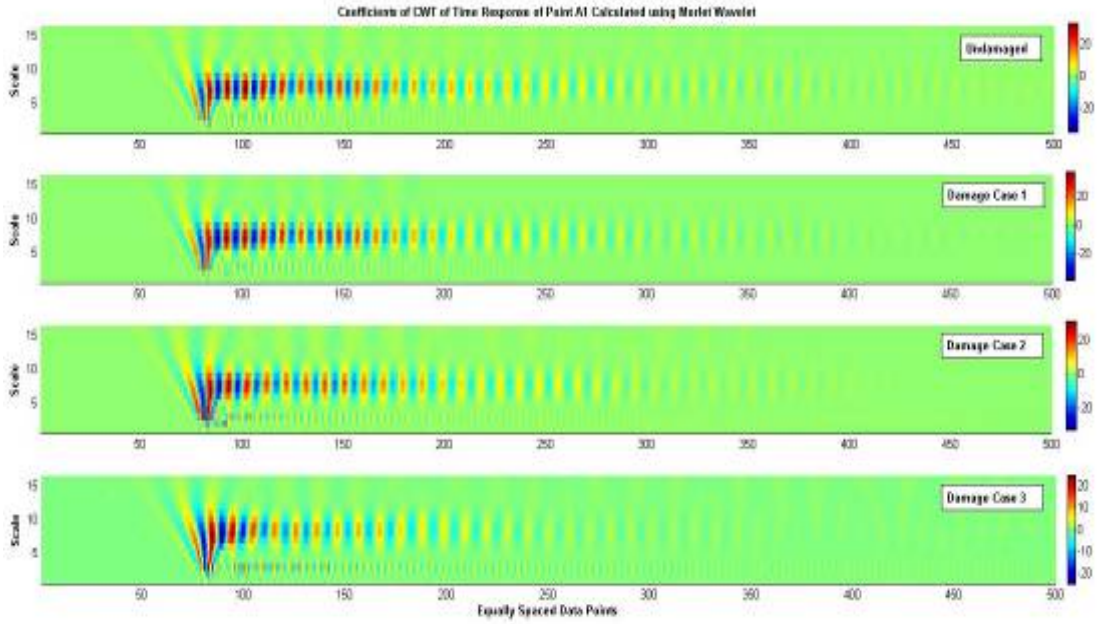

Figure 5.22 Coefficients of CWT of response data of point A1, morlet with scale 16

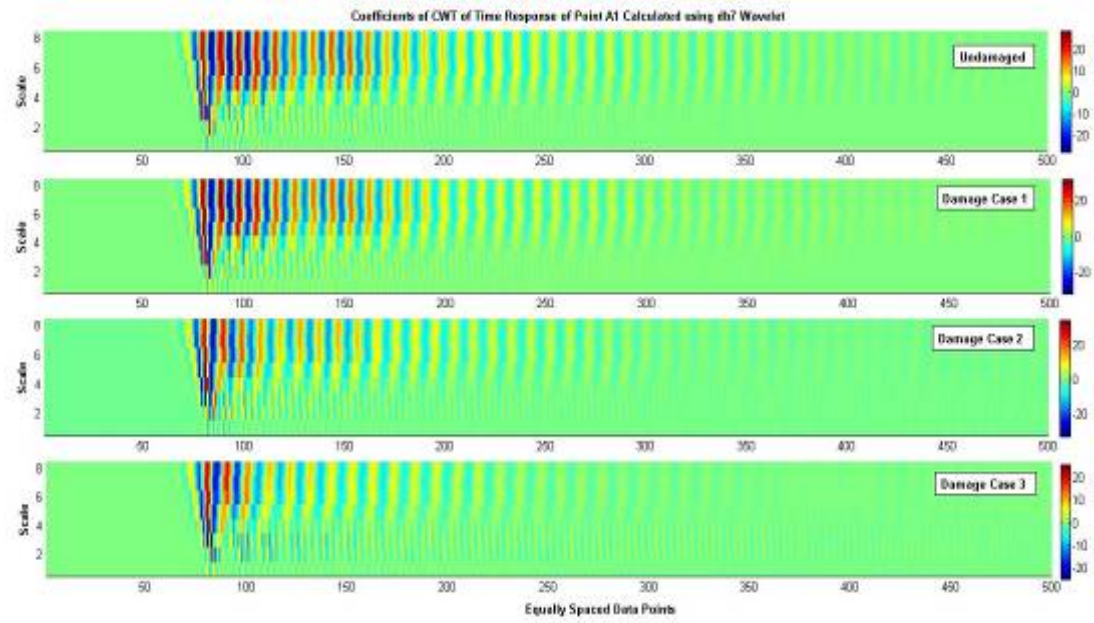

Figure 5.23 Coefficients of CWT of response data of point A1, db7 with scale 8

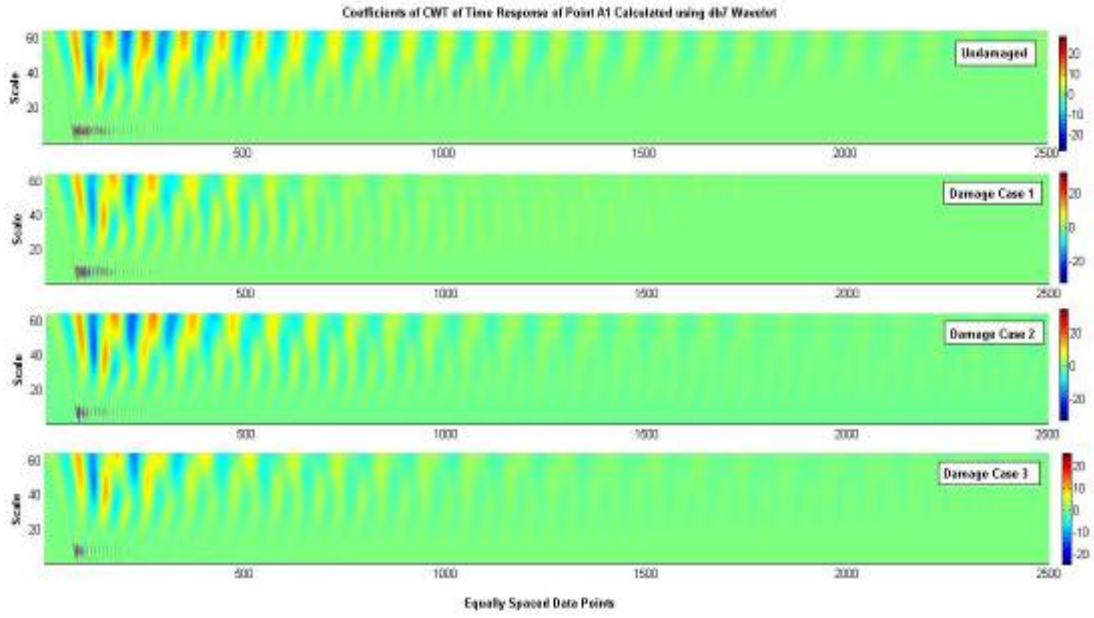

Figure 5.24 Coefficients of CWT of response data of point A1, db7 with scale 64

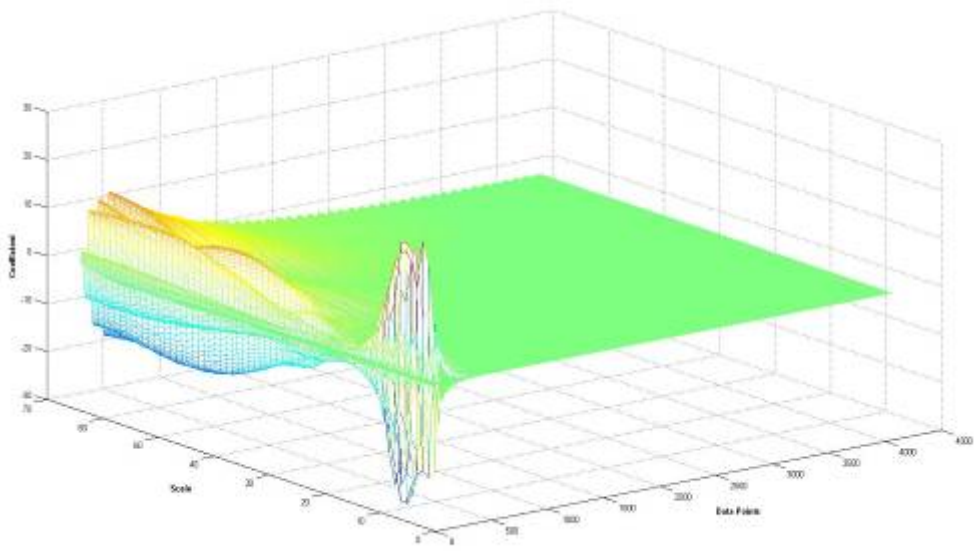

Figure 5.25 3D map of CWT coefficients of undamaged case response data of point A1, db7 with scale 64

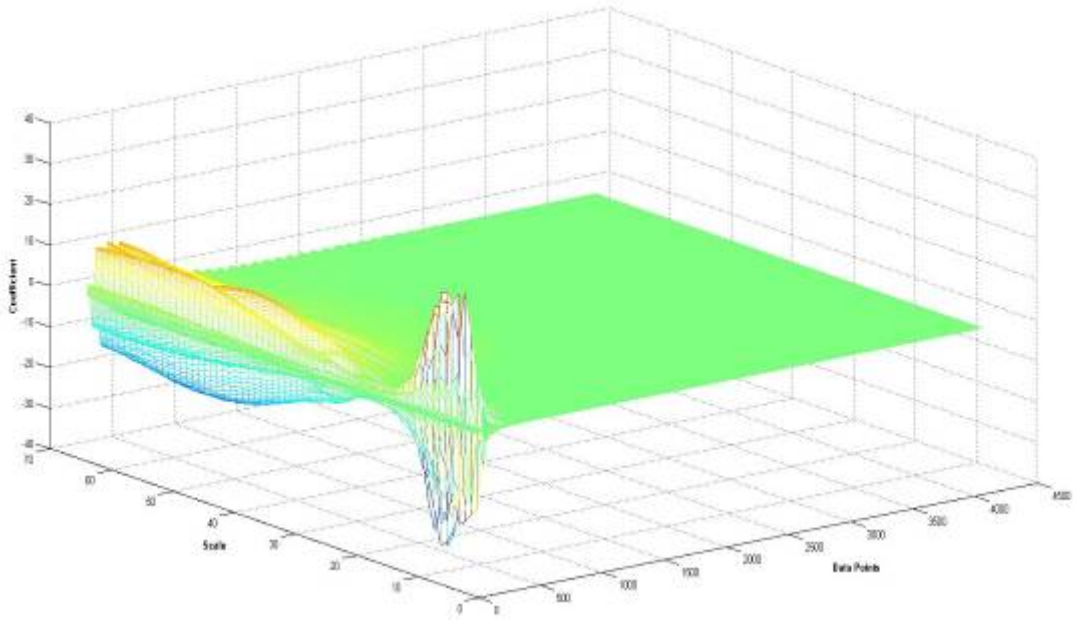

Figure 5.26 3D map of CWT coefficients of damage case 1 response data of point A1, db7 with scale 64

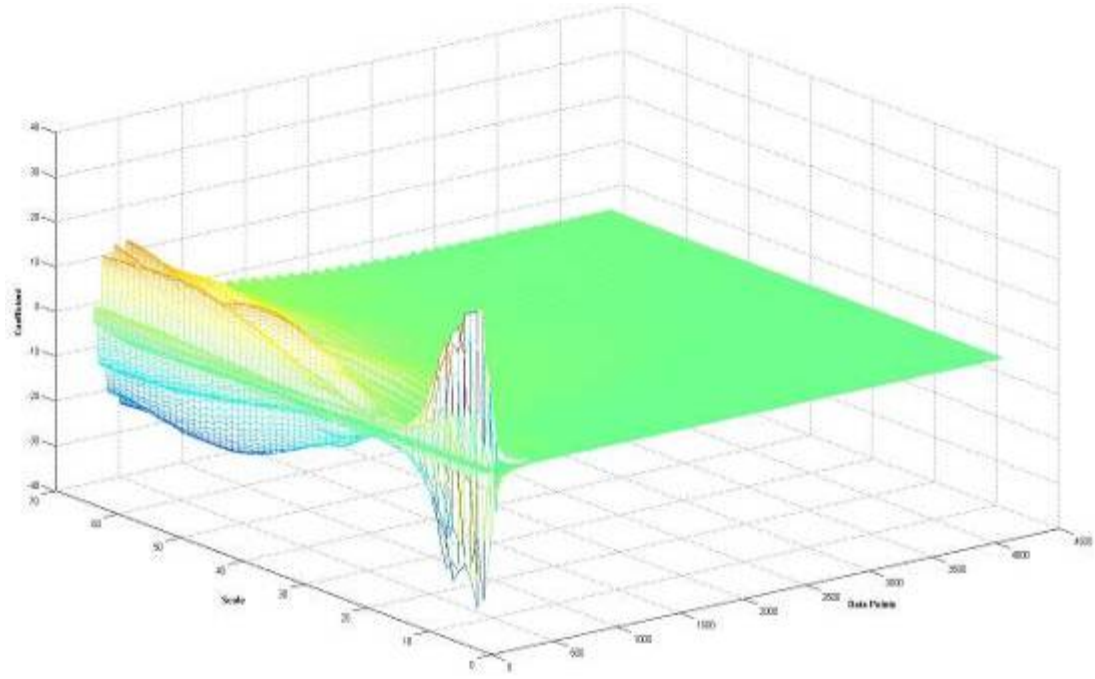

Figure 5.27 3D map of CWT coefficients of damage case 2 response data of point A1, db7 with scale 64

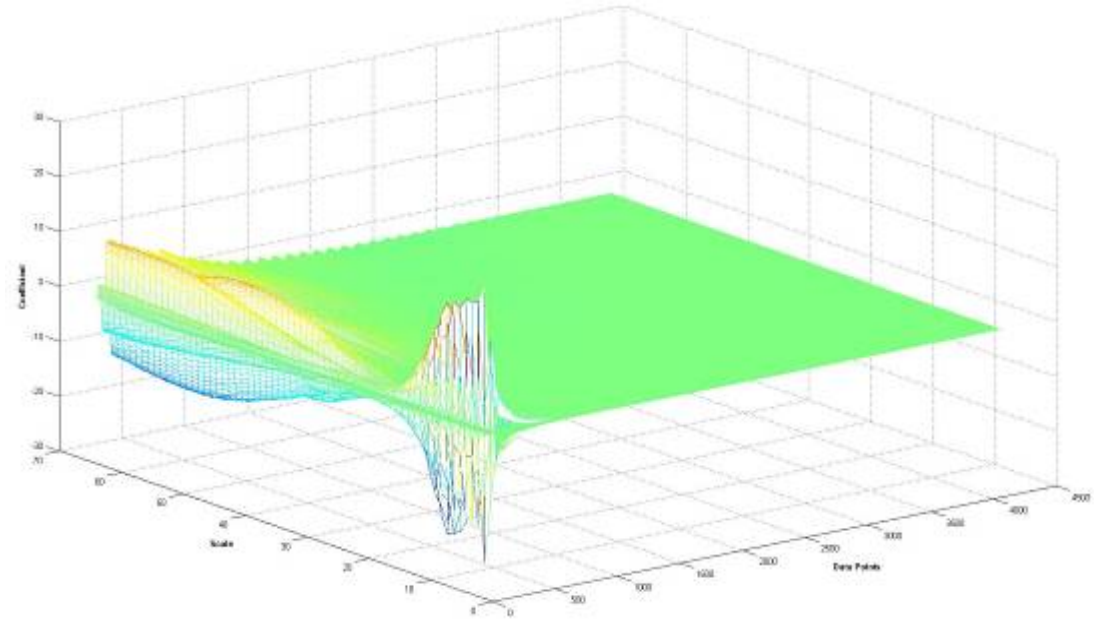

Figure 5.28 3D map of CWT coefficients of damage case 3 response data of point A1, db7 with scale 64

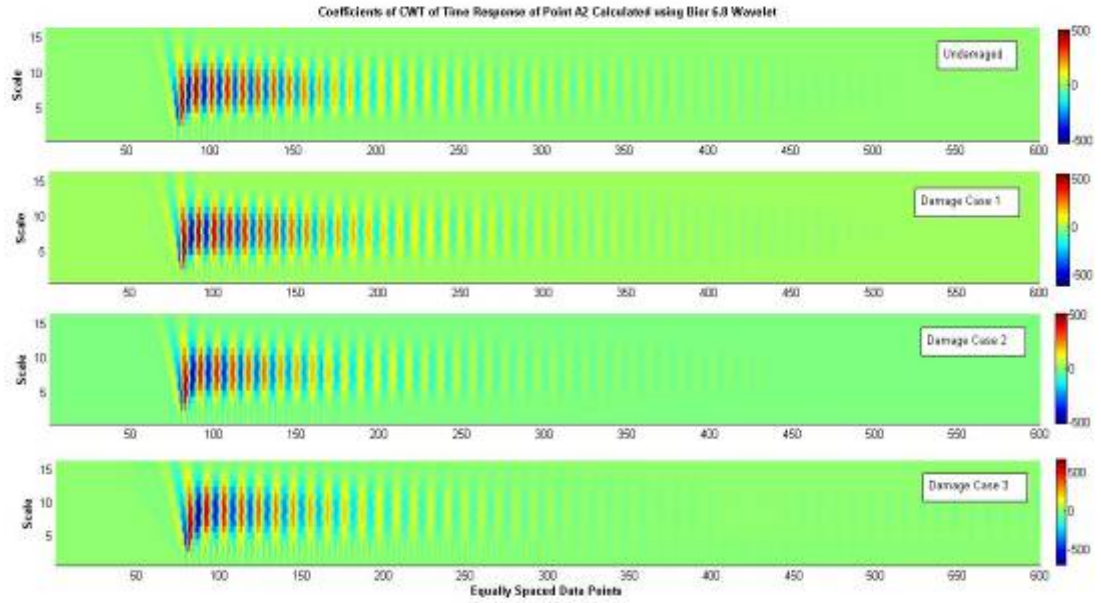

Figure 5.29 Coefficients of CWT of response data of point A2, bior 6.8 with scale 16

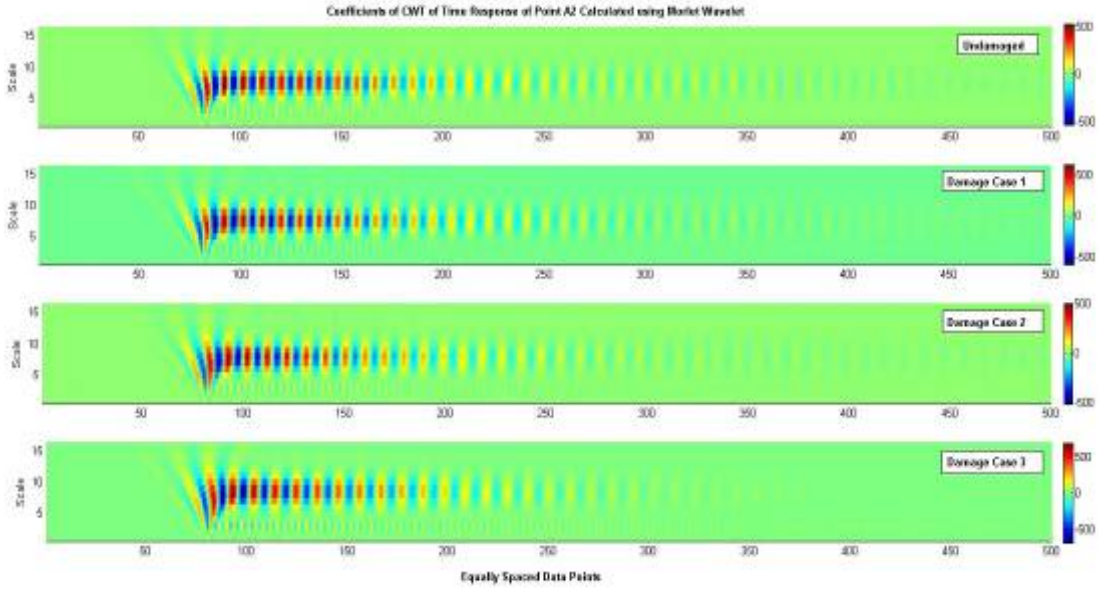

Figure 5.30 Coefficients of CWT of response data of point A2, morlet with scale 16

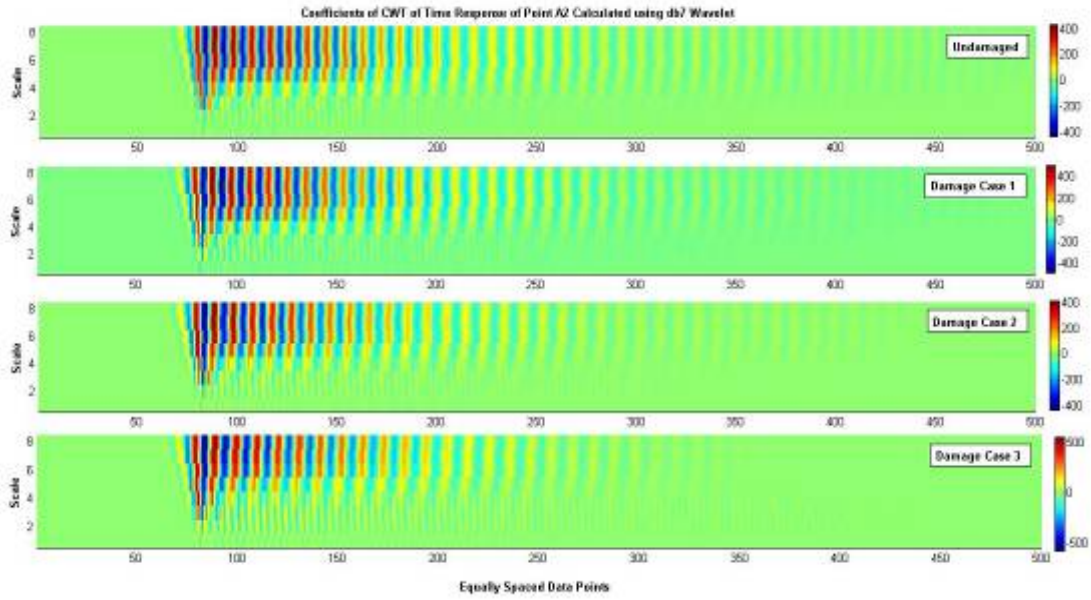

Figure 5.31 Coefficients of CWT of response data of point A2, db7 with scale 8

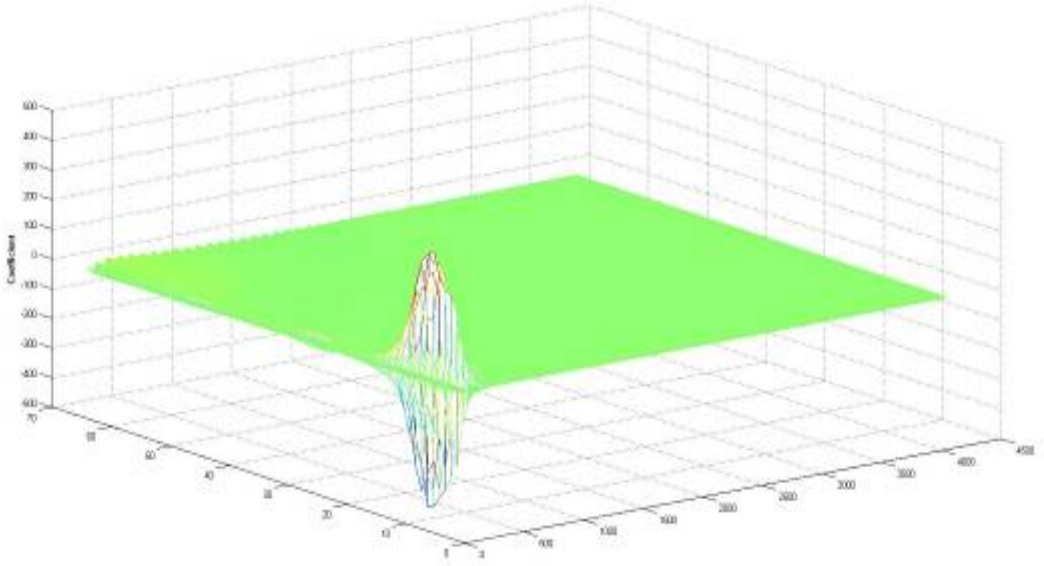

Figure 5.32 3D map of CWT coefficients of undamaged case response data of point A2, db7 with scale 64

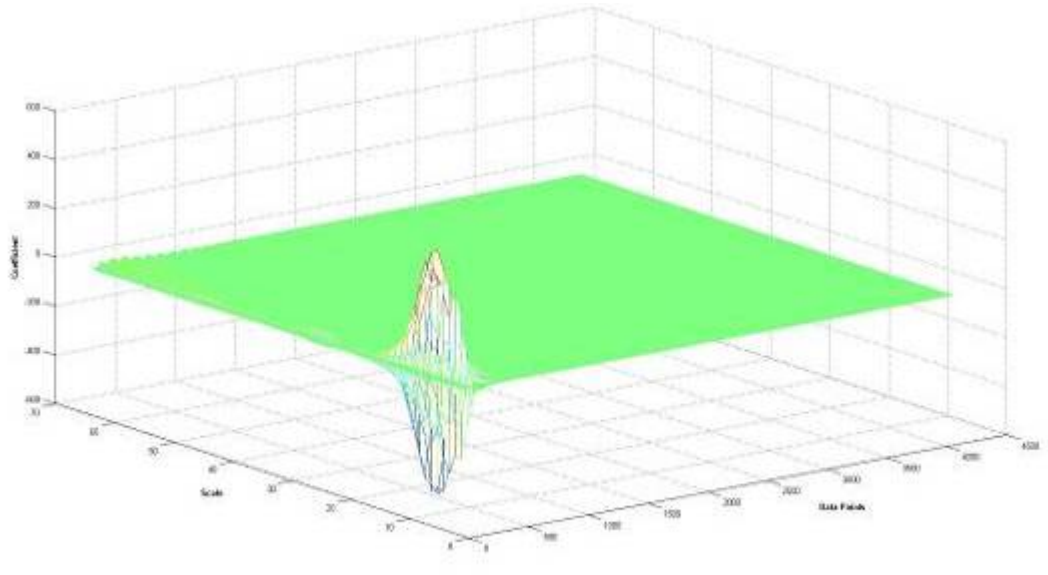

Figure 5.33 3D map of CWT coefficients of damage case 1 response data of point A2, db7 with scale 64

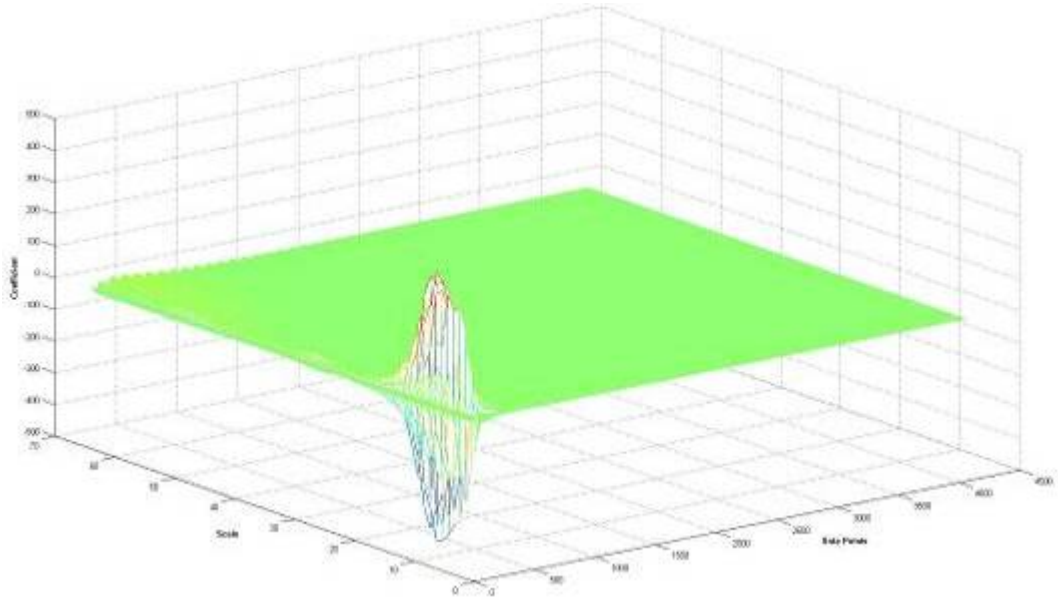

Figure 5.34 3D map of CWT coefficients of damage case 2 response data of point A2, db7 with scale 64

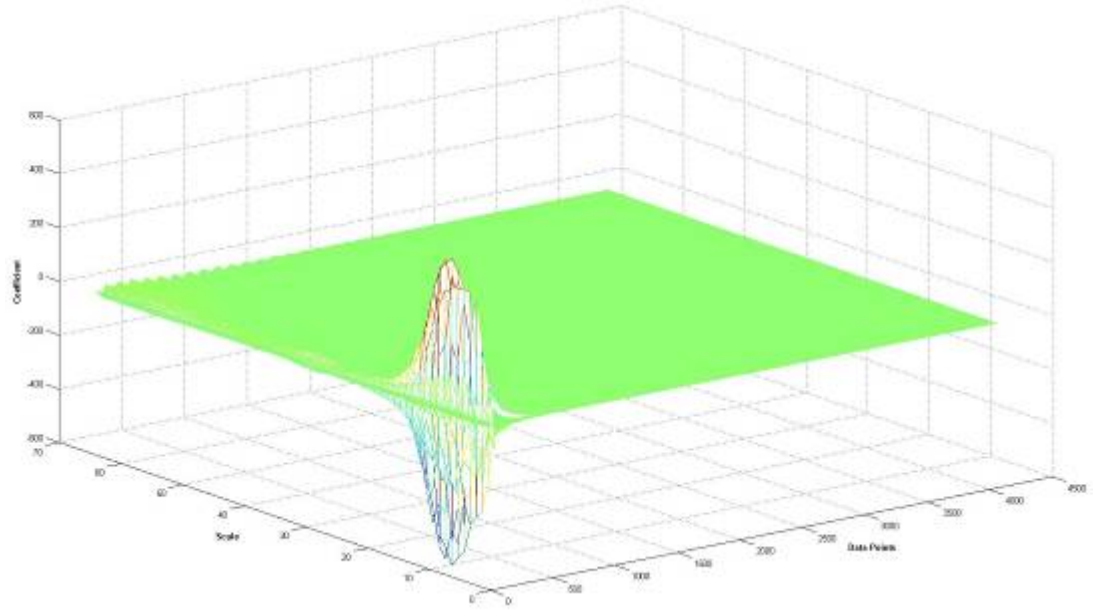

Figure 5.35 3D map of CWT coefficients of damage case 3 response data of point A2, db7 with scale 64

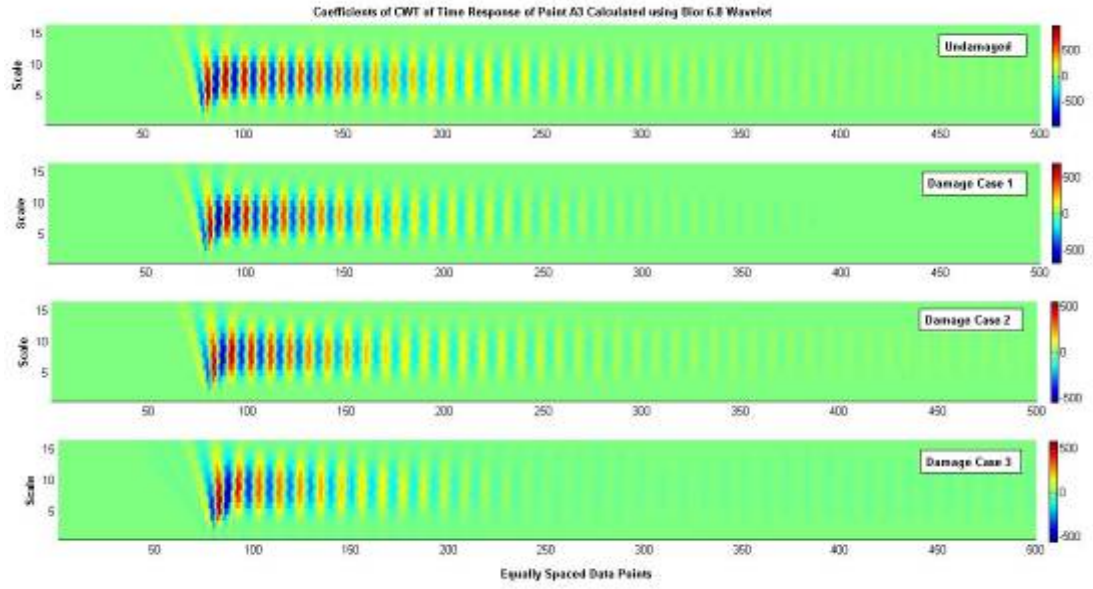

Figure 5.36 Coefficients of CWT of response data of point A3, bior 6.8 with scale 16

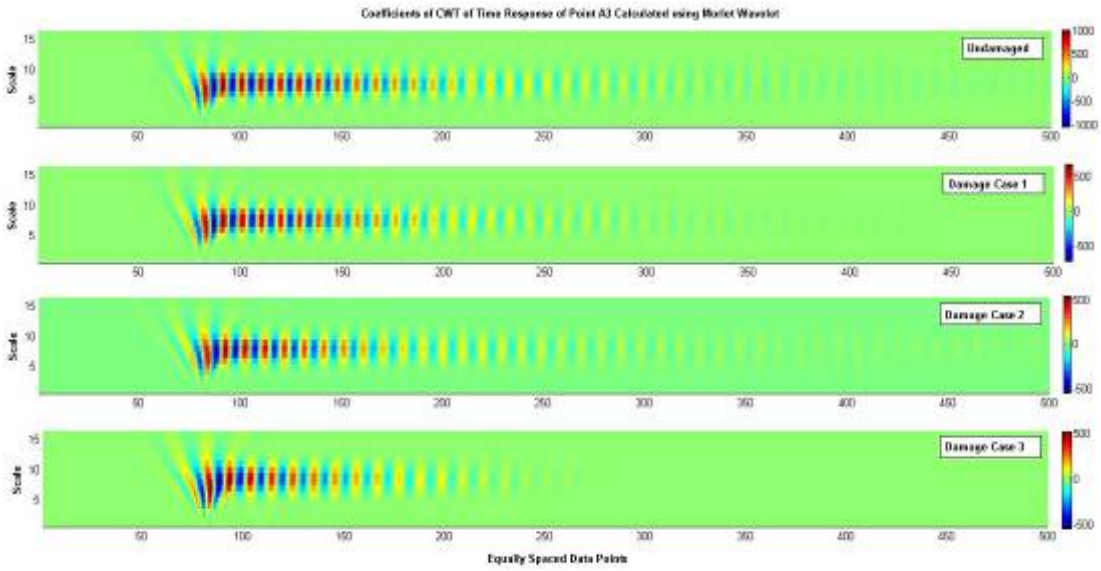

Figure 5.37 Coefficients of CWT of response data of point A3, morlet with scale 16

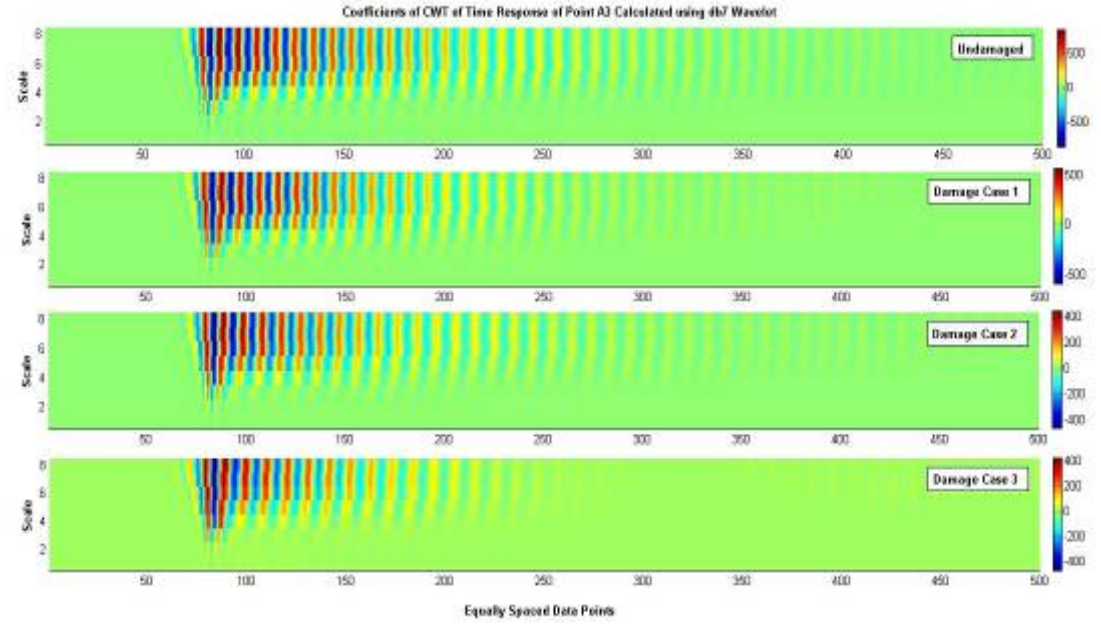

Figure 5.38 Coefficients of CWT of response data of point A3, db7 with scale 8

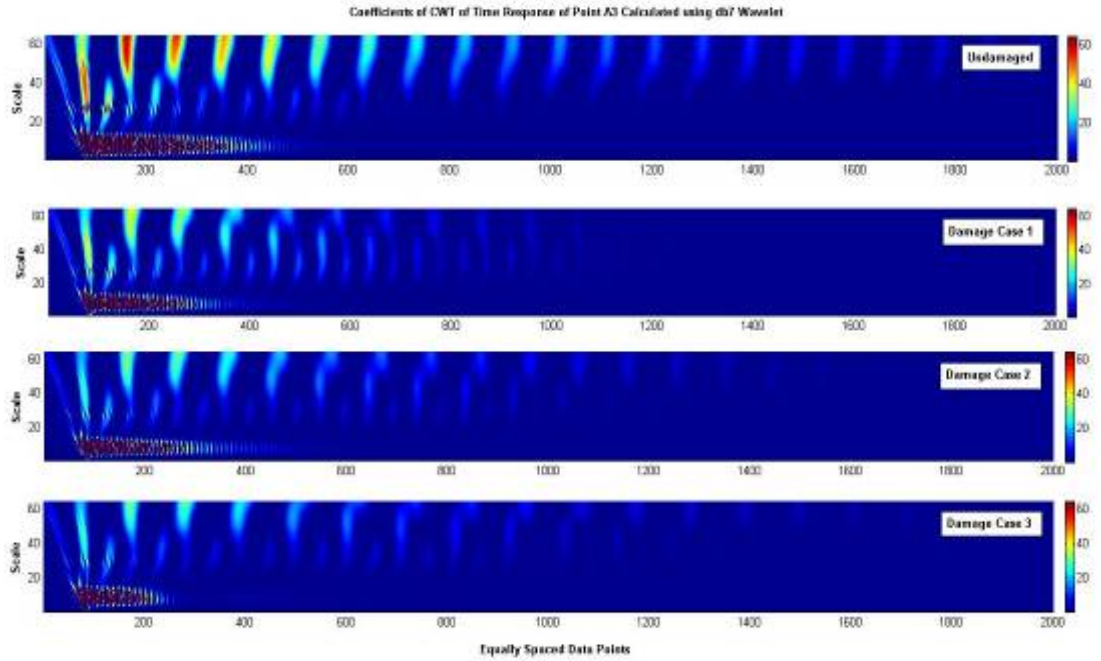

Figure 5.39 Coefficients of CWT of response data of point A3,db7 with scale 64

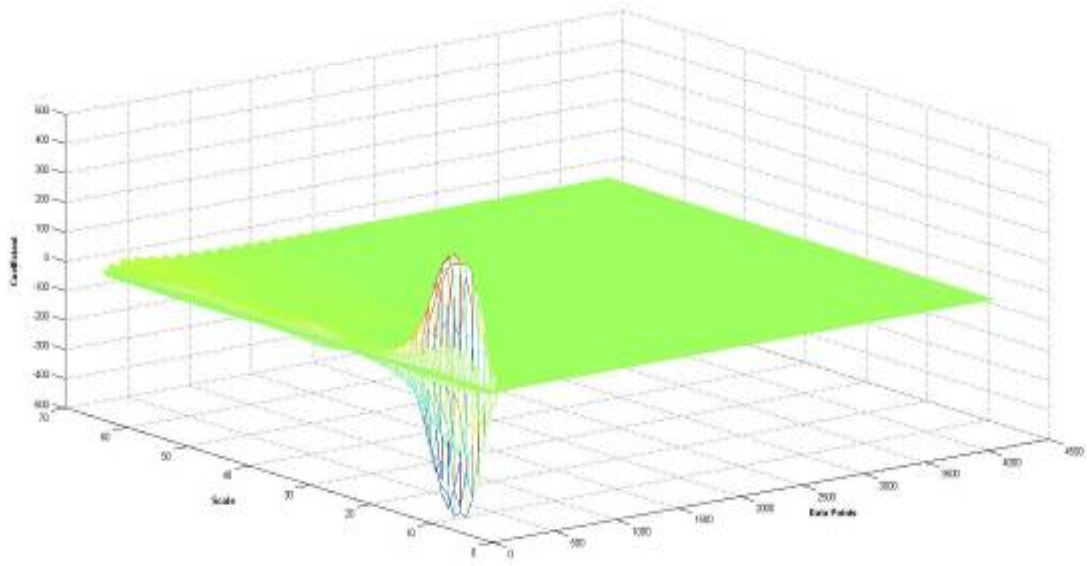

Figure 5.40 3D map of CWT coefficients of undamaged case response data of point A3,db7 with scale 64

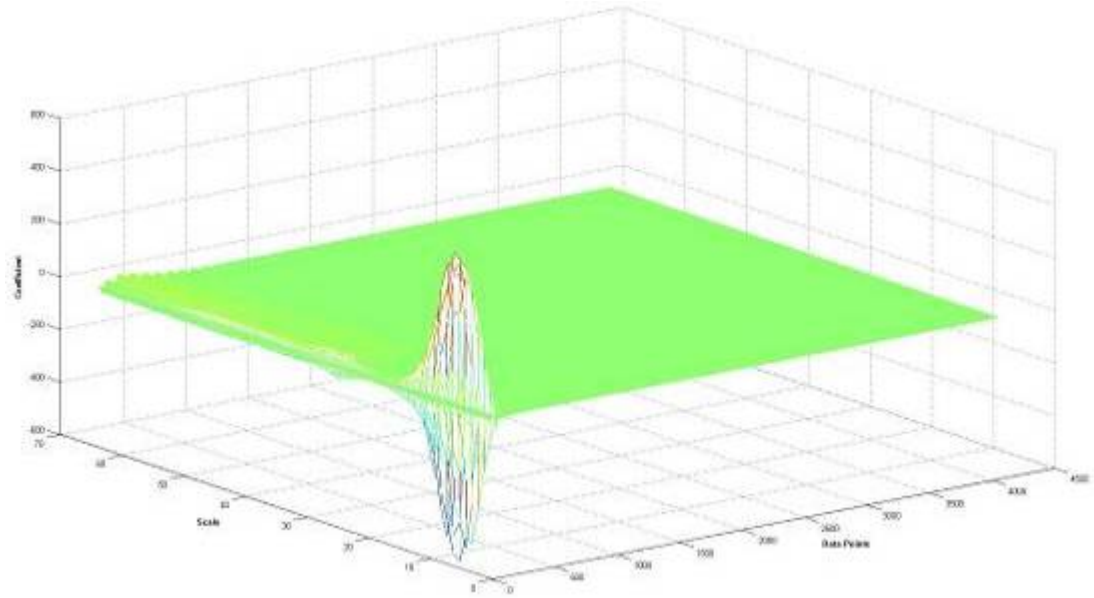

Figure 5.41 3D map of CWT coefficients of damage case 1 response data of point A3,db7 with scale 64

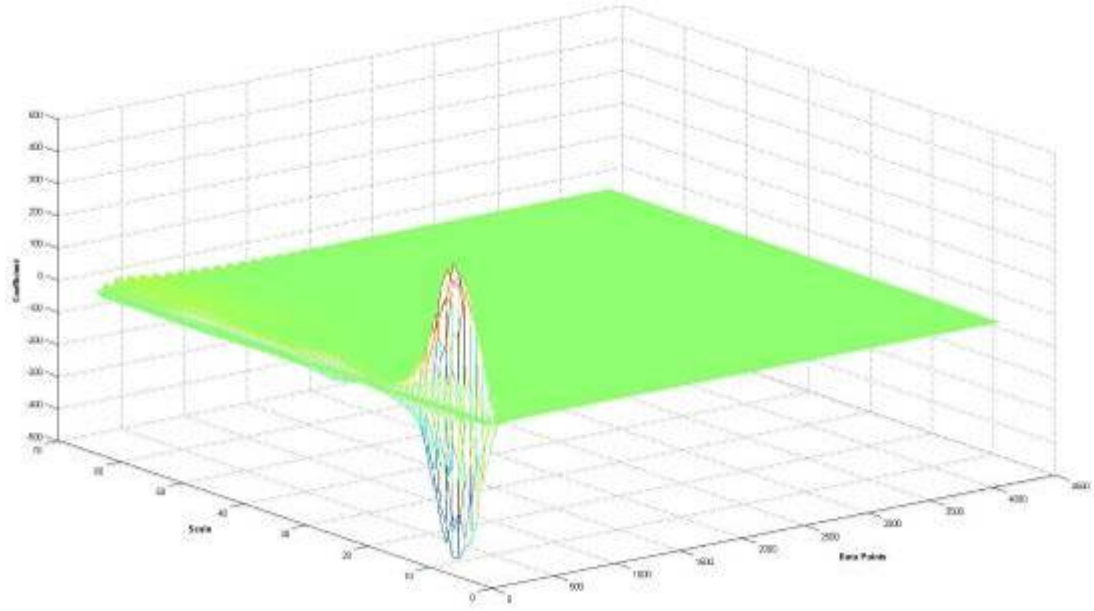

Figure 5.42 3D map of CWT coefficients of damaged case 2 response data of point A3,db7 with scale 64

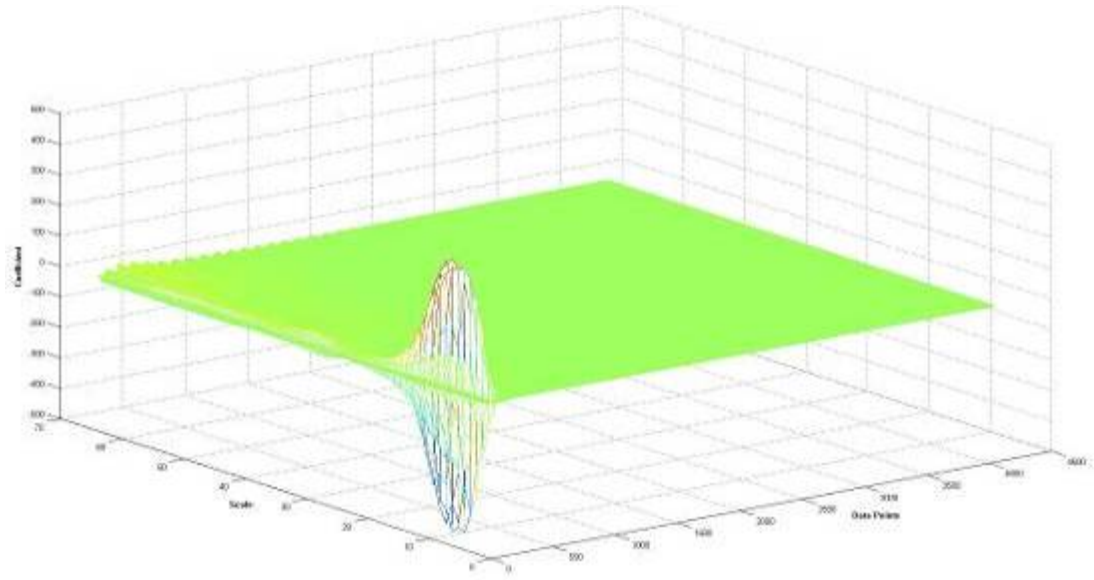

Figure 5.43 3D map of CWT coefficients of damaged case 3 response data of point A3,db7 with scale 64

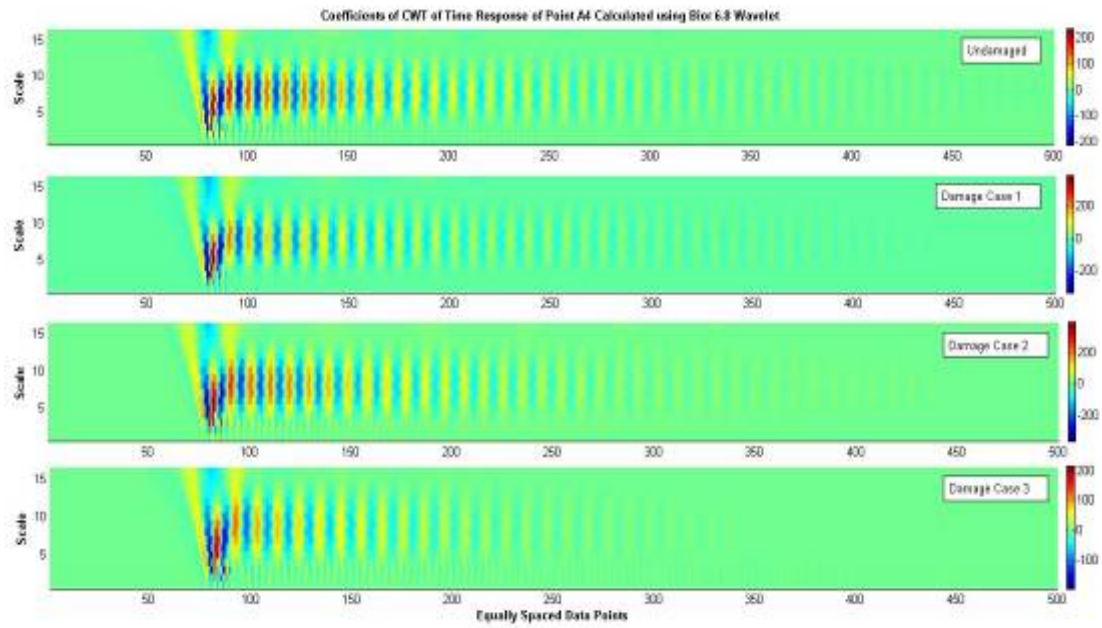

Figure 5.44 Coefficients of CWT of response data of point A4, bior 6.8 with scale 16

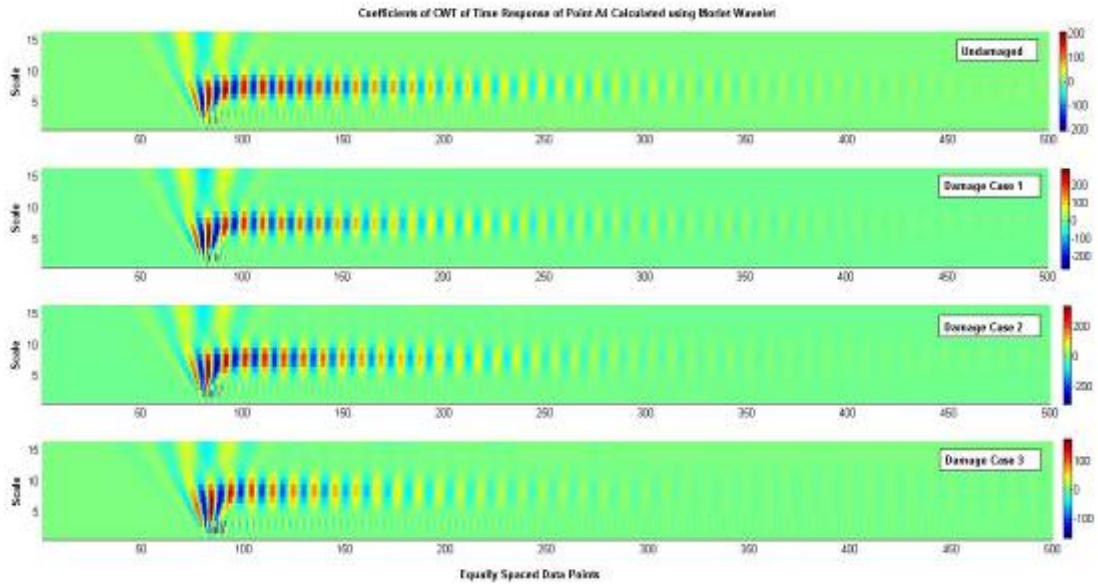

Figure 5.45 Coefficients of CWT of response data of point A4, morlet with scale 16

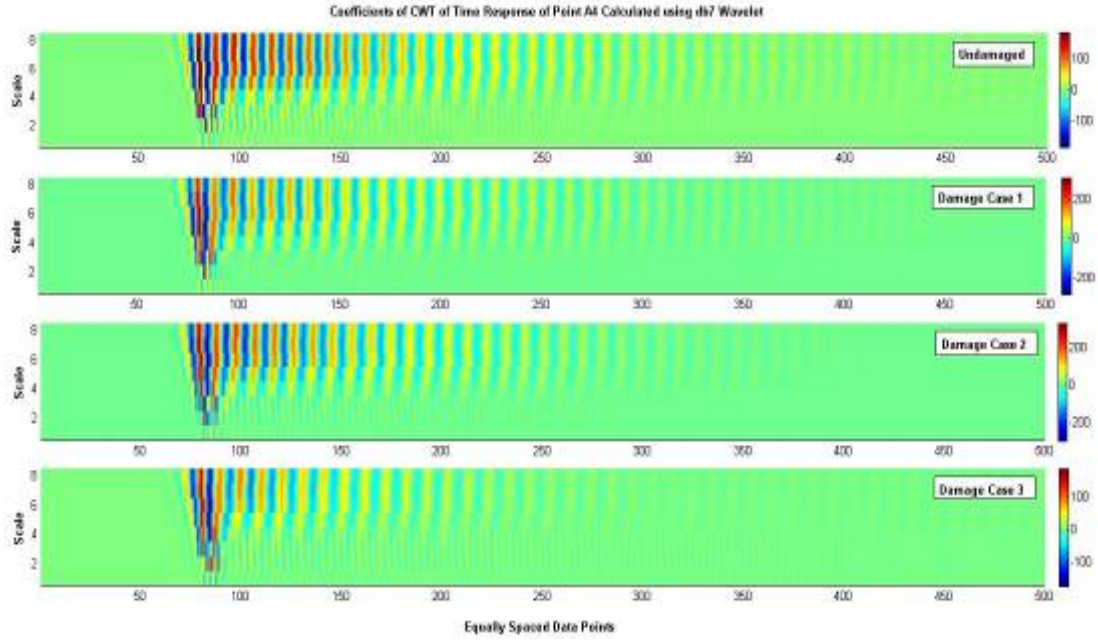

Figure 5.46 Coefficients of CWT of response data of point A4,db7 with scale 8

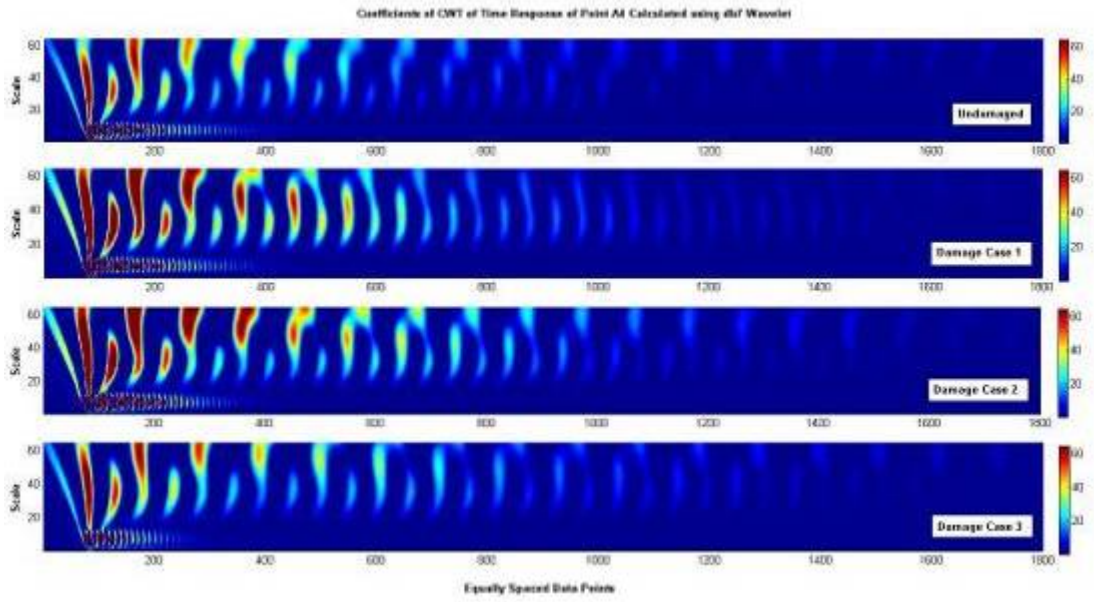

Figure 5.47 Coefficients of CWT of response data of point A4, db7 with scale 64

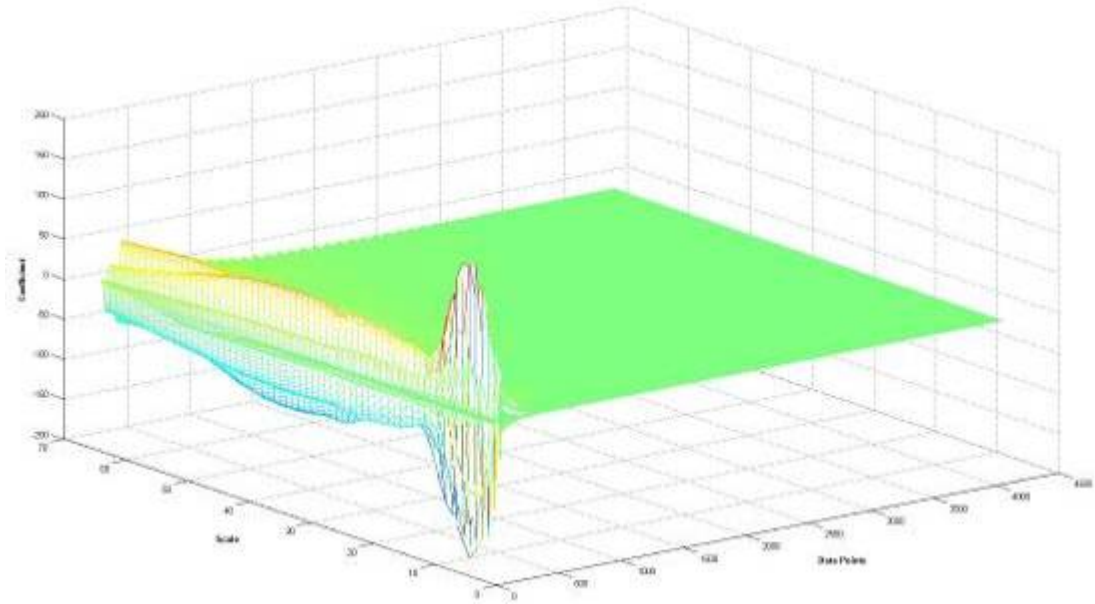

Figure 5.48 3D map of CWT coefficients of undamaged case response data of point A4, db7 with scale 64

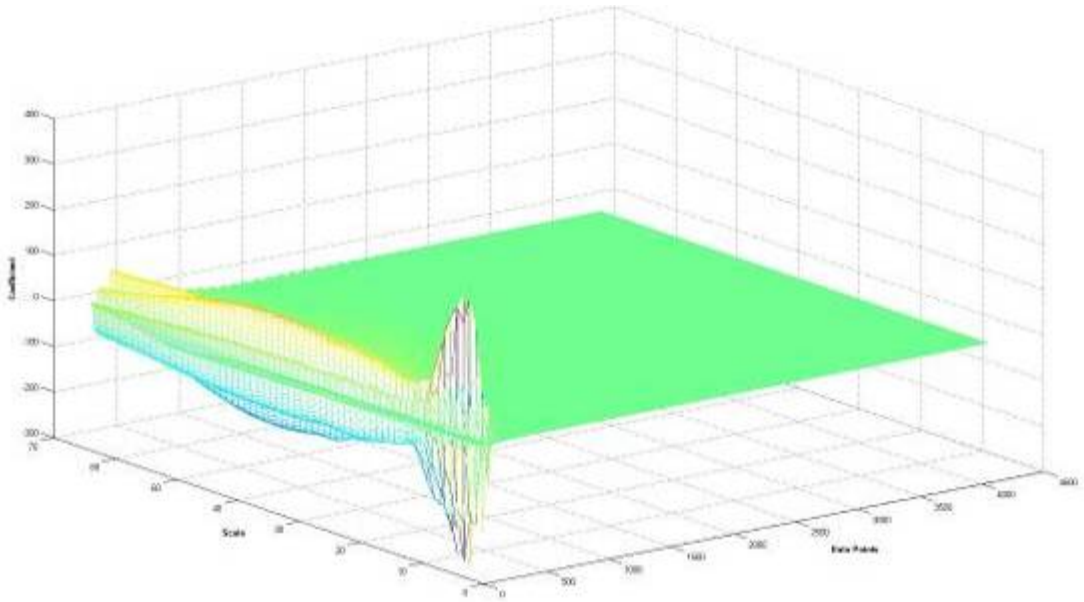

Figure 5.49 3D map of CWT coefficients of damaged case 1 response data of point A4, db7 with scale 64

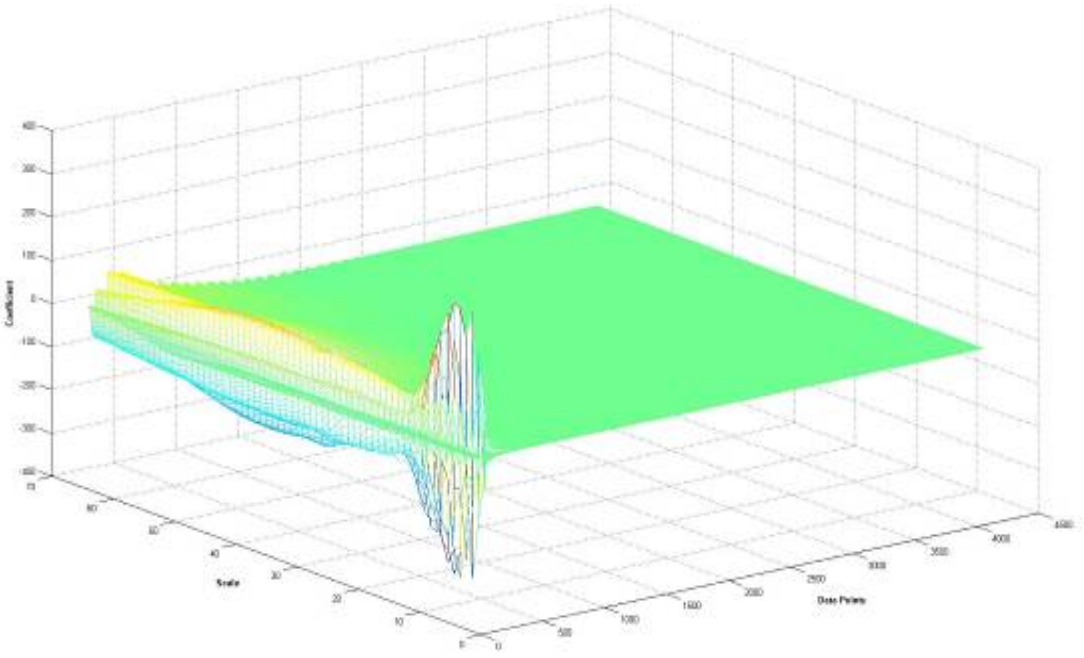

Figure 5.50 3D map of CWT coefficients of damaged case 2 response data of point A4, db7 with scale 64

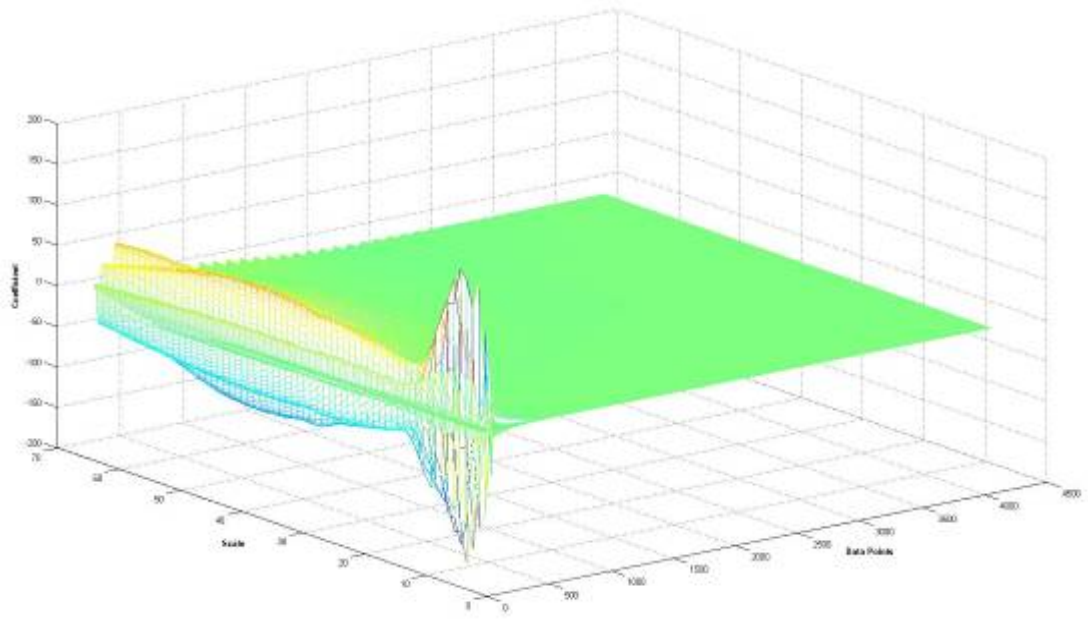

Figure 5.51 3D map of CWT coefficients of damaged case 3 response data of point A4, db7 with scale 64

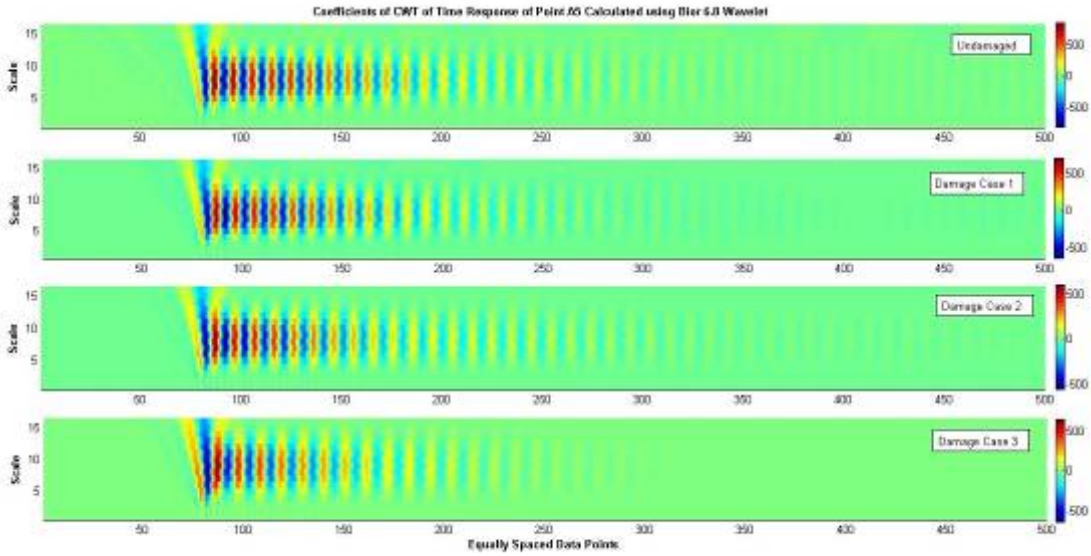

Figure 5.52 Coefficients of CWT of response data of point A5, bior 6.8 with scale 16

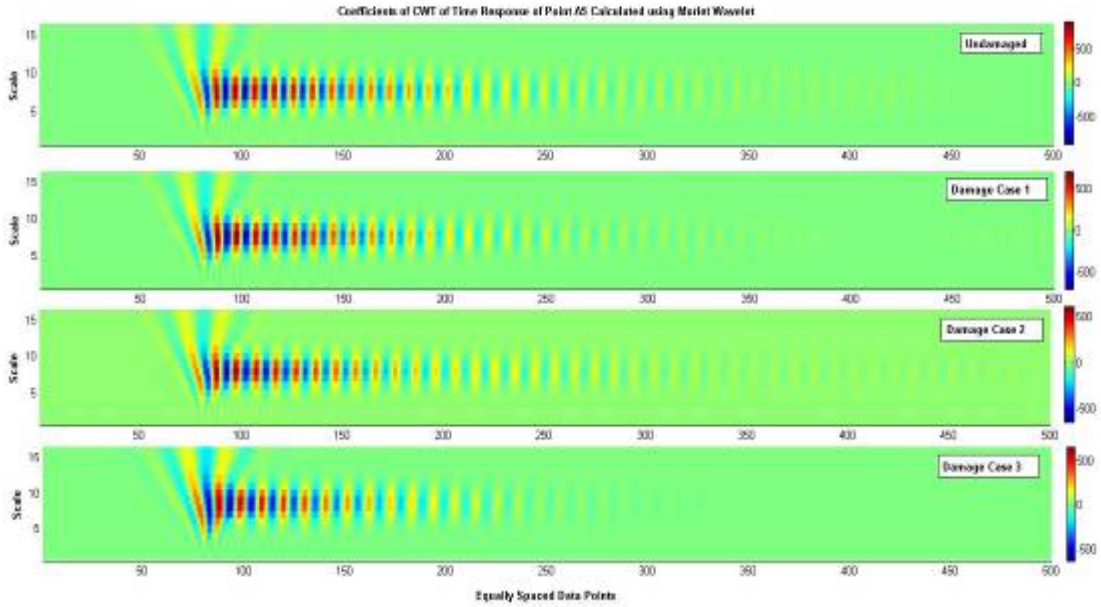

Figure 5.53 Coefficients of CWT of response data of point A5, morlet with scale 16

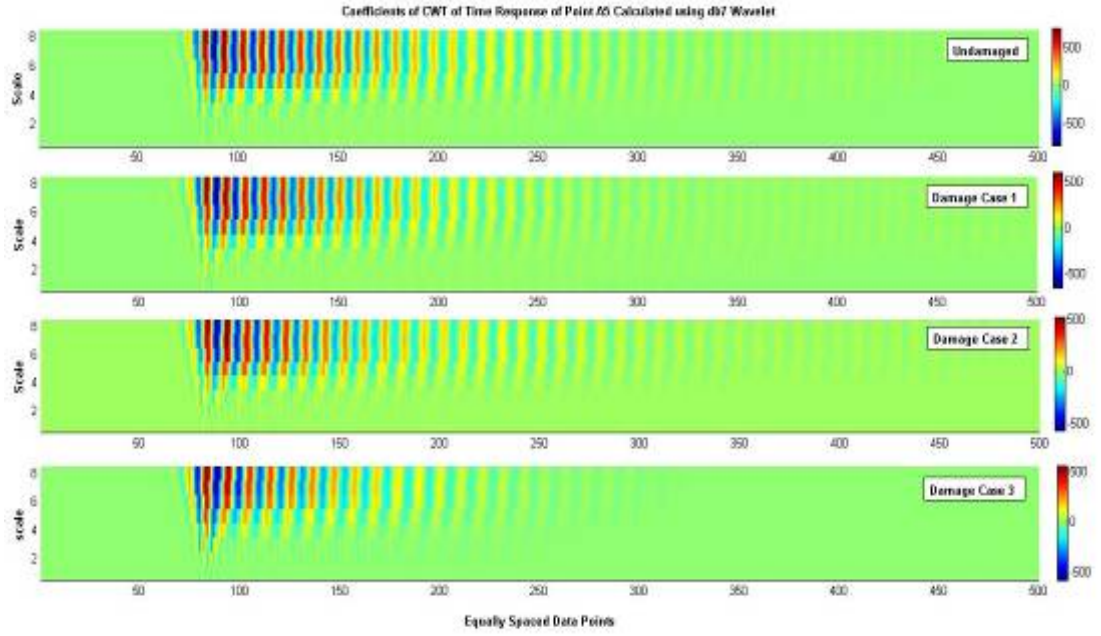

Figure 5.54 Coefficients of CWT of response data of point A5, db7 with scale 8

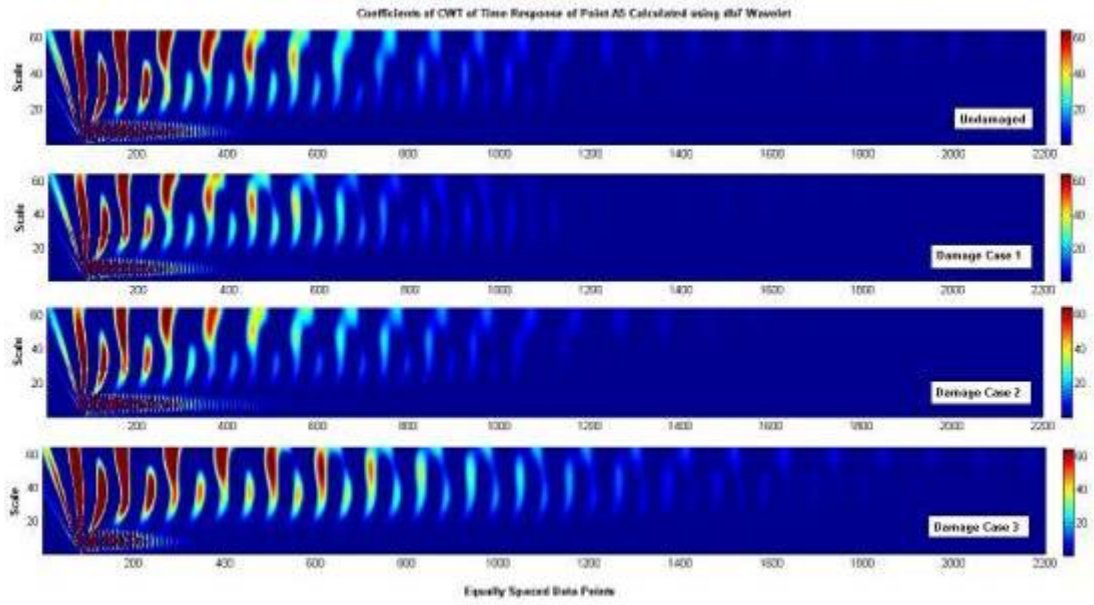

Figure 5.55 Coefficients of CWT of response data of point A5, db7 with scale 64

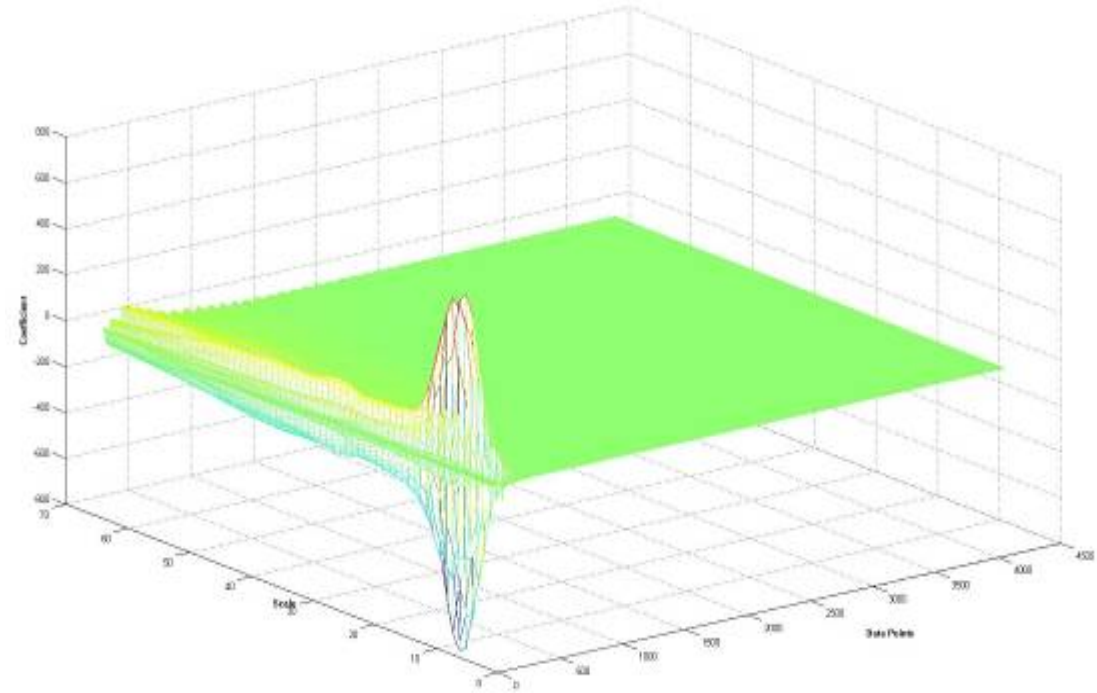

Figure 5.56 3D map of CWT coefficients of undamaged case response data of point A5, db7 with scale 64

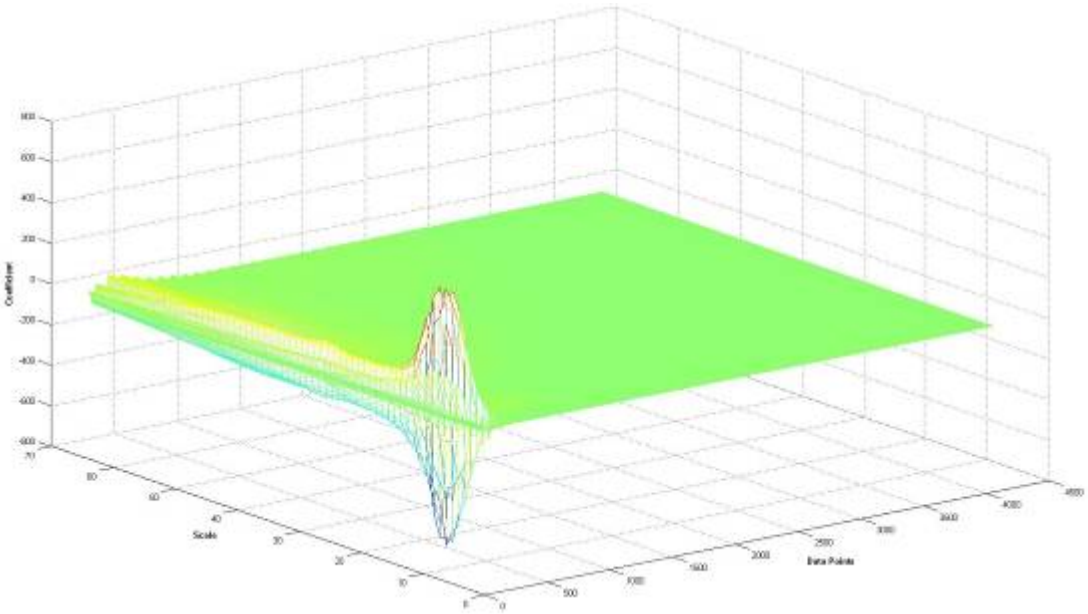

Figure 5.57 3D map of CWT coefficients of damaged case 1 response data of point A5, db7 with scale 64

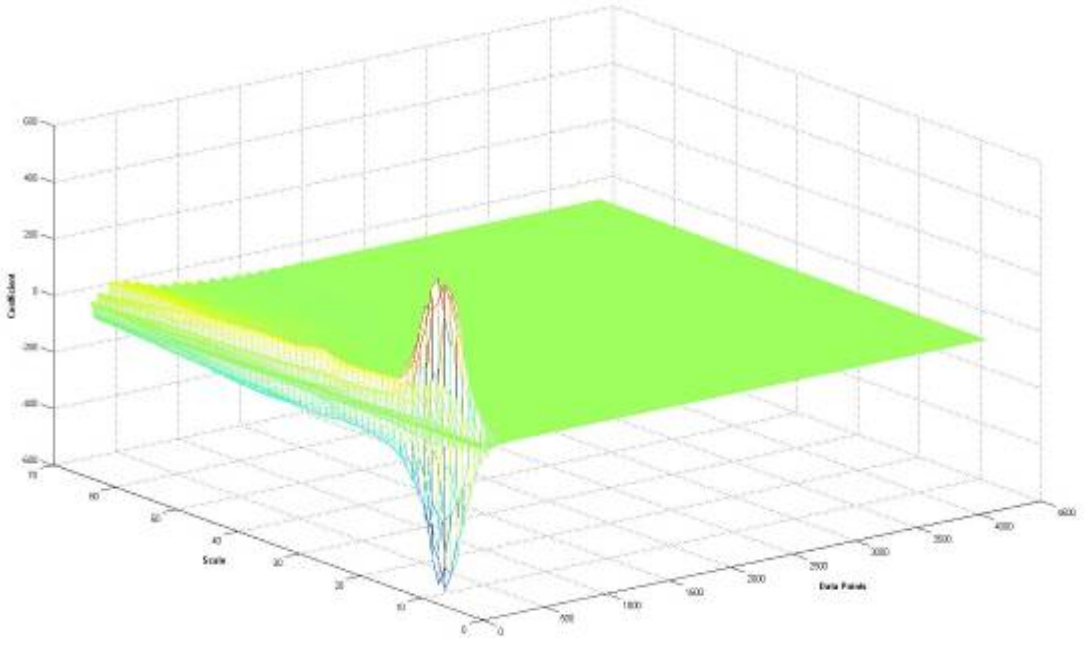

Figure 5.58 3D map of CWT coefficients of damaged case 2 response data of point A5, db7 with scale 64

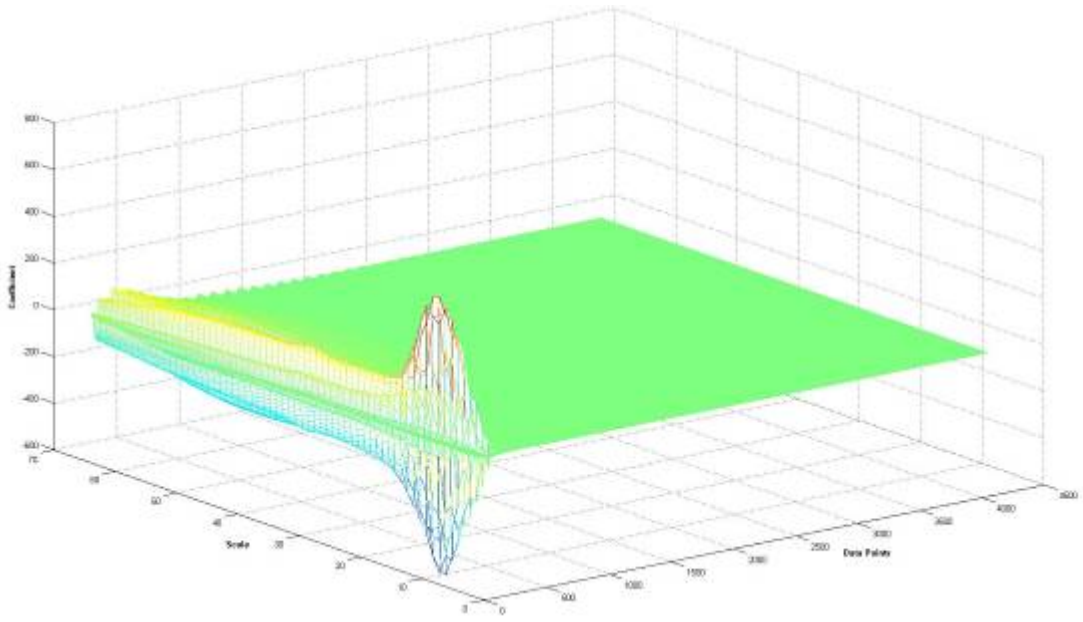

Figure 5.59 3D map of CWT coefficients of damaged case 3 response data of point A5, db7 with scale 64

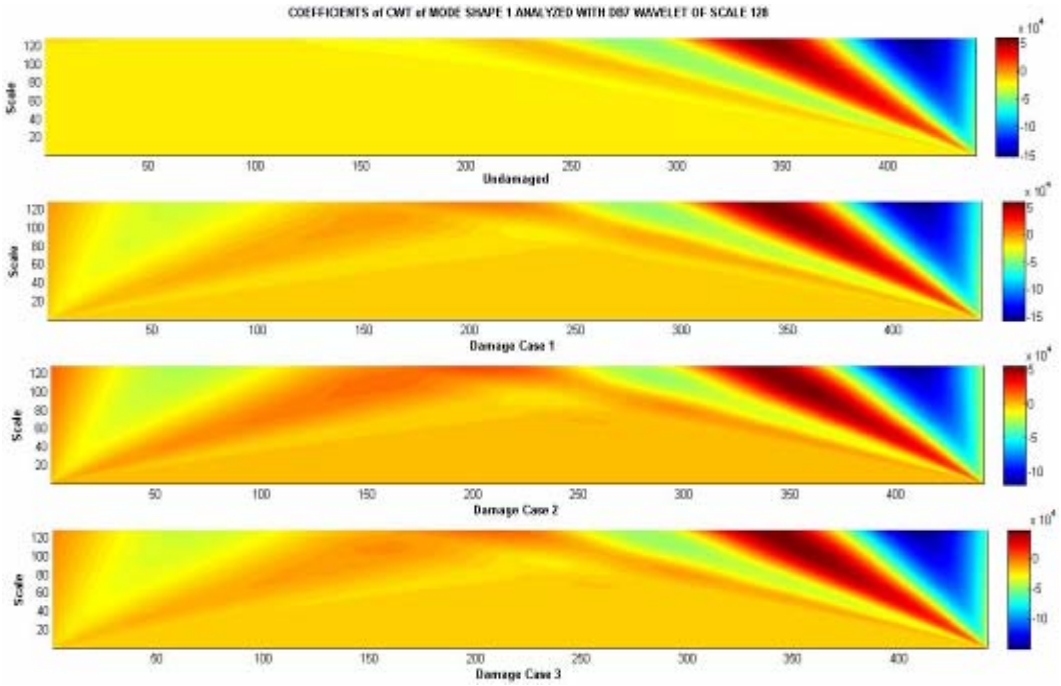

Figure 5.60 Coefficients of CWT of mode shape 1 data, db7 with scale 128

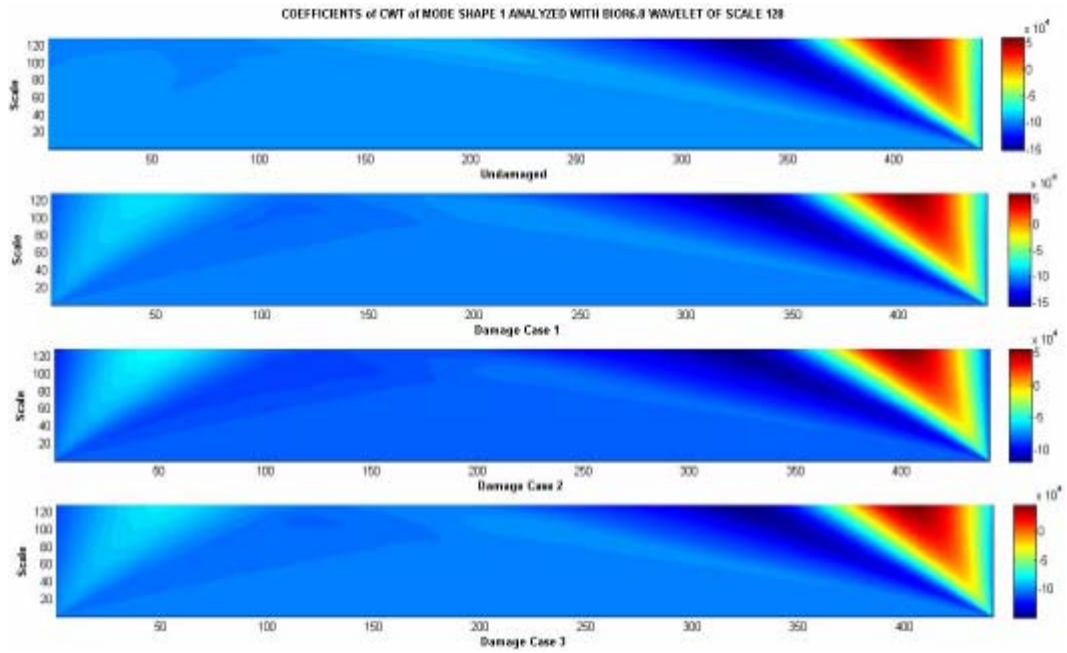

Figure 5.61 Coefficients of CWT of mode shape 1 data, bior 6.8 with scale 128

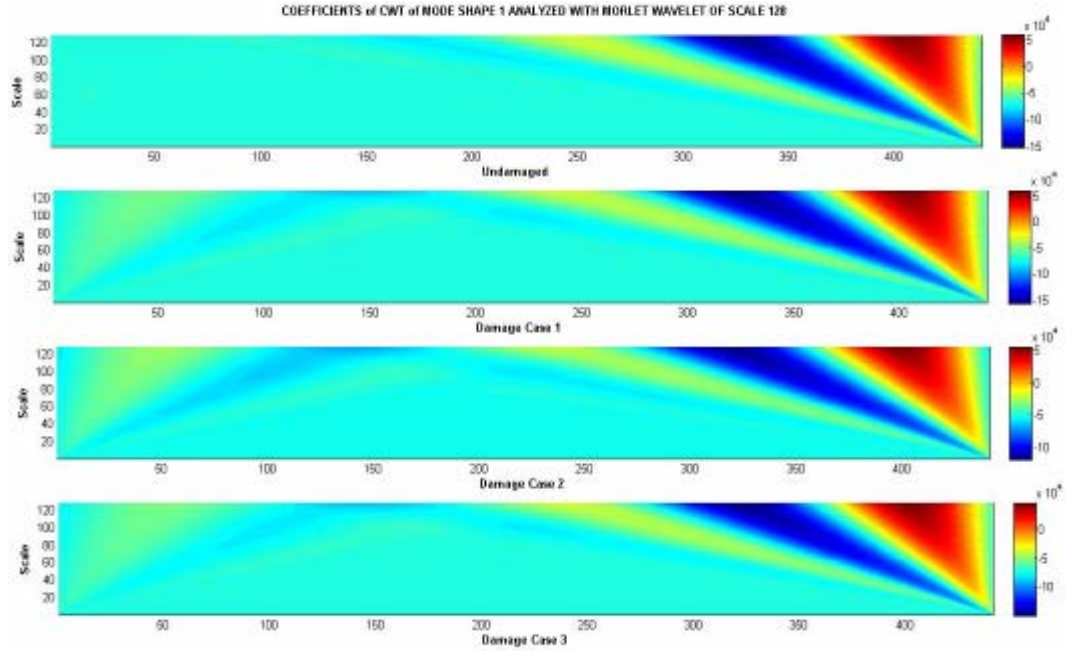

Figure 5.62 Coefficients of CWT of mode shape 1 data, morlet with scale 128

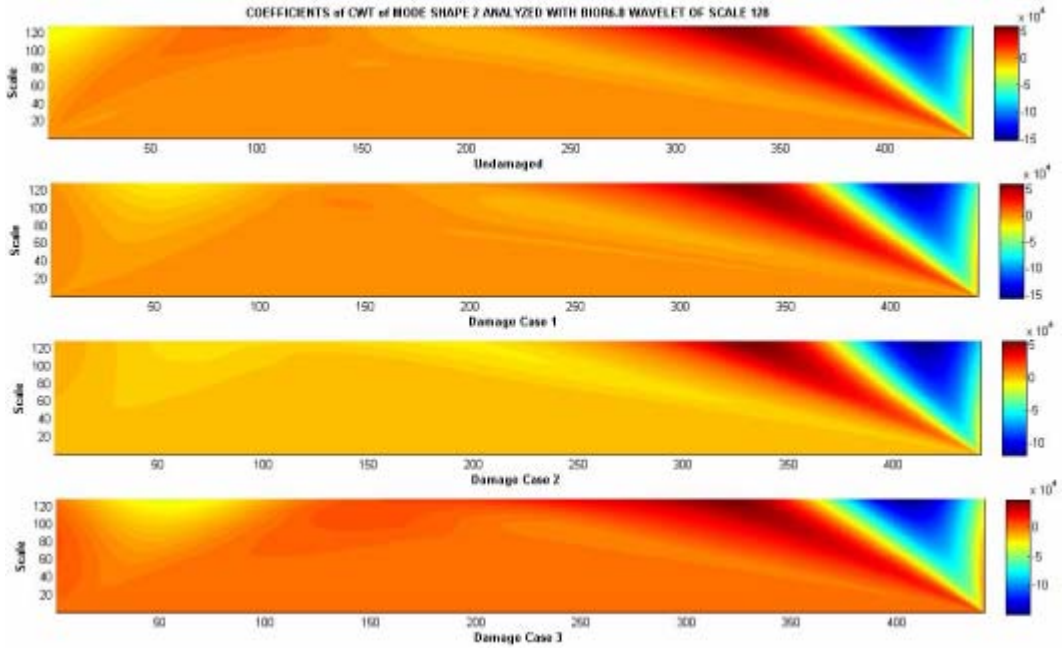

Figure 5.63 Coefficients of CWT of mode shape 2 data, bior 6.8 with scale 128

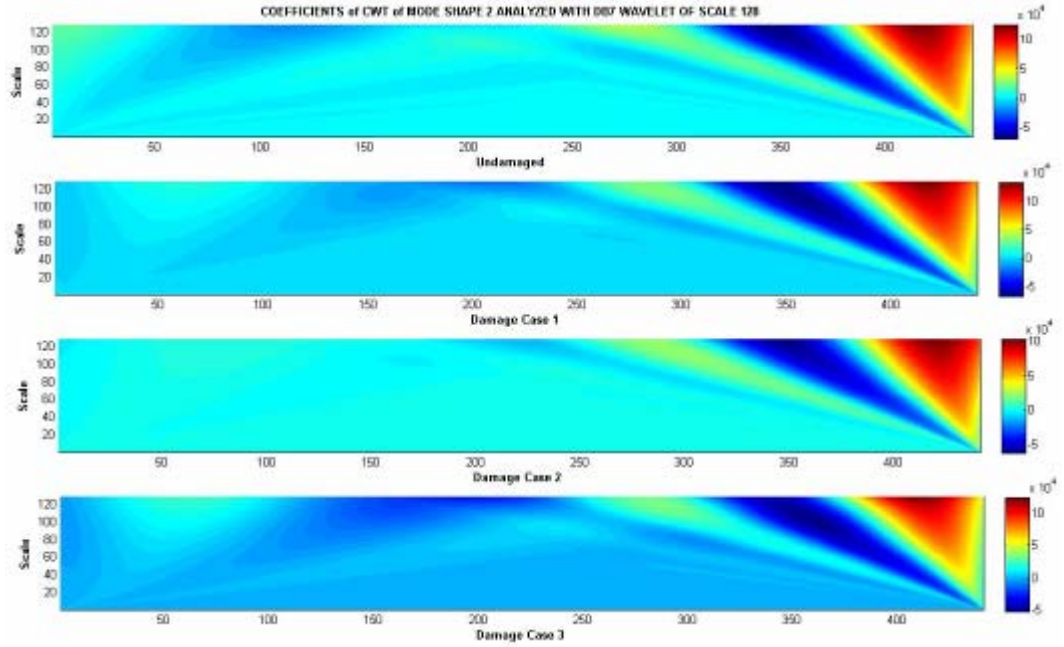

Figure 5.64 Coefficients of CWT of mode shape 2 data, db7 with scale 128

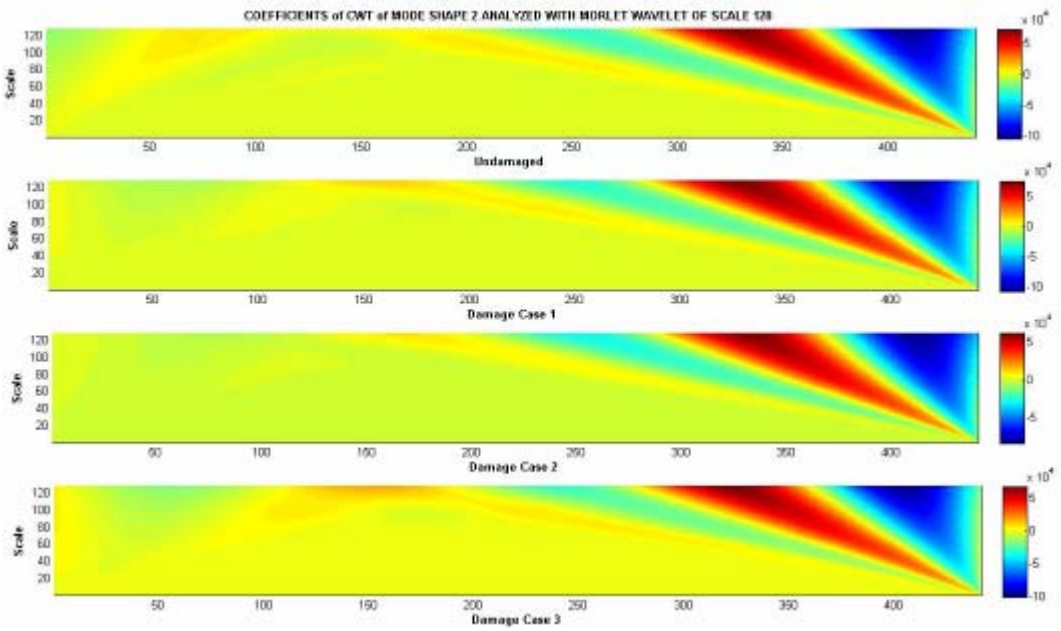

Figure 5.65 Coefficients of CWT of mode shape 2 data, morlet with scale 128

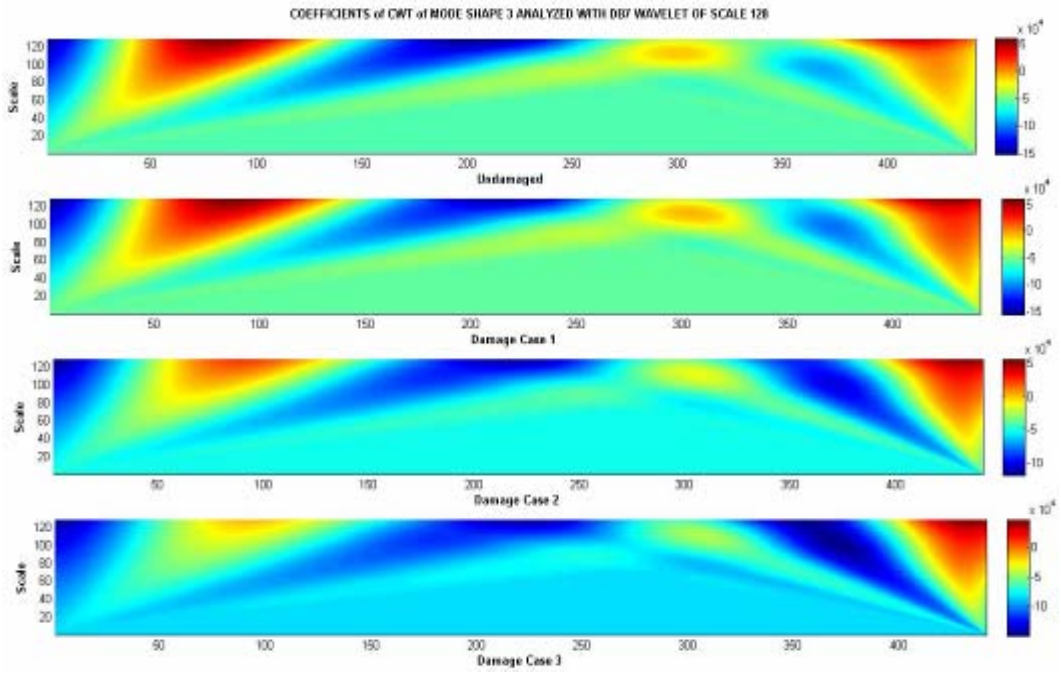

Figure 5.66 Coefficients of CWT of mode shape 3 data, db7 with scale 128

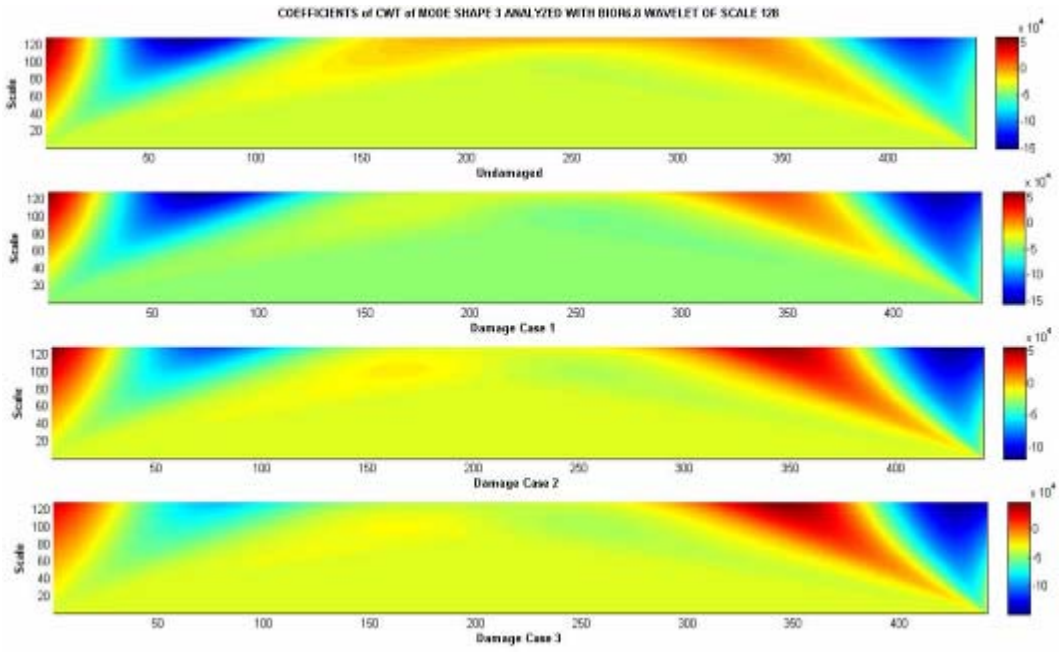

Figure 5.67 Coefficients of CWT of mode shape 3 data, bior 6.8 with scale 128

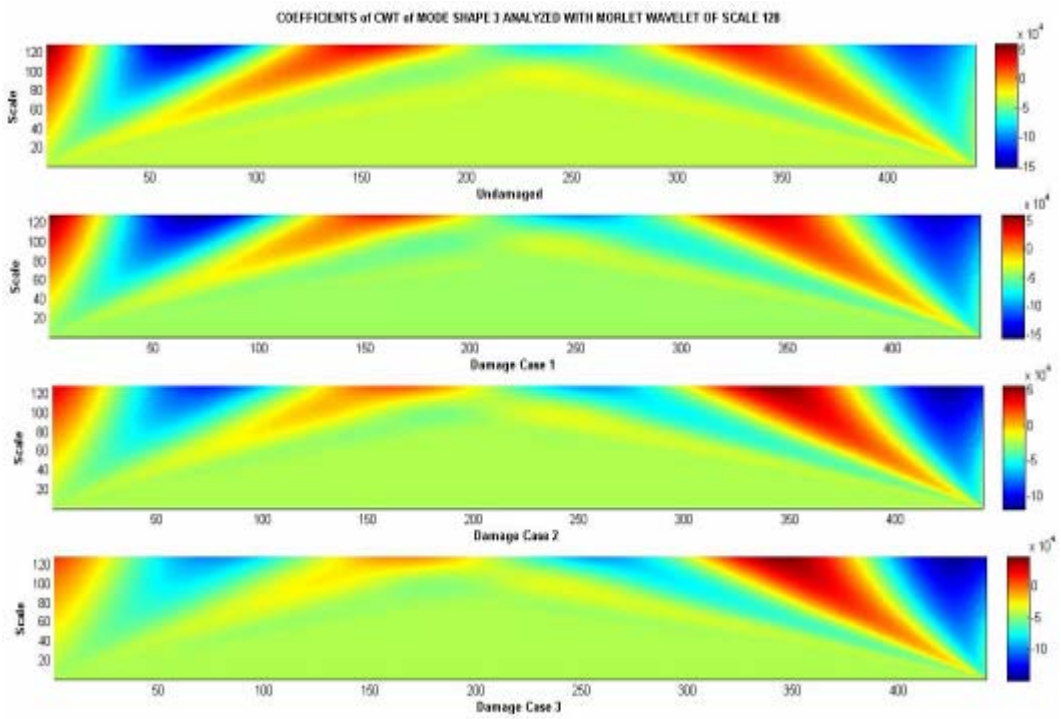

Figure 5.68 Coefficients of CWT of mode shape 3 data, morlet with scale 128

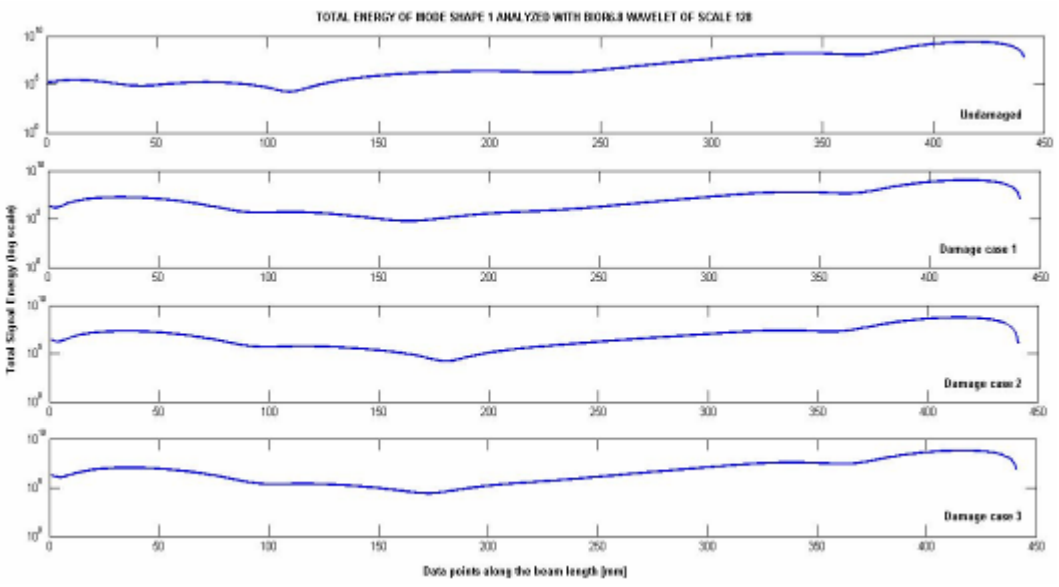

Figure 5.69 Total energy of mode shape 1 data processed with bior 6.8 at scale 128

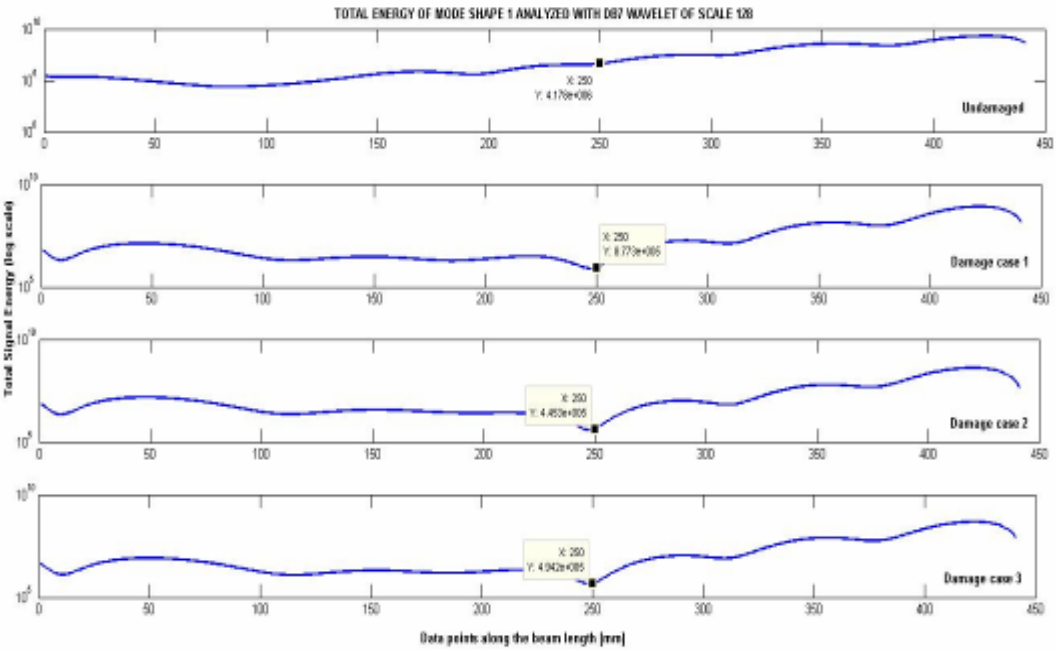

Figure 5.70 Total energy of mode shape 1 data processed with db7 at scale 128

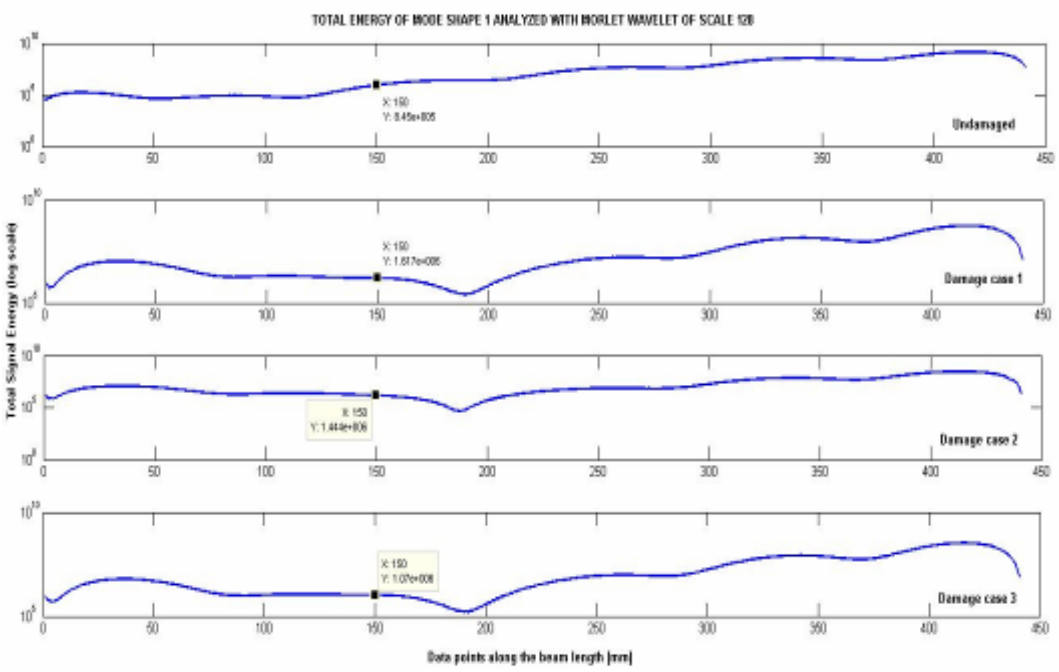

Figure 5.71 Total energy of mode shape 1 data processed with morlet at scale 128

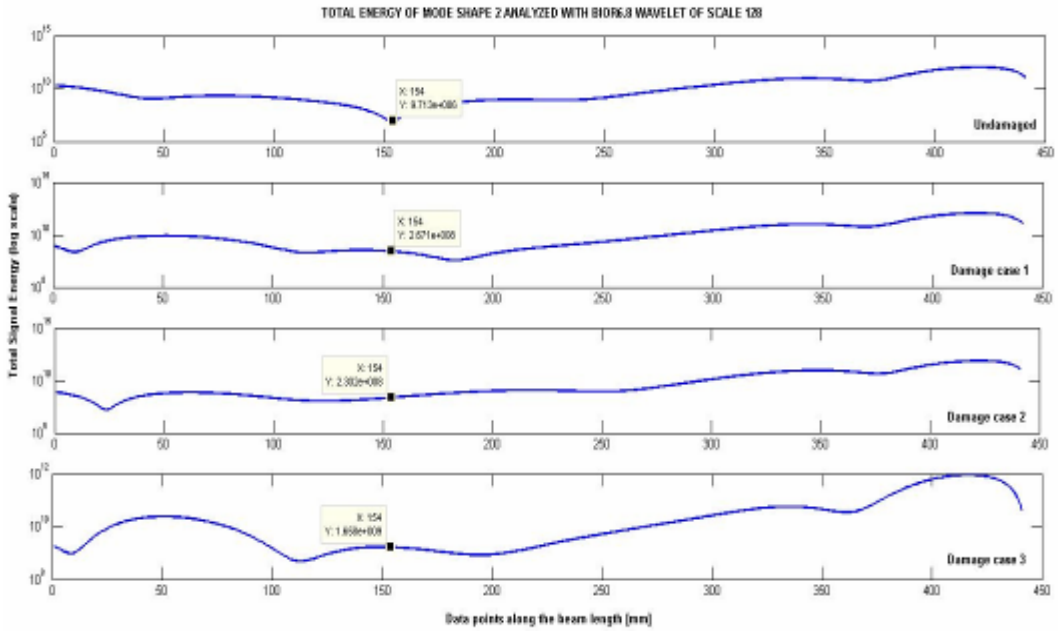

Figure 5.72 Total energy of mode shape 2 data processed with bior 6.8 at scale 128

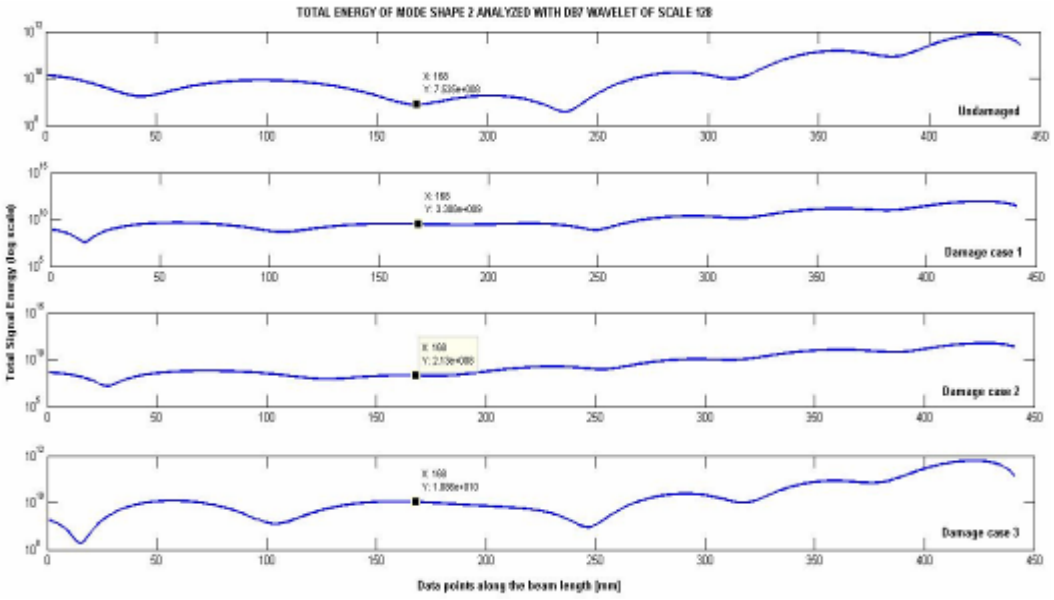

Figure 5.73 Total energy of mode shape 2 data processed with db7 at scale 128

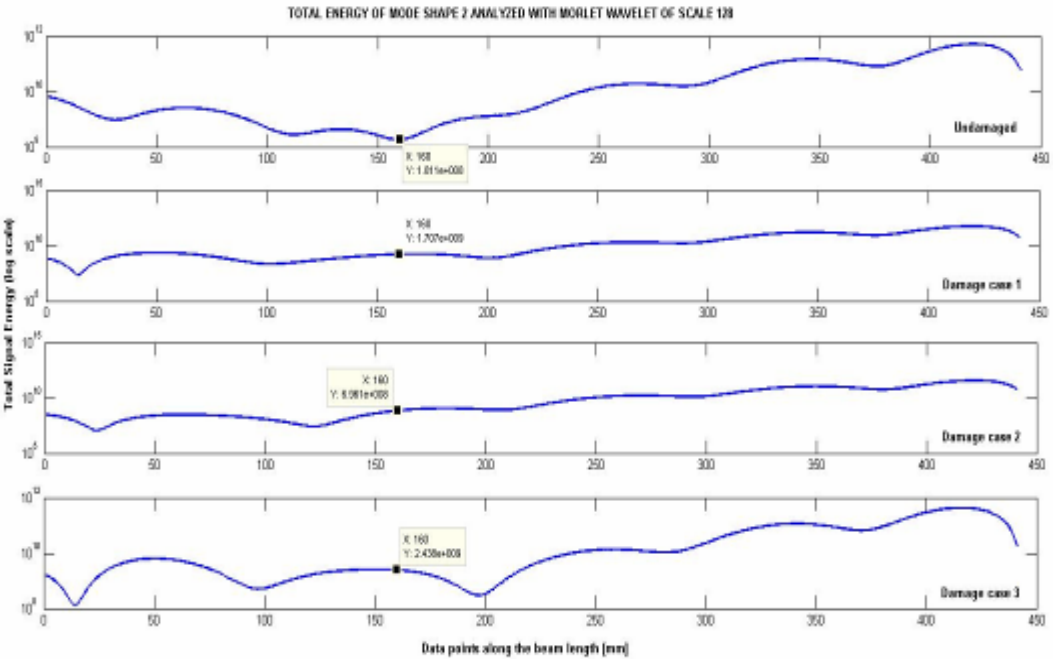

Figure 5.74 Total energy of mode shape 2 data processed with morlet at scale 128

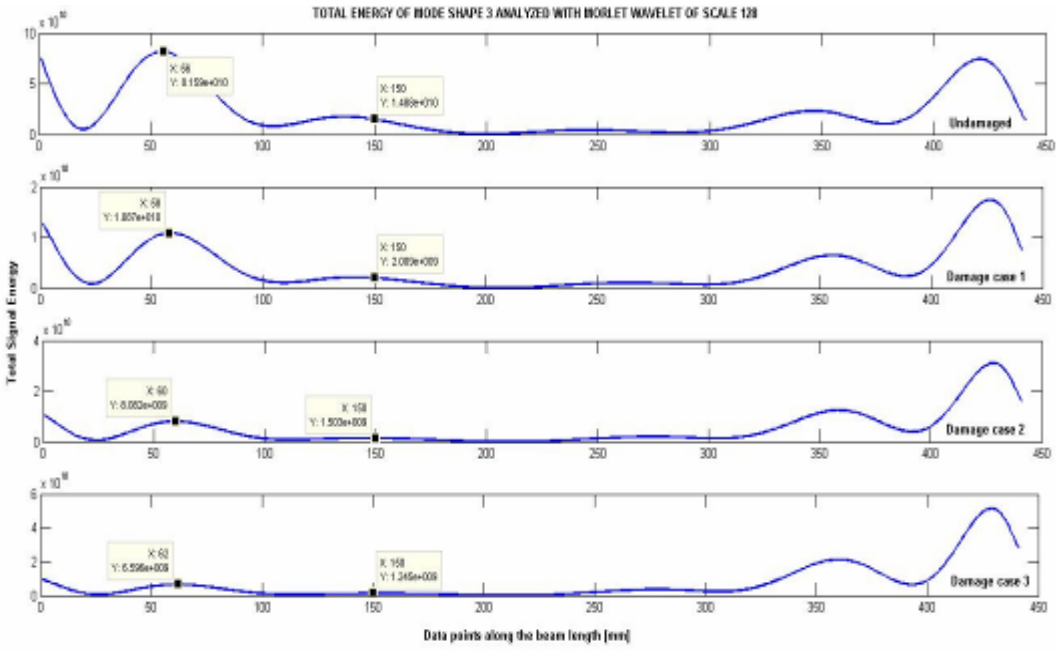

Figure 5.75 Total energy of mode shape 3 data processed with morlet at scale 128

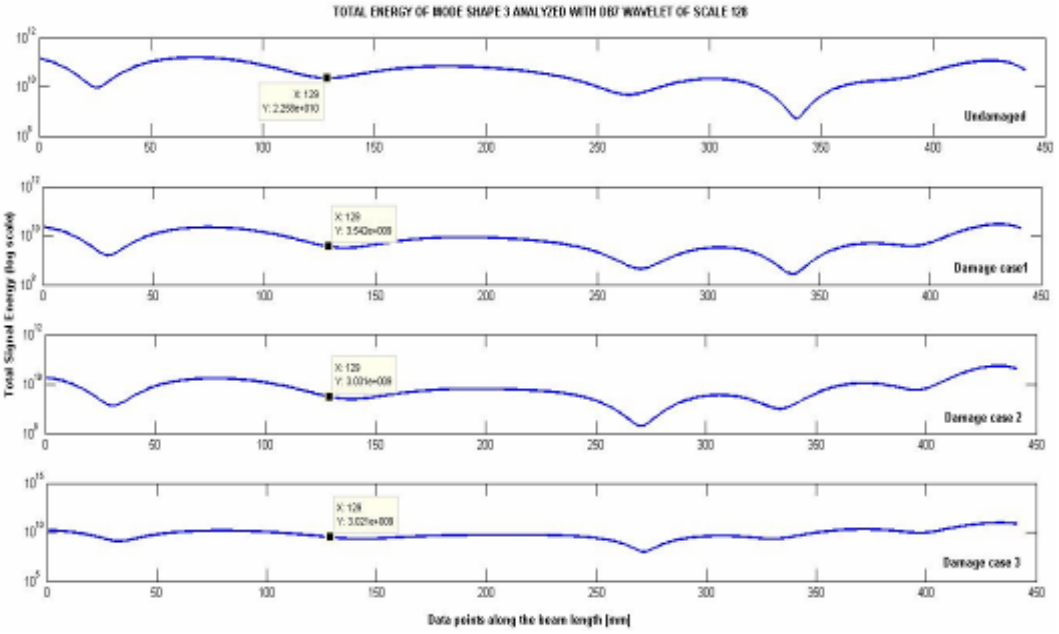

Figure 5.76 Total energy of mode shape 3 data processed with db7 at scale 128

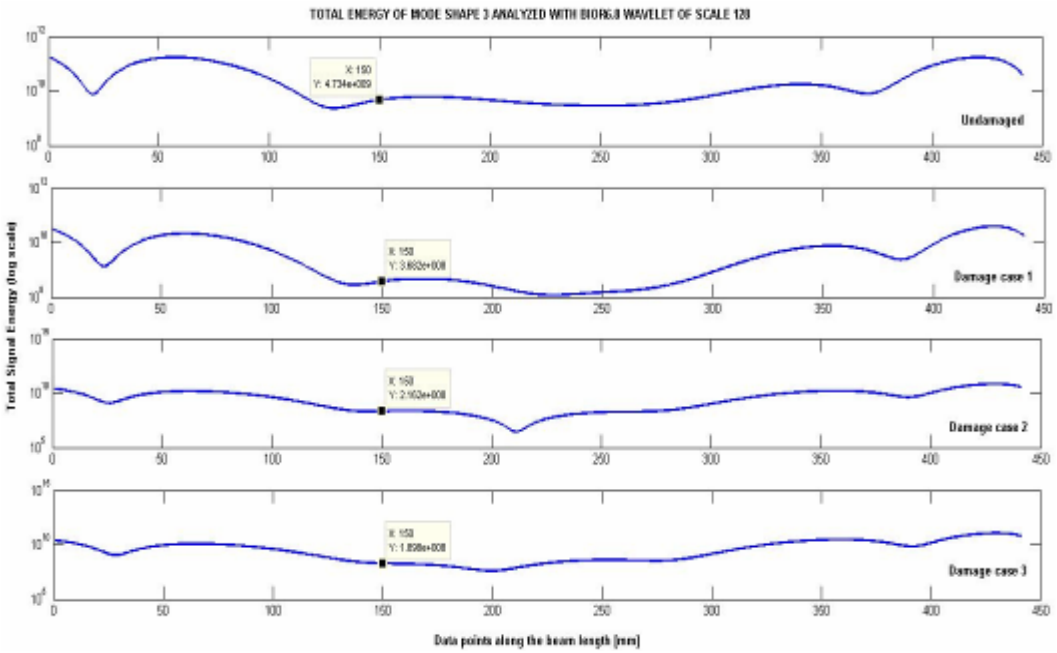

Figure 5.77 Total energy of mode shape 3 data processed with bior 6.8 at scale 128

CHAPTER 6

SUMMARY AND CONCLUSIONS

In this thesis, different damage assessment methods for identification of damages in structural systems were studied. The methods used the experimentally measured acceleration signals obtained at various damage levels as the input in the analysis process. Acceleration data was acquired from a cantilever beam with a cut in varying depths. Natural frequencies, mode shapes and FRFs were used as the modal indicators of damage whereas magnitudes of CWT coefficients and energy indices calculated from these coefficients were utilized as the wavelet indicators of damage.

When components develop structural damages like a cut, then the dynamic behavior of the component start to change as dimensional properties of the cut change. The bulk of research conducted in the past concentrated mainly on the effect of crack on natural frequencies, mode shapes and FRFs. Also, there were some separate works studying the effect of crack on wavelet transform coefficients obtained by using a specific mother wavelet and the energy indices calculated from the wavelet transform results. In this study, performance of several different methods in detection and localization of a cut was aimed in parallel to previous studies. Also, a comparison of results obtained by using different mother wavelets in the CWT analysis of response data was conducted.

One of the methods used for the damage identification was an extension of a method recently developed in another study[40]. In order to verify the method's capability and also compare the results with that of other methods in detecting and locating cut type damage, the time response data of a cracked beam which was damaged at various levels were recorded and processed.

A number of case studies were performed to demonstrate the applicability of the suggested technique and also compare it with different methods. Case studies performed indicated that suggested method was good at detecting the presence of a cut. The method's output was also consistent with the damage level. It should be noted that for the wavelet analysis two different types of input data was used: one being the transverse vibration response of various measurement points along the tested beam while the other one was the corresponding mode shape data of the tested beam. Each analysis was repeated for each damage level. The methods that were successful in damage detection are CWT scale wise energy indices and CWT coefficients of first three mode shapes.

For the identification of the size of a cut, satisfactory results were not obtained. Yet the modified method of wavelet transform energy rate indices suggested some relation between the energy level and the cut depth which was the only parameter that was altered during the tests. The normalization of the calculated energy indices was done in order to exclude the effect of forcing amplitude on the identification of the cut.

It should be noted that for the modal analysis, only the first three modal parameters were used. Results of these methods suggested the presence of a cut, yet to give any information for the position of the cut along the beam length. Modal and FRF results were the least informative among the modal analysis results with the exception of the first mode.

The forcing position for all the measurements was kept the same on the beam, i.e., the excited modes was always the same, which could play an important role in the modal as well as in the sensitivity of wavelet analysis results in damage identification process. Moreover, only three different mother wavelets were utilized in the CWT process where the scaling level of decomposition was limited by a certain value. The reasons of this limitation were the limited data points of the analyzed signal and the length of time required for analyses. Furthermore, mode shape data that was analyzed was obtained through curve fitting tool of Microsoft Excel XP ® which fit a polynomial curve to each measured mode shape data. In general, the informative part of a signal is found in the lower frequency region. This is exactly where the most substantial changes were observed in the two dimensional (2D) map, which was actually three dimensional (3D), of CWT coefficients for various damage levels.

It has been concluded that energy rate indices associated with CWT coefficients promise to be most indicative and open for development tool for the assessment of the damage for the beam under the test. The versatility of this tool lies in the insensitivity to the type of mother wavelet used in the analysis.

The study can further be extended to include the higher modal parameters in order to predict crack parameters, such as depth of crack. Also the excitation point of the impulse forcing can be altered in order to excite different modes of the structure being tested. The position of sensors must be also taken into account which may also cause to miss some modes that could be sensitive to damage. For the wavelet analysis part the followings can be further investigated:

- Effect of many different mother wavelets in the results of CWT for damage identification can be tested since every wavelet type has different characteristic properties,

- Number of scales used for the CWT process can be increased so that the effect of coefficients obtained at higher scales, i.e., lower frequencies, can be observed,
- More accurate mode shape data as the input to the CWT process can yield better results,
- Energy calculations based on the CWT of mode shape data can be done at some larger intervals of the horizontal length of the beam instead of point by point calculations. This is anticipated to yield better results.

Finally, the wavelet analysis methods used may also be tested by variations in the crack position as well as the material of the tested beam.

REFERENCES

[1] Doebling, S.W., Farrar, C.R., Prime, M.B., 1998. A summary review of vibration-based damage identification methods. Shock and Vibration Digest 30 (2), 91–105.

[2] Doebling S. W., Farrar C. R., Prime M. B. and Shevitz D. W., 1996. Damage Identification and Health Monitoring of Structural and Mechanical Systems from Changes In Their Vibration Characteristics; a Literature Review. Report No: LA-13070-MS, Los Alamos National Laboratory.

[3] Jian-Gang Han ,Wei-Xin Ren, Zeng-Shou Sun, 2005. Wavelet packet based damage identification of beam structures. International Journal of Solids and Structures (42), 6610–6627.

[4] Ren, W.X., DeRoeck, G., 2002a,b. Structural damage identification using modal data. I: Simulation verification. II: Test verification. Journal of Structural Engineering, ASCE 128 (1), 87–95, 96–104.

[5] Farrar, C.R., Doebling, S.W., Duffey, T.A., 1999. Vibration-based damage detection. In: SD2000, Struct. Dyn. Forum.

[6] Gabor, D., 1946. Theory of communication. IEEE Journal (21), 149–157.

[7] Daubechies, I., 1992. Ten Lectures on Wavelets. CBMS-NSF Regional Conference Series in Applied Mathematics. Dept. Of Mathematics, Univ. Of Lowell, MA, Society for Industrial and Applied Mathematics, Philadelphia.

[8] Mallat, S., 1989. A theory for multiresolution signal decomposition: The wavelet representation. IEEE Transactions on Pattern Analysis and Machine Intelligence (11), 674–693.

[9] Coifman, R.R., Wickerhauser, M.V., 1992. Entropy-based algorithms for best basis selection. IEEE Transactions of Information Theory (38), 713–718.

[10] Dimarogonas A.D., 1976. Vibration Engineering. St. Paul, M.A.: West Publishers.

[11] Chondros T., 1977. Dynamic response of cracked beams. MSc thesis, University of Patras, Greece.

[12] Cawley P, Adamas RD., 1979. Defect location in structures by a vibration technique. American Society of Mechanical Engineers Design Engineering Technical Conference, St. Louis, paper (79)-DET-46.

[13] Petroski H. J., 1981. Simple static and dynamic models for the cracked elastic beam. International Journal of Fracture (17), R71–0R76.

[14] Dimarogonas A. D., Paipetis S. A., 1983. Analytical Methods In Rotor Dynamics, Applied Science Publishers Ltd.

[15] Chondros T. G., Dimarogonas A. D., 1980. Identification of cracks in welded joints of complex structures. Journal of Sound and Vibration (69), 531–8.

[16] Rizos P. F., Aspragathos N., Dimarogonos A. D., 1990. Identification of Crack Location & Magnitude in a Cantilever Beam from the Vibration Modes. Journal of Sound and Vibration (138), 381-388.

[17] Liang R. Y., Choy F. K., Hu J., 1991. Detection of cracks in beam structures using measurements of natural frequencies. Journal of the Franklin Institute 328 (4), 505–18.

[18] Ostachowicz W. M. and Krawczuk M., 1991. Analysis of the Effect of Cracks on the Natural Frequencies of a Cantilever Beam. Journal of Sound and Vibration (150), 191-201.

[19] Ruotolo R. and Surace C., 1977. Damage Assessment of Multiple Cracked Beams: Numerical Results & Experimental Validation. Journal of Sound and Vibration (206), 567-5887.

[20] Williams E. J. and Messina A., 1999. Applications of the Multiple Damage Location Assurance Criteria. Proceedings of the International Conference on Damage Assessment of Structures (DAMAS 99), Dublin, Ireland 256–264.

[21] Chaudhari, T. D. and Maiti, S. K., 1999. Crack Detection in Geometrically Segmented Beams. Damage Assessment of Structures, Proceedings of the International Conference on Damage Assessment of Structures (DAMAS 99), Dublin, Ireland 343–353.

[22] Hanselka H., Melcher M., Campanile L.F., and Kaiser S., 1997. A Demonstrator for On-line Health Monitoring of Adaptive Structures. Structural Damage Assessment Using Advanced Signal Processing Procedures, Proceedings of DAMAS '97, University of Sheffield, 225–236.

[23] Morassi A., 1997. Damage Detection and Fourier Coefficients. Structural Damage Assessment Using Advanced Signal Processing Procedures. Proceedings of DAMAS '97, University of Sheffield, UK. 387–397.

[24] Aydoğan, M.Ö., 2003. Damage Detection in Structures Using Vibration Measurements. M. Sc. Thesis, Department of Mechanical Engineering, Middle East Technical University, Ankara.

[25] Doebling, S. W. and C. R. Farrar, 1997. Using Statistical Analysis to Enhance Modal-Based Damage Identification. In Structural Damage Assessment Using Advanced Signal Processing Procedures, Proceedings of DAMAS '97, University of Sheffield, UK. 199–210.

[26] Ahmadian, H., Mottershead, J. E., and Friswell, M. I., 1997. Substructure Modes for Damage Detection. Structural Damage Assessment Using Advanced Signal Processing Procedures, Proceedings of DAMAS '97, University of Sheffield, UK. 257–268.

[27] Sun Z., 2003. Wavelet Packet Based Structural Health Monitoring and Damage Assessment. PhD. Dissertation, Department of Civil Engineering, Hong Kong University of Science and Technology, Hong Kong.

[28] Ettouney M., Daddazio, R., Hapij, A., and Aly A., 1998. Health Monitoring of Complex Structures, Smart Structures and Materials. Industrial and Commercial Applications of Smart Structures Technologies, Proceedings of SPIE, Vol. 3, (326), 368–379.

[29] Wang, W.J., McFadden, P.D., 1996. Application of wavelets to gear box vibration signals for fault detection. Journal of Sound and Vibration 192 (5) ,927–939.

[30] Sung D. U., Kim C. G., Hong C. S., 2002. Monitoring of impact damages in composite laminates using wavelet transform. Composites part B (33), 35–43.

[31] Zhang L.X., Li Z., and Su X.Y., 2001. Crack detection in beams by wavelet analysis. Proceedings of SPIE (4537), 229–232.

[32] Liew K. M., Wang Q., 1998. Application of Wavelet Theory for Crack identification in Structures. Journal of Engineering Mechanics (124), 152–7.

[33] Chang C. C., Chen L. W., 2003. Vibration damage detection of a Timoshenko beam by spatial wavelet based approach. Applied Acoustics (64), 1217–1240.

[34] Naldi G. and Venini P., 1997. Postprocessing Singular Solutions by the Wavelet Transform. Structural Damage Assessment Using Advanced Signal Processing Procedures. Proceedings of DAMAS ‘97, University of Sheffield, UK. 109–120.

[35] Lu C. J., Hsu Y. T., 1999. Application of wavelet transform to structural damage detection. In: 17th International Modal Analysis Conference, Kissimee, USA, 908–914.

[36] Bieman C., Staszewski W. J., Boller C., and Tomlinson G. R., 1999. Crack detection in metallic structures using piezoceramic sensors. Key Engineering Materials (167), 112–121.

[37] Wang, Q., Deng, X., 1999. Damage detection with spatial wavelets. International Journal of Solids and Structures 36 (23), 3443–3468.

[38] Peng Z. K. and Chu F. L., 2004. Application of the wavelet transform in machine condition monitoring and fault diagnostics: a review with bibliography. Mechanical Systems and Signal Processing (18), 199–221.

[39] Hughes D. R., Ghoshal A., Rowe E., Sundaresan M. J., , Schulz M. J., and Feaster J. T., 2004. Health monitoring of thick materials using piezoceramic patches, time signals, and wavelet transmittance functions. Shock and Vibration (11), 47–66.

[40] Han Jian-Gang, Ren Wei-Xin and Sun Zeng-Shou, 2005. Wavelet packet based damage identification of beam structures. International Journal of Solids and Structures (42), 6610–6627.

[41] Kim Y.Y. and Kim E.H., 2000. A new damage detection method based on wavelet transform. In: Proceedings of the International Modal Analysis Conference 1207–12.

[42] Kim H. And Mehlem H., 2003. Damage detection of structures by wavelet analysis. Engineering Structures (26), 347–362.

[43] Spanos PD., Failla G., Santini A., and Pappatico M., 2005. Damage detection in Euler–Bernoulli beams via spatial wavelet analysis. Structural Control and Health Monitoring, doi: 10.1002 / stc. 118.

[44] Ovanesova A. V., Suarez L. E., 2004. Applications of wavelet transform to damage detection in frame structures. Engineering Structures (26), 39–49.

[45] Castro E., Garcia-Hernandeza M. T., Gallego A., 2006. Damage detection in rods by means of the wavelet analysis of vibrations: Influence of the mode order. Journal of Sound and Vibration (296), 1028–1038.

[46] Law S. S., Li X. Y., Zhu X. Q., and Chan S. L., 2005. Structural damage detection from wavelet packet sensitivity. Engineering Structures (27), 1339–1348.

[47] Li Z., Xia S., Wang J., and Su X., 2006. Damage detection of cracked beams based on wavelet transform. International Journal of Impact Engineering (32), 1190–1200.

[48] Cohen A., Daubechies I., Feauveau J.C., 1992. Biorthogonal basis of compactly supported wavelets. Comms on Pure and Applied Mathematics (45), 485–560.

[49] Gurley, K., Kareem, A., 1999. Application of wavelet transform in earthquake, wind and ocean engineering. Engineering Structures (21), 149–167.

[50] Farrar C. R., Sohn H., Hemez F. M., Anderson M.C., Bement M. T., Cornwell P. J., Doebling, S. D., Lieven, N., Robertson, A. N., and Schultze J. F. , 2003. Damage Prognosis: Current Status and Future Needs. Los Alamos National Laboratory report, LA-14051-MS.

[51] Yen, G.G., Lin, K.C., 2000. Wavelet packet feature extraction for vibration monitoring. IEEE Transactions on Industrial Electronics 47 (3), 650–667.

[52] Tsai C., Hsieh C., and Huang S., 2006. Enhancement of Damage-Detection of Wind Turbine Blades Via CWT-Based Approaches. IEEE Transactıons on Energy Conversıon,Vol. 21, no. 3. 776-781.

[53] MATLAB Wavelet Toolbox 4, 2006. Version R2006a, The Mathworks Inc., USA.

APPENDIX A

1. Introduction

The fixed end of the experimentally tested beam as shown in Figure 4.2 looks like as if it were free to move in vertical direction, although a support was put beneath the clamped end of the beam and it was very tightly squeezed in horizontal plane so that it can not move in any direction. Because of this ambiguity in the behavior of the end condition of the test beam, two analytically simulated beams are analyzed. One end of the beam was fixed in all directions for the first simulation case where the same end was fixed only in horizontal directions for the second simulation case. The modal analysis results of all the three cases are compared to decide on the type of end condition

2. Verification Of The Test Setup

2.1 Experimental Analysis

The experimental data that was collected from 5 different points on the test beam was processed at Pulse software programme for modal analysis. The first three natural frequencies and mode shape estimations were obtained from the analysis program.

2.2 Results

2.2.1 Natural Frequencies

Natural frequencies were obtained through processing the measured vibration response data at Pulse software programme.

The first three natural frequencies belonging to the first three transverse vibration modes are given in the following table.

Table A.1 First Three Transverse Natural Frequencies of the Beam

	NATURAL FREQUENCY [Hz]
FIRST	65
SECOND	441
THIRD	1190

2.2.2 Mode Shapes

Mode shapes obtained from experimental results were estimated again through the Pulse software program. First three lateral mode shapes are depicted in Figures A.1 to A.3.

2.3 Analytical Analysis

2.3.1 Modeling the Beam

First of all, the geometry of the beam was modeled in ANSYS ®. Then the proper material type and also the meshing were selected. Geometry and the meshing of the test beam are shown in Figures A.4 and A.5, respectively. Note that in the aforementioned figures the y direction corresponds to the vertical direction in the real test setup. Afterwards, for the test beam at hand a proper material type was selected, where some properties of the selected material are tabulated in Table A.2.

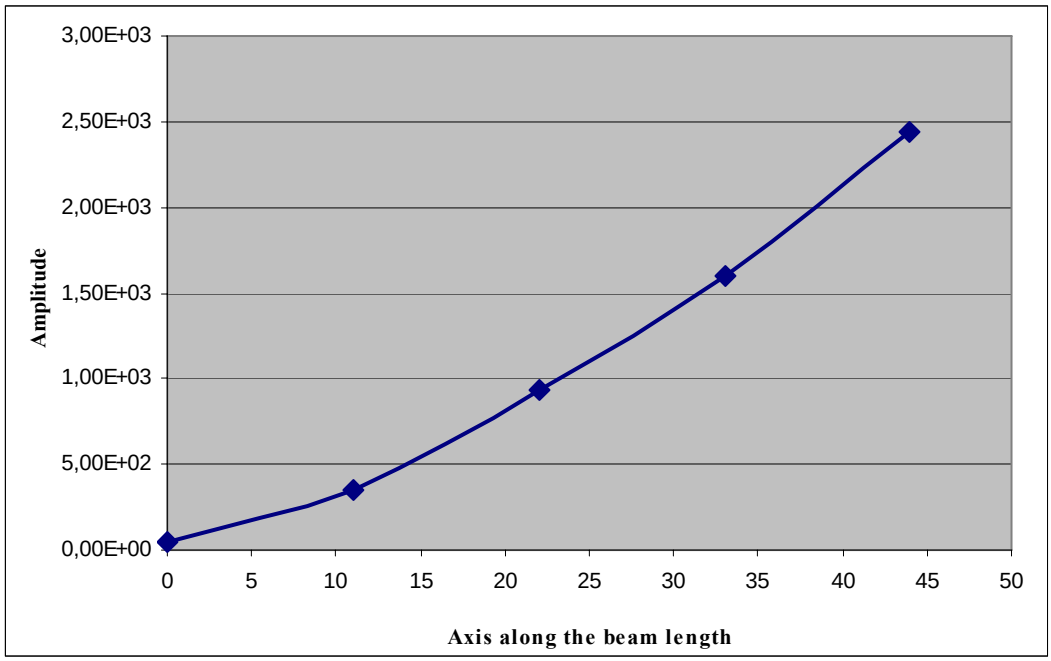

Figure A.1 Mode Shape 1

Figure A.2 Mode Shape 2

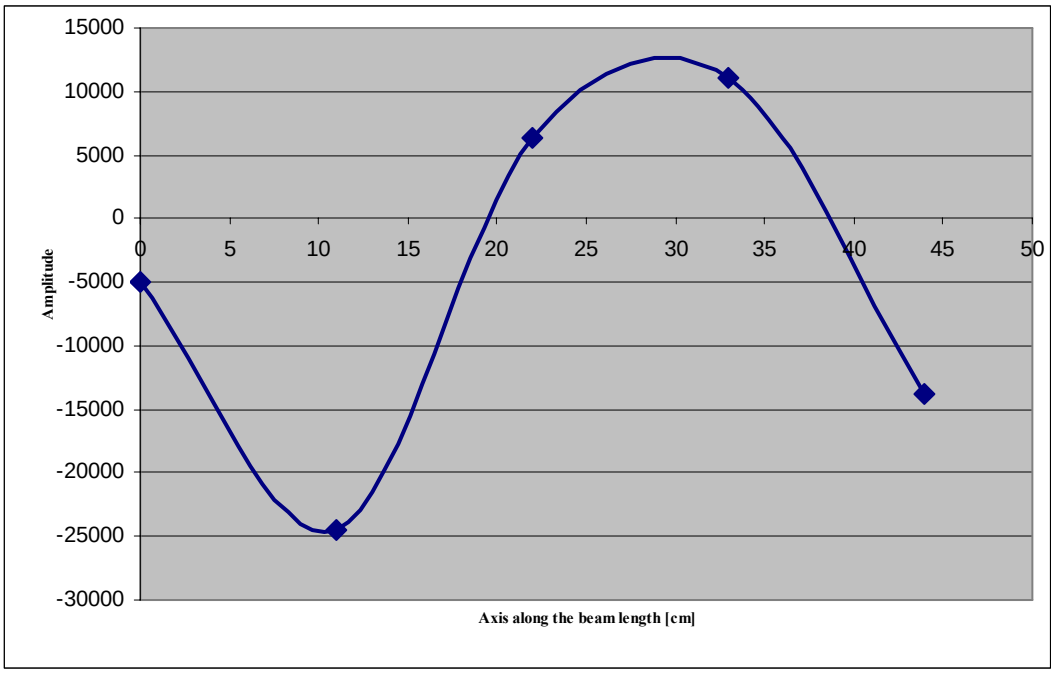

Figure A.3 Mode Shape 3

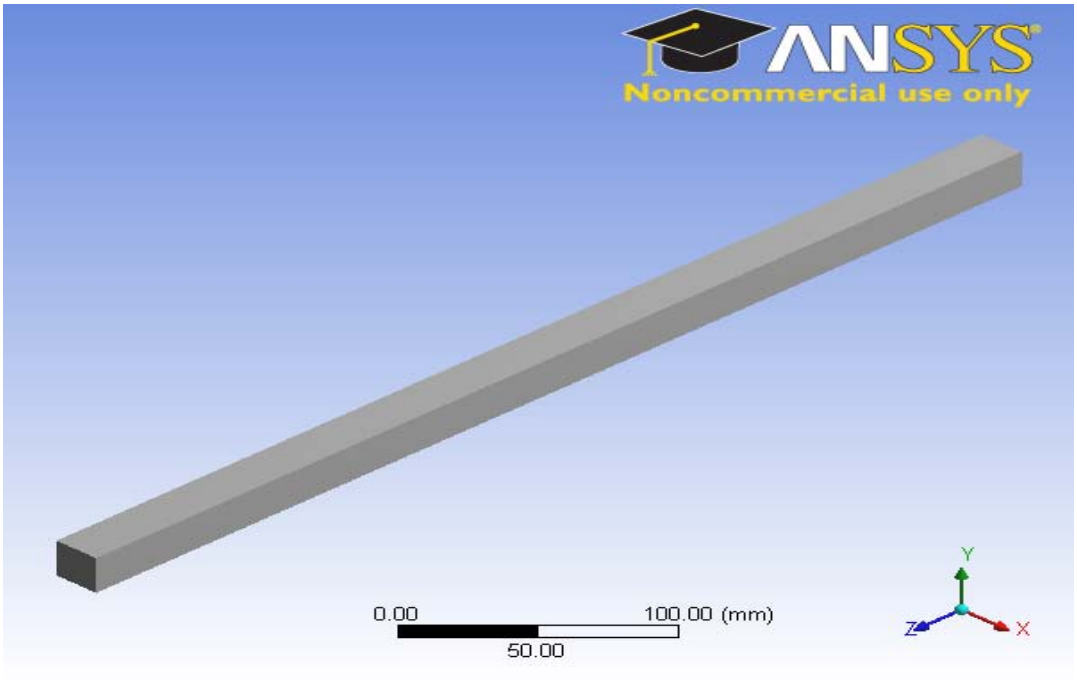

Figure A.4 Geometry of the Test Beam

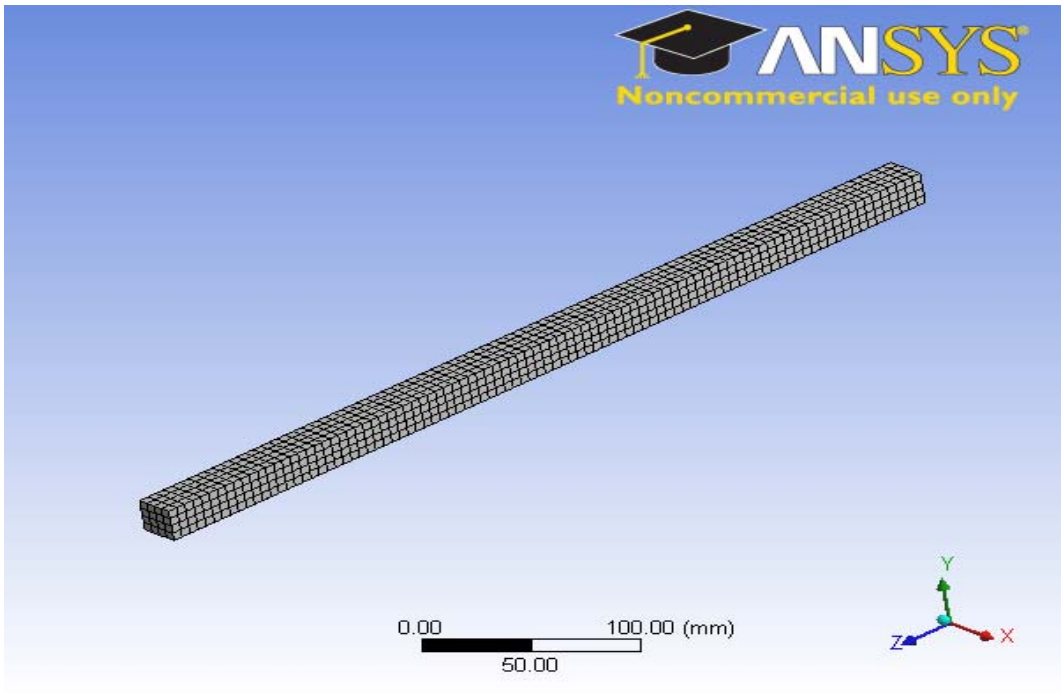

Figure A.5 Meshing of the Test Beam

Table A.2 Material Properties of the Modeled Beam

PROPERTY	VALUE	UNIT
Volume	1,8433e+005	mm³
Mass	0,51059	kg
Young's Modulus	71000	MPa
Poisson's Ratio	0,33	
Density	2,77e-006	kg/mm³
Thermal Expansion	2,3e-005	1/°C
Tensile Yield Strength	280	MPa
Compressive Yield Strength	280	MPa
Tensile Ultimate Strength	310	MPa

2.3.2 Defining the End Conditions

2.3.2.1 X-Y-Z Fixed Case

Cantilever beam model was attained by fixing the displacements of the points along the two yellow lines that is depicted in Figure A.6. Note that all the displacement components along those yellow lines are zero. Since the actual beam was squeezed from the sides, the end condition was simulated along lines.

2.3.2.2 X-Y Fixed Case

In this case end condition of the beam was modeled similar to the previous case except Y direction was set free. In other words, points along the yellow lines that are shown in Figure A.10 were set free to move along the Z direction. Recall that Y direction in all the figures corresponds to Z direction in the actual test setup. Thus, the suspected case of Figure 4.2 could be simulated in this analysis.

2.3.3 Results

2.3.3.1 X-Y-Z Fixed Case Results

2.3.3.1.1 Natural Frequencies

The first three natural frequencies belonging to the first three lateral vibration modes are given in the following table.

Table A.3 First Three Lateral Natural Frequencies of the X-Y-Z Fixed Beam

	NATURAL FREQUENCY [Hz]
FIRST	67.5
SECOND	427.8
THIRD	1198.5

2.3.3.1.2 Mode Shapes

The first three lateral mode shapes which were obtained from the analysis solution are depicted in Figures A.7 to A.9.

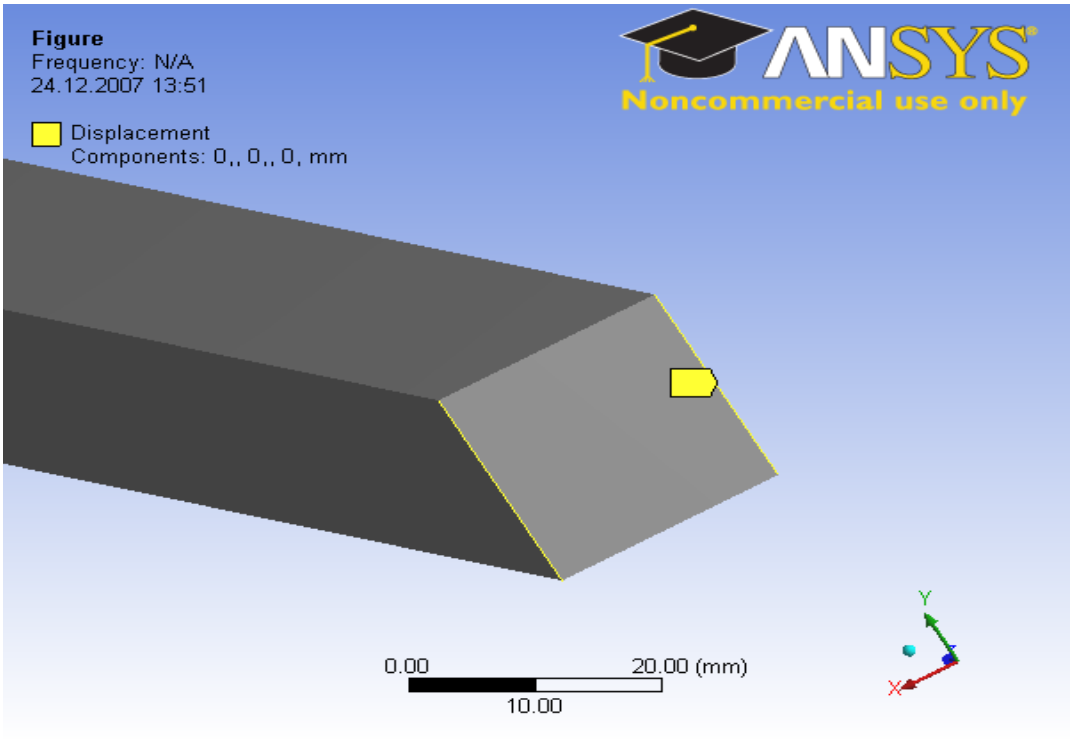

Figure A.6 X-Y-Z Fixed Boundary Condition of Test Beam

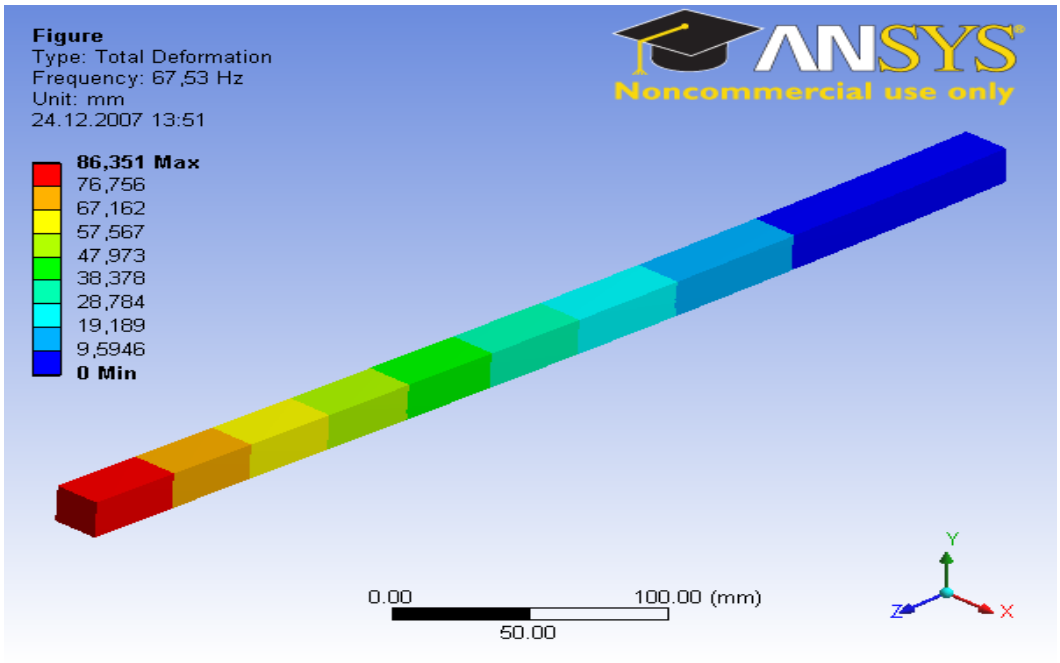

Figure A.7 Mode Shape 1 of X-Y-Z Fixed end Case

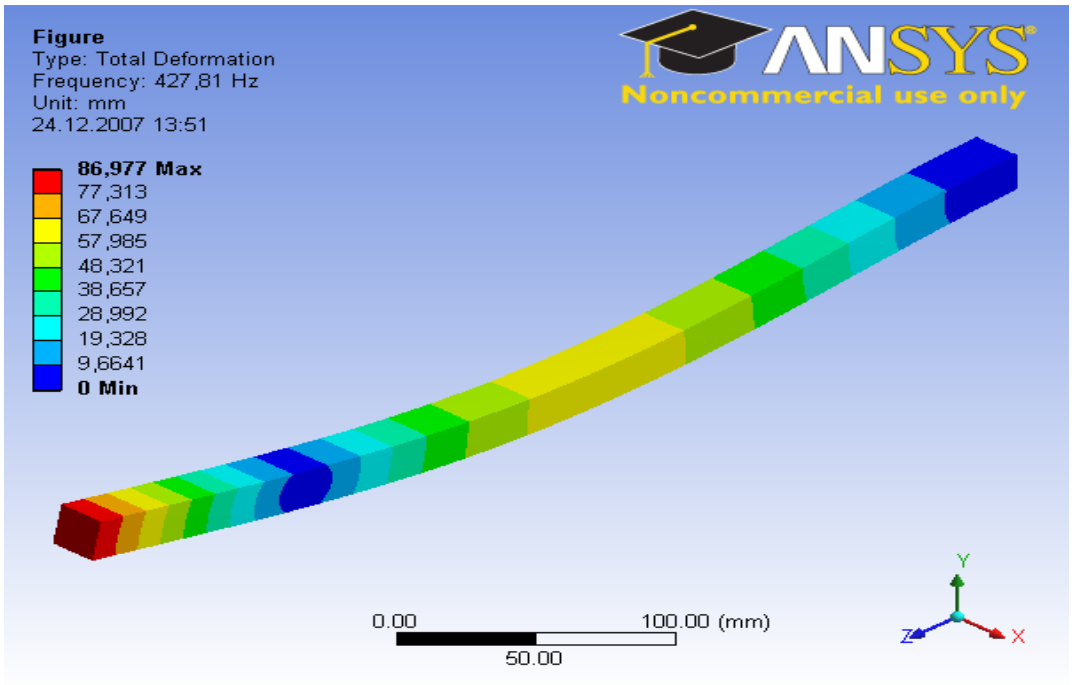

Figure A.8 Mode Shape 2 of X-Y-Z Fixed end Case

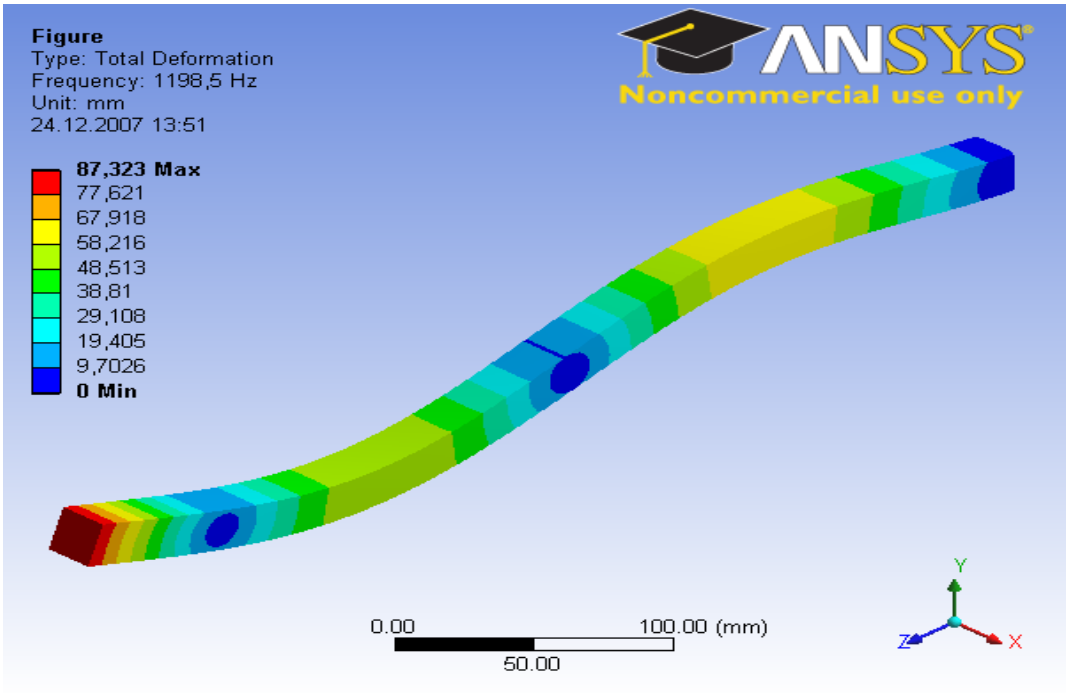

Figure A.9 Mode Shape 3 of X-Y-Z Fixed end Case

2.3.3.2 X-Y Fixed Case Results

In this case end condition of the beam was modeled similar to the previous case except Y direction was set free. In other words, points along the yellow lines that are shown in Figure A.10 were set free to move along the Z direction. Recall that Y direction in all the figures corresponds to Z direction in the actual test setup. Thus, the suspected case of Figure 4.2 could be simulated in this analysis.

2.3.3.2.1 Natural Frequencies

The first three natural frequencies belonging to the first three lateral vibration modes are given in the following table.

Table A.4 First Three Lateral Natural Frequencies of the X-Z Fixed Beam

	NATURAL FREQUENCY [Hz]
FIRST	71.9
SECOND	111.1
THIRD	608.9

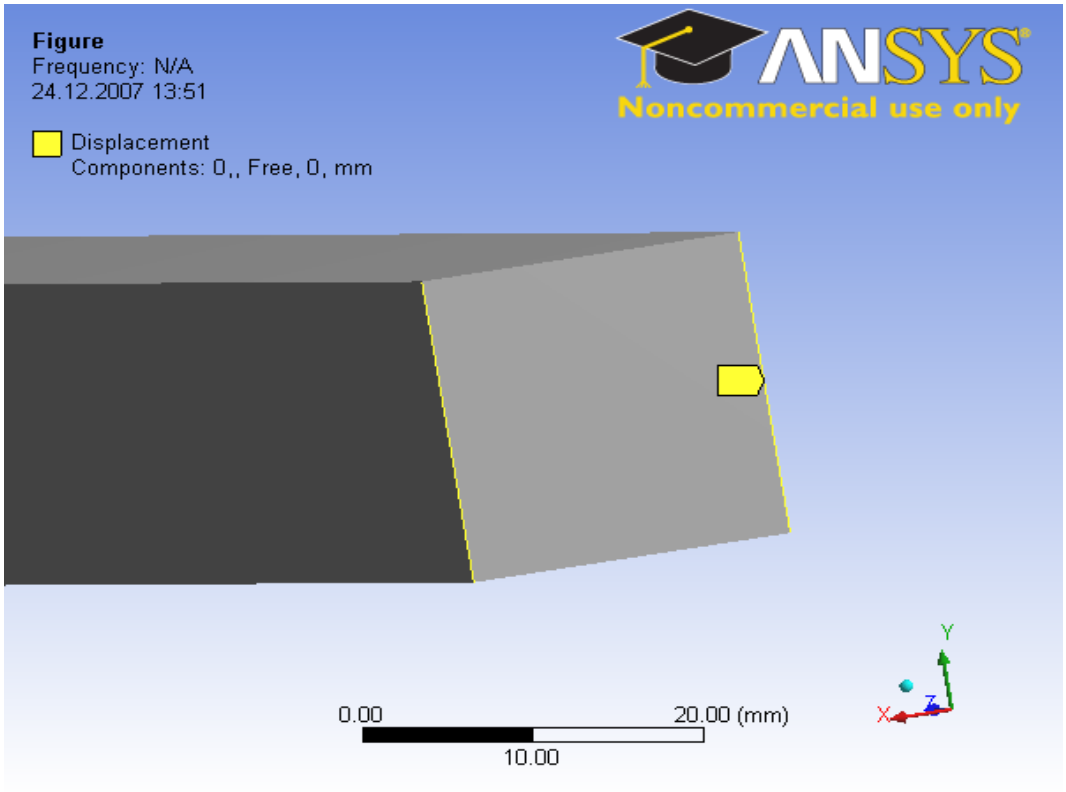

Figure A.10 X-Z Fixed Boundary Condition of Test Beam

2.3.3.2.2 Mode Shapes

The first three lateral mode shapes which were obtained from the analysis solution are depicted in Figures A.11 to A.13.

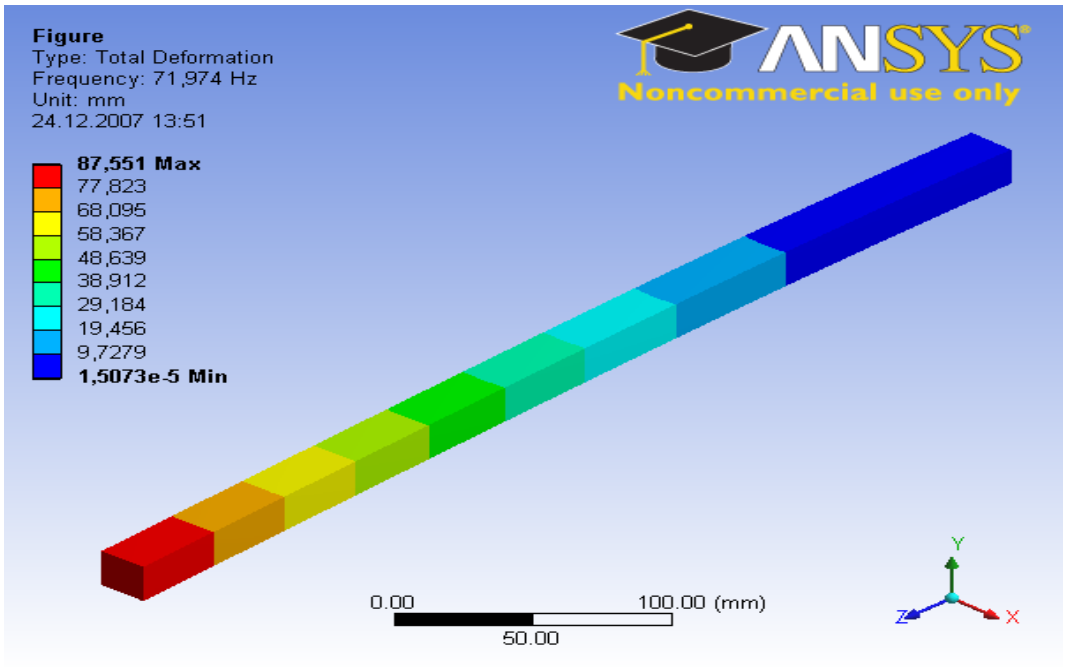

Figure A.11 Mode Shape 1 of X-Z Fixed end Case

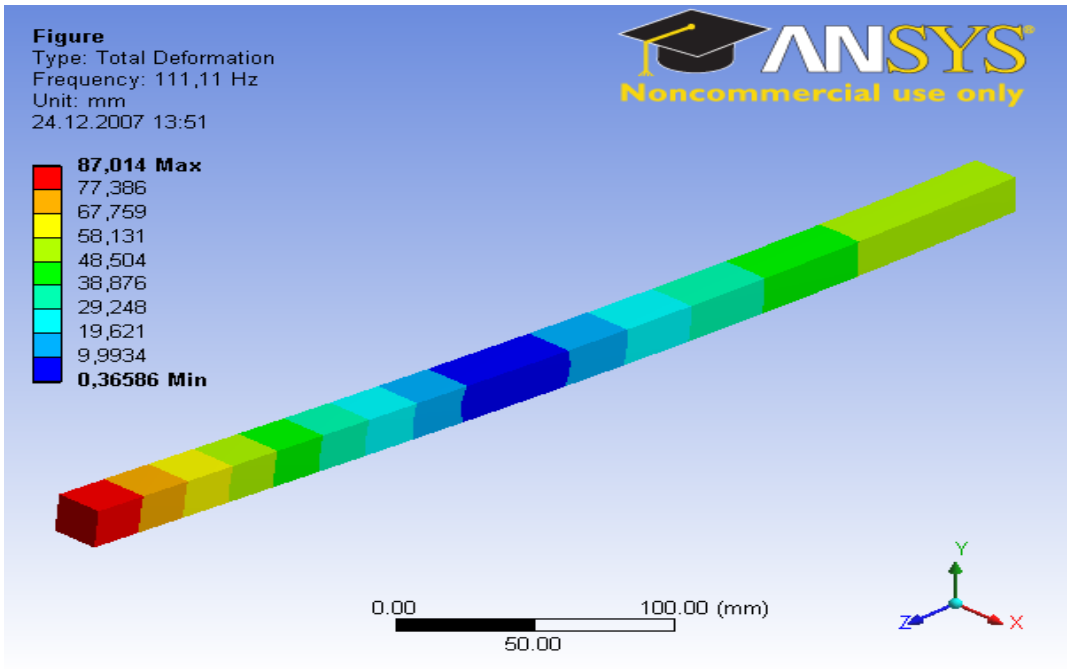

Figure A.12 Mode Shape 2 of X-Z Fixed end Case

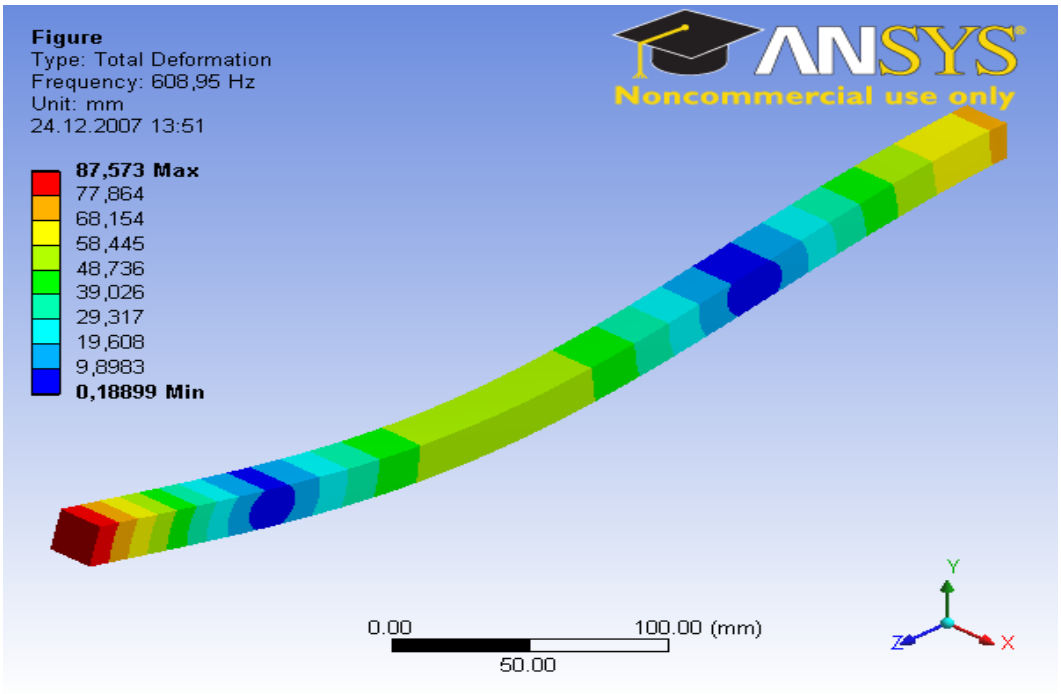

Figure A.13 Mode Shape 3 of X-Z Fixed end Case

3. Discussions

When the natural frequencies obtained from measurement and analytical data are tabulated, it is clearly seen that the actual test beam behaved as if it was a cantilever beam. Table A-5 shows first three lateral natural frequencies of all the three cases. As shown in Table A-6 experimental results and cantilever beam modeled simulation results are in agreement whereas the results of the other case are not acceptable. This result is also supported by the mode shape graphics. When the mode shape figures of different analysis cases are observed it is noticed that mode shapes of Figures A-1 to A-3 match those of Figures A-7 to A-9, respectively. However, among the mode shapes that were calculated from the simulated beam where one end was fixed in X-Z direction, only the first mode shape was similar to that of the experimentally obtained one. These mode shapes are depicted in Figures A-1 and A-11, respectively.

Table A-5 Natural Frequencies of Various Cases

Natural Frequency	Experimental Result [Hz]	Analytical Result (X-Y-Z fixed) [Hz]	Analytical Result (X-Z fixed) [Hz]
FIRST	65	67.5	71.9
SECOND	441	427.8	111.1
THIRD	1190	1198.5	608.9

Table A-6 % Deviations of Analytical Results from Experimental Results for Natural Frequencies

Natural Frequency	Experimental Result [Hz]	% Deviation of X-Y-Z Fixed Case	% Deviation of X-Z Fixed Case
FIRST	65	3.7	9.5
SECOND	441	3	297
THIRD	1190	0.7	95

4. Conclusion

In this study, modal analysis of three different cases of a beam was conducted. From the natural frequency and mode shape results of those analysis cases it was shown that the end condition of the experimentally tested beam was very similar to that of the analytically simulated beam where one end was completely fixed in all directions. To sum up, the beam that was tested experimentally behaved as if it was a cantilever beam although it looks like as if it was not cantilevered.